Experimental Demonstration of Two-Dimensional Spatial Squeezing

Nicolai Grosse

A thesis submitted for the degree of
Bachelor of Science Honours of the
The Australian National University

November 2002

Declaration

This thesis is an account of research undertaken with the supervision of Dr Ping Koy Lam and Dr Nicolas Treps in the Quantum Optics Group between February 2002 and November 2002 at The Department of Physics, Faculty of Science, The Australian National University, Canberra, Australia.

Except where acknowledged in the customary manner, the material presented in this thesis is, to the best of my knowledge, original and has not been submitted in whole or part for a degree in any university.

Nicolai Grosse
12th November 2002

Acknowledgements

I'm taking this moment to quietly reflect on all the people in my life who are so wonderful in many ways. This year has been fantastic. I've had the opportunity to be involved in exciting research with wonderful people. I would like to thank Ping Koy for offering me this honours project, and scholarship too. The enthusiasm of the whole quantum optics team (Andrew, Thomas, Ping Koy, Hans, Aska, Kirk, Ben, Warwick, Nicolas) has been an inspiration. Nicolas, it was really good working with you. In the lab, and discussions, and also BBQs There is no way that I could have built and run the experiment without you. I think that we made a really good team, and I feel that I've learnt alot this year. Thankyou also for proof reading my chapters and taking the time to make comments. From the first half of the year I'd like to thank Ben and Warwick for sharing their office, and also the weekly discussions with Hans, Ping Koy and Nicolas to get me up to speed. Thankyou Ping Koy for all the help you have given me throughout this year, and making clear, lots of concepts that were initially unclear. Thankyou too for all the last minute proof reading, and also your positive outlook. Now lots of thankyous as people pop randomly into my head. Conor and Tim, for keeping me company through my 25hr editing marathon! Simon, for all your help and humour and cricket bowling tips. John, for calling late afternoon beers at deck world, and also helping with the laser beam calibration. Adele for talking with me at the end of some very long winter days. Taira, for your random appearances. The whole honours crowd Tim, Adele, Kirk, Simon, Aska, Stu, Conor, Doug, Ingrid, Taira, Phil, Anne, Annabel, for when assignments were always due yesterday. Katie, Jenny and Nick of the Mephisto quartet for making music so much fun. Aska, your beautiful creativity, and strength of friendship will always inspire me. Violette, you are the best sister in the universe! Thankyou Mama and Papa for your love, and showing me that love is the most important thing.

Abstract

This thesis presents the first experimental demonstration of two-dimensional spatial squeezing. A dual squeezer was used to produce two beams of temporally squeezed light. Specially designed wave-plates were required to generate the necessary spatially orthogonal modes. These modes were mixed on an optical cavity to form a multi-mode superposition that converted the original temporal correlations into the desired spatial correlations. We used this light to improve the sensitivity of a two-dimensional beam displacement measurement to below the quantum noise limit. Our setup was also configured to generate a one-dimensional spatially squeezed state of light that did not require either of the two input modes to suffer substantial loss. This was the first experimental demonstration of a proper spatial squeezing measurement.

Contents

List of Figures

List of Tables

Chapter 1

Introduction

Scientific concepts are inner pictures. Heinrich Hertz

This chapter introduces the idea of two-dimensional spatial squeezing, why it is interesting, and how it may relate to improvements in instrument precision.

1.1 What is spatial squeezing?

Spatial squeezing allows position measurements of a laser beam to be made below the standard quantum limit in sensitivity. To find out what this really means, will require an explanation of beam displacement measurements, the quantum noise limit, and how it may be surpassed with the use of squeezed light.

1.1.1 Beam displacement measurements

A split detector is commonly used for the purpose of measuring the position of a laser beam. For one-dimensional measurements, a split detector consists of two independent

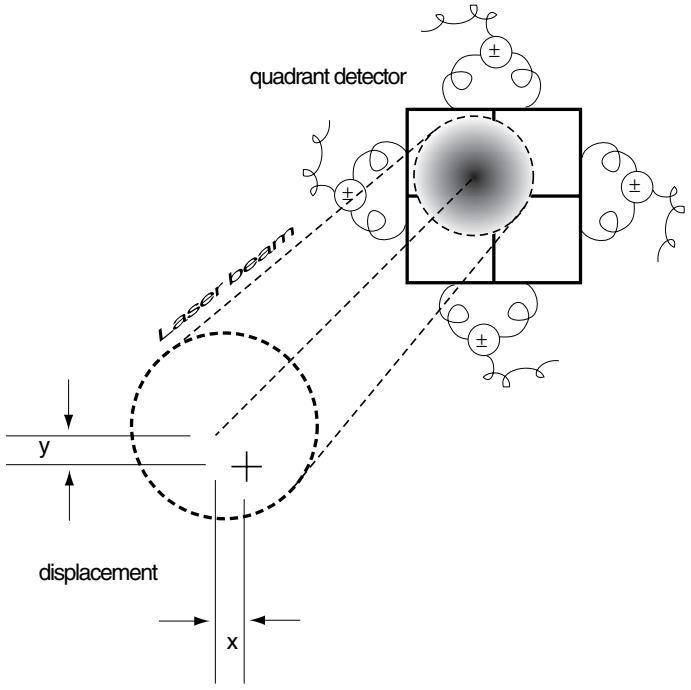

Figure 1.1: Beam displacement from centre measured with a quadrant detector.

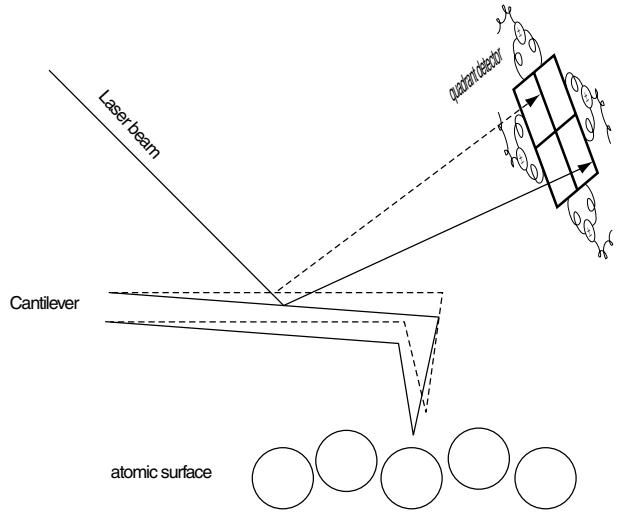

Figure 1.2: Schematic of an atomic force microscope. A laser beam reflects from a displaced cantilever onto a quadrant detector.

photodetectors mounted side by side. The difference photocurrent is formed to produce an error signal. This is often referred to as a differential measurement. When the beam is perfectly centred on the split detector, the photocurrents from each detector element are balanced, and the error signal is zero. If the beam should walk away from the centre, then the photocurrents will not be balanced. For small beam displacements (less than the width of the laser beam), the error signal (S) is directly proportional to the displacement (x) and the maximum intensity (I_0) of the beam, that is

$$S \propto I_0 x \tag{1.1}$$

Two-dimensional beam displacement measurements may be performed using a split detector that consists of four elements placed side by side to form a square, called a quadrant detector. See Figure 1.1. The photocurrents are added/subtracted in such a way as to give two differential measurement signals corresponding to horizontal and vertical beam displacements.

1.1.2 Atomic force microscopy

Beam displacement measurements such as this are used in an atomic force microscope (AFM). As shown in Figure 1.2. An AFM can create a height map of a surface down to the molecular level. It consists of a silicon cantilever that terminates with a very fine needle. The tip of the needle feels a force from the atoms in the surface which causes the cantilever to bend and change angle. A laser beam is then focussed onto the highly reflective cantilever. The change in angle of the cantilever corresponds to a change in the position of the laser beam, which is measured on a split detector. The sample, which is attached to a piezo electric mount, is then scanned in position to build up a three-dimensional map of the surface.

1.1.3 Quantum noise limit

Is there a limit in sensitivity for a beam displacement measurement? The answer is yes. In most cases there will be various noises present such as seismic, acoustic, thermal, radiation pressure, electronic, which will limit the sensitivity of the measurement. In some regime, these noise will be low enough that limit in sensitivity is entirely due to the quantum nature of light. We know that light is a continuous electromagnetic wave, but we also know that its energy is delivered in discrete packets called photons. For the light that a laser produces, which is a good approximation to a coherent state and has Poissonian statistics, the photons are randomly ordered in time, ie. there is no correlation between arrival times of photons on a detector. It must be remembered that where a photon is in the transverse space of a beam is also random. For a Gaussian beam, this means that the probability of detecting a photon follows a Gaussian distribution. For a split detector beam displacement measurement, this implies that the number of photons detected on each element will be uncorrelated with its neighbours. The anti-correlation component will produce a noise in the error signal at what is called the quantum noise limit (QNL). Another name for this is the shot noise limit (SNL). This corresponds to a minimum displacement that may be measured, and from [11] for a Gaussian beam, this is given by

$$d_{SNL} = \sqrt{\frac{\pi}{8}} \frac{\omega_0}{\sqrt{N}} \tag{1.2}$$

Where ω_0 is the width of the Gaussian beam, and N is the number of photons collected from the duration of the measurement. For a beam that is maximally tightly focussed the width is on the order of the wavelength, and we get

$$d_{SNL} \propto \frac{\lambda}{\sqrt{N}} \tag{1.3}$$

To boost the number of photons detected, and hence improve the spatial resolution of the measurement, one may either increase the laser power, or increase the integration time. An increase in laser power is not always desirable, as for example one may reach the point where the cantilever in an AFM begins to respond to the radiation pressure noise of the light, thereby increasing the noise in the displacement measurement. An increase in integration time is usually not desired either, as the frequency response of the measurement is lowered, and therefore any action happening on short time scales will be missed. One can imagine that for very demanding applications it may not be possible to find a compromise, and sensitivity will have to be sacrificed. However, as we shall see, the optical technique of producing squeezed light may come to the rescue.

1.1.4 Spatial squeezing

Amplitude squeezed light has the property that its photon number fluctuations are below that of shot noise. In the last decade it has been shown that squeezed light could improve the sensitivity of measurements beyond the quantum noise limit [1]. Some examples include; the improvement in position measurement of test masses in an interferometric gravitational wave detector [6], and improvement of absorption measurements [7]. These, however, all relied on the temporal nature of squeezing, ie. photon correlations in time.

The photon statisitics of an ordinary beam, a temporally squeezed beam, and a spatially squeezed beam are shown hitting two halves of a split detector in Figure 1.3. For an

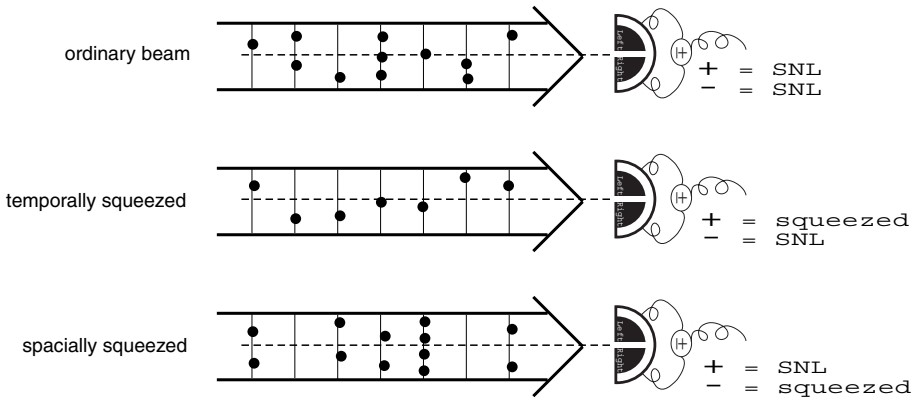

Figure 1.3: Conceptual picture of the photon distribution in light hitting a one dimensional split detector and the resulting noise level for sum/difference mesurements. Shown for coherent state, temporally squeezed state, and spatially squeezed state.

ordinary shot noise limited beam, the number of photons at each moment in time is randomly drawn from a Poissonian distribution with a mean photon number corresponding to the intensity of the beam. A temporally squeezed beam has photons that are correlated in time, ie. they prefer to come one at a time. It is for this reason that when this beam is detected on a single detector, that the photon number fluctuations are below the shot noise limit. However, if this beam is detected on a split detector, there will be no improvement for a beam displacement measurement. This is because the photons are arriving effectively one at a time, but in a random spatial position at the split detecter. This gives rise to anti-correlations of the photocurrents in the split detector, which translate into noise in the displacement signal. The result is that the signal stays at the SNL, ie. using temporal squeezing alone gives no improvement.

How can temporal squeezing be converted into spatial squeezing? The clever technique proposed by [3] used a waveplate that gave one half of a dim squeezed beam a 180° phase flip. This squeezed mode was then mixed with an ordinary bright Gaussian mode. The effect of the flipped squeezed mode on the bright Gaussian can be seen in Figure 1.3. Where the single photons have been re-distributed to form pairs, and guarantee a photon at each half of the split detector, thereby giving a spatial correlation. This has the effect of lowering the noise floor of the displacement measurement to below the SNL, and is therefore spatially squeezed.

1.2 Previous work in one dimension

The first ever continuous wave one-dimensional spatial squeezing experiment was performed in 2001 by N. Treps, *et al.* [11]. They demonstrated (2.5 ± 0.2)dB of spatial squeezing. And an improvement in the signal to noise floor ratio of a beam displacment modulation at 4.5MHz by a factor of 1.7 below the shot noise. It was a landmark experiment that has opened a new pathway into the field of quantum imaging.

1.3 How can this be extended to two dimensions?

The technique by [3] may be extended to two dimensions by using a second squeezed beam that is phase flipped along the other axis (vertical). See Figure 1.4. This will have the

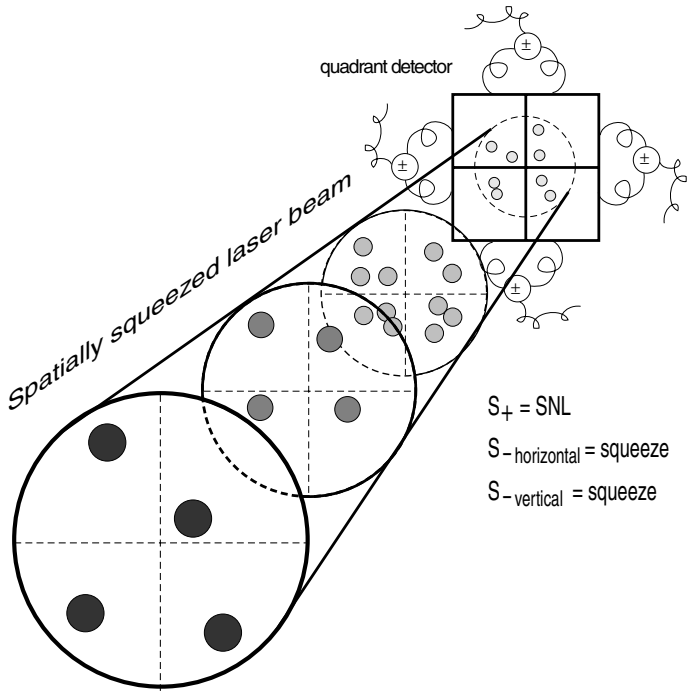

Figure 1.4: Conceptual picture of the photon distribution for a light beam that is squeezed in two dimensions.

effect of re-distributing the photons in such a way that they arrive at the quadrant detector with effectively one addressed to each quadrant. This will reduce the anti-correlations, and hence the differential noise measured for both horizontal and vertical axes. This is two-dimensional spatial squeezing.

1.4 Our work

Our aim was to experimentally demonstrate two-dimensional spatial squeezing. The motivation was of course that we wanted to prove whether it could be done in practice. Our method involved the operation of two temporal squeezers, and the utilisation of a new optical mode mixing technique.

1.5 Thesis structure

This thesis has been written in such a way that each section and chapter flows on from the next in a linear fashion. The confident reader may of course advance beyond material that they are already familiar with.

- Chapter 2 is largely a review of quantum optics theory. However, the reader is urged not to miss the very important, and perhaps unfamiliar, theory of spatial squeezing and spatial differential measurements. These are crucial to understanding the concepts behind spatially squeezed light.

- Chapter 3 is a thorough investigation of the special optical components that were required for the experiment. The theoretical aspects and modelling are addressed,

followed by the experimental characterization of these components and a discussion of their utilisation in the experiment.

- Chapter 4 goes into detail about the experimental setup, locking techniques, and method of data analysis.
- Chapter 5 presents all the 2D spatial squeezing results and their interpretation.
- The final chapter is a summary of what we have accomplished, and also a look into the future of spatial squeezing.

Chapter 2

Theory

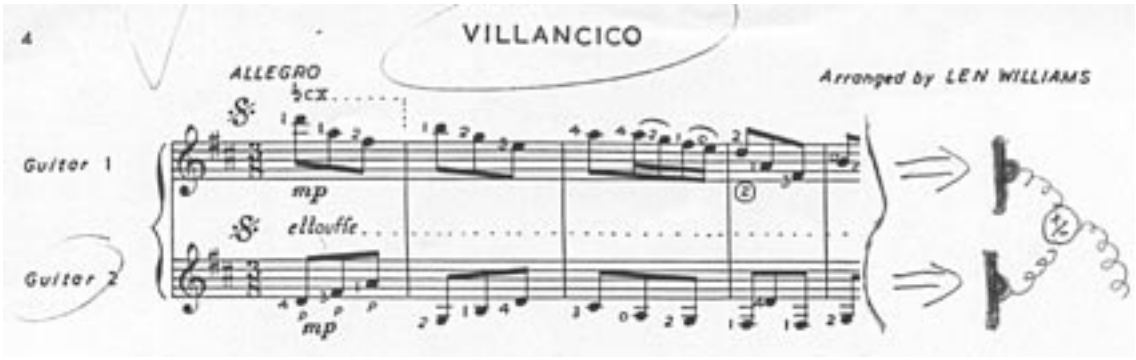

Figure 2.1: A differential measurement performed on the musical notes in a guitar duet. Observe the strong anti-correlation in the first two bars.

Most of this Chapter is a review of the quantum optics theory that will give us insight into the quantum nature of light. Theoretical tools will be developed to enable the calculation of some results that lead to useful experimental techniques. Spatial differential measurements will be dealt with and the origin of the noise in these measurements will be revealed. This knowledge will then be used to predict the spatial-multi-mode light necessary for two dimensional spatial squeezing.

2.1 Quantum description of light

What we are seeking here is an understanding of the quantum nature of light. The treatment here is very brief, and for details the reader is advised to turn to the standard literature on the subject [12], [1], [2], [4].

2.1.1 Quantization of the electromagnetic field

Classical electromagnetism is completely contained within Maxwell's set of equations, which predict the phenomenon of light as the continuous propagation of energy by harmonic oscillation of electric and magnetic fields. Experiments in the early 20th century revealed that light also consisted of discrete packets (quanta) of energy. Due to their

particulate nature, they were given the name photons. Measured properties of photons are that they carry $p = \hbar k$ of linear momentum, and $L = \pm\hbar$ angular momentum. Where $k = 2\pi/\lambda$ is the wave-number inversely proportional to the wavelength, and $\hbar$ is Planck's constant. A deeper level of quantum theory was developed by Dirac, that was used to uncover the origin of photons. The method of second quantization was applied to the situation of an electromagnetic field bounded in a finite space, giving rise to a set of discrete modes. The result was that there exist operators that raise and lower the occupation number of photons in a single mode, defined as the creation $\hat{a}_k^\dagger$ and annhilation $\hat{a}_k$ operators, where k labels the mode. Since photons are spin $S = 1$ particles, they are from the boson family of particles with integer value spins ($S = 0, 1, 2, 3, \ldots$), and hence obey the boson commutation relation

$$[\hat{a}_k, \hat{a}_{k'}^\dagger] = \delta_{kk'} \tag{2.1}$$

Where $k^{'}$ refers to another mode. From now on we will be dealing with a single mode, and the relation thus simplifies to

$$[\hat{a}, \hat{a}^\dagger] = 1 \tag{2.2}$$

The Hamiltonian of the quantized system is

$$\mathcal{H} = \hbar\omega(\hat{a}^\dagger\hat{a} + \frac{1}{2}) \tag{2.3}$$

Whose eigenstates form the basis of number states $|n\rangle$ (also called Fock states). The number operator is defined as $\hat{n} = \hat{a}^\dagger\hat{a}$ and returns the occupation number n as its eigenvalue when operated on the number state, that is

$$\hat{n}|n\rangle = n|n\rangle \tag{2.4}$$

The effect of creation and annhiliation operators on a number state may be seen from

$$\hat{a}|n\rangle = \sqrt{n}|n-1\rangle \tag{2.5}$$
$$\hat{a}^\dagger|n\rangle = \sqrt{n+1}|n+1\rangle \tag{2.6}$$

The lowest energy state of the system $|0\rangle$ is called the vacuum state. Note that its energy of $\frac{1}{2}\hbar\omega$ is not zero. This vacuum energy is present in every possible mode at every point in position space. These operators alone are not a satisfying description of light as they themselves do not correspond to observable quantities. This is because they are not Hermitian operators complying with the condition $(\hat{o})^* = \hat{o}$. We can, however, form a Hermitian operator from these two to give what is called the general quadrature operator.

$$\hat{X}^\theta = \hat{a}e^{-i\theta} + \hat{a}^\dagger e^{i\theta} \tag{2.7}$$

It is convenient to work with this operator evaluated for $\theta = 0$ and $\theta = \frac{\pi}{2}$ giving an operator pair

$$\hat{X}^+ = \hat{a}^\dagger + \hat{a} \tag{2.8}$$
$$\hat{X}^- = i(\hat{a}^\dagger - \hat{a}) \tag{2.9}$$

Where $\hat{X}^+$ and $\hat{X}^-$ are referred to as the amplitude and phase quadratures respectively. These may of course be used to re-express the original general quadrature operator as

$$\hat{X}^\theta = \hat{X}^+ \cos\theta + \hat{X}^- \sin\theta \tag{2.10}$$

The story does not end here, but we must digress briefly to explain the Heisenberg uncertainty principle so that we may then apply it to light.

2.1.2 Heisenberg uncertainty principle

Imagine that we have an ensemble of identical experimental systems, and we wish for example, to make a measurement of the position and momentum of a single particle. Classical physics does not put a limit on how fine a measurement we could make of both observables with instruments of unlimited precision. However, the Heisenberg uncertainty principle (HUP) from quantum physics tells us that we could not even in principle perform perfect simultaneous measurements of the two aforementioned observables on the particle. The HUP is usually expressed as

$$\sigma_A^2 \sigma_B^2 \geq (\frac{1}{2i}\langle[\hat{A}, \hat{B}]\rangle)^2 \tag{2.11}$$

Where $\hat{A}$ and $\hat{B}$ are the operators of the corresponding observables with expectation value of the commutator $\langle[\hat{A}, \hat{B}]\rangle$, and σ_A, σ_B are their standard deviations $\sigma_A^2 = \langle\hat{A}^2\rangle - \langle\hat{A}\rangle^2$ and so on. A pair of observables which do not commute, ie. $[\hat{A}, \hat{B}] \neq 0$ are called incompatible observables. Position $\hat{x}$ and momentum $\hat{p}$ are non-commuting, and therefore incompatible observables because their commutation relation gives $[\hat{x}, \hat{p}] = i\hbar$ and we get the following uncertainty relation

$$\sigma_p \sigma_x \geq \frac{\hbar}{2} \tag{2.12}$$

This means that a precision measurement of one observable always comes at the expense of making its incompatible observable more uncertain. Returning now to optics and applying the HUP to our pair of quadrature operators we find that $[\hat{X}^+, \hat{X}^-] = 2i$ which leads to the uncertainty relation

$$\sigma_{X^+} \sigma_{X^-} \geq 1 \tag{2.13}$$

A state of light for which ($\sigma_{X^+}\sigma_{X^-} = 1$) is called a minimum uncertainty state. For this state, the fluctuations in each quadrature give rise to measurements at a level of precision that are said to be at the standard quantum limit (SQL). States having variances (square of the standard deviation) that are both equal to one, ie. ($\sigma_{X^+} = \sigma_{X^-} = 1$) , are called quantum noise limited (QNL), or equivalently, shot noise limited (SNL). Both QNL and SNL will be used interchangebly from now on.

2.1.3 Vacuum state

As mentioned earlier, a number state having zero photons $|0\rangle$ is called the vacuum state. Although it contains no photons, it still has quadrature fluctuations at the minimum uncertainty state, and is therefore QNL. When doing quantum optical calculations, it is important to include the vacuum state entering from unused ports of beamsplitters etc.

2.1.4 Coherent state

A coherent state $|\alpha\rangle$ is the state light emitted by an ideal laser. It may be expressed as a superposition of number states

$$|\alpha\rangle = e^{-\frac{|\alpha^2}{2}|} \sum_n^\infty \frac{\alpha^n}{\sqrt{n!}} |n\rangle \tag{2.14}$$

The form of this expansion means that a coherent state has a photon number distribution that is Poissonian with an expectation value at α. For very bright coherent states, ie. a large coherent amplitude α, the Poissonian distribution may be approximated as a Gaussian distribution. For bright coherent states the actual expectation value of the photon number is $\langle \hat{n} \rangle = |\alpha|^2$. A coherent state may be produced by the application of the displacement operator

$$\hat{D}_\alpha = e^{\alpha \hat{a}^\dagger - \alpha^* \hat{a}} \tag{2.15}$$

on the vacuum state to give

$$\hat{D}_\alpha |0\rangle = |\alpha\rangle \tag{2.16}$$

Note that a coherent state is QNL (also SNL). The idea of shot noise in SNL arises from the statistical nature of the detection of photons from a coherent state. The rule for Poissonian statistics is that there is no correlation between arrival times of successive 'shot' (lead shot for bullets!) being dropped onto a hard surface. The term 'no correlations' means having an ensemble of prepared systems that drop their shot at their own random moment of choice.

2.1.5 Squeezed state

A state may be regarded as squeezed if either one of the quadrature amplitude standard deviations falls below the value of one. The HUP of course requires that the other quadrature standard deviation rise above the value of one. A squeezed state $|\alpha_r\rangle$ may be generated by the application of the squeezing operator $\hat{S}_r$ on the vacuum state $|0\rangle$ to create a squeezed vacuum, which is then operated on by the displacement operator $\hat{D}_r$

$$\hat{S}_r = e^{\frac{1}{2}(r^* \hat{a}^2 - r \hat{a}^{\dagger 2})} \tag{2.17}$$

$$|\alpha_r\rangle = \hat{D}_\alpha \hat{S}_r |0\rangle \tag{2.18}$$

Where r is the squeezing parameter and belongs to the set of real numbers. This has the following effect on the quadrature standard deviations

$$\sigma_{X+} = e^{-r} \tag{2.19}$$

$$\sigma_{X-} = e^{r} \tag{2.20}$$

Note that one quadrature will always be squeezed at the expense of the other. Also note that this is still a minimum uncertainty state because the product of the standard deviations is equal to one. The expectation value of the photon number becomes

$$\langle \hat{n} \rangle = |\alpha|^2 + \sinh r^2 \tag{2.21}$$

One may often encounter the term *squeezed vacuum* in the literature for a state with zero coherent amplitude α. It may be seen from the equation above that a squeezed vacuum

does have probability of containing some photons due to the extra squeezing term. An important point to be aware of is that these three states; vacuum, coherent and squeezed, are not the only ones possible. One can in principle construct any state the imagination may conjure up using a superposition of states from the complete number state basis $|n\rangle$.

2.1.6 Linearized quadrature operators

In quantum optics, linearization has proven to be a very useful tool, not only in aiding calculation, but also in gaining insights into the physics behind the results. The linearization is performed at the very beginning with the creation and annhiliation operators. Looking at the creation operator for the moment (treatment for the annhilation operator is identical)

$$\hat{a}(t) \approx \alpha + \delta\hat{a}(t) \tag{2.22}$$

Where α is a complex valued constant and corresponds to the classical field amplitude. And $\delta\hat{a}(t)$ represents all the time varying fluctuations. The following assumptions are inherent to the linearization

$$\begin{aligned} \langle\delta\hat{a}(t)\rangle &= 0 && (2.23)\\ |\delta\hat{a}(t)| &\ll |\alpha| && (2.24) \end{aligned}$$

The first actually follows on from the definition of α as the expectation value of $\hat{a}$, ie. $\alpha = \langle\hat{a}\rangle$. Conceptually this is the separation of mean field from the fluctuations. The second line is a reminder that the fluctuations are much smaller than the classical coherent amplitude α. As will be seen, these linearization assumptions greatly simplify the analysis of problems, as they allow terms to be thrown away that are small in comparison to their neighbours. After linearization, the variances of the quadratures are given by

$$\begin{aligned} \sigma^2_{X_a^+} &= \langle(\delta\hat{a}^\dagger + \delta\hat{a})^2\rangle && (2.25)\\ &= \langle(\delta\hat{X}^+)^2\rangle && (2.26)\\ \sigma^2_{X_a^-} &= \langle(i\delta\hat{a}^\dagger - i\delta\hat{a})^2\rangle && (2.27)\\ &= \langle(\delta\hat{X}^-)^2\rangle && (2.28) \end{aligned}$$

Using linearized operators, assuming that α is real, and throwing away any products of more than two fluctuation terms (ie. the quadratic terms), the expectation value of the photon number becomes

$$\begin{aligned} \hat{n}(t) &= \hat{a}^\dagger\hat{a} && (2.29)\\ &= [\alpha^* + \delta\hat{a}^\dagger(t)][\alpha + \delta\hat{a}(t)] && (2.30)\\ &= \alpha^2 + \alpha[\delta\hat{a}(t) + \delta\hat{a}^\dagger(t)] + \delta\hat{a}^\dagger(t)\delta\hat{a}(t) && (2.31)\\ &\approx \alpha^2 + \alpha\delta\hat{X}_a^+(t) && (2.32) \end{aligned}$$

The variance of the linearized photon number is then found to be

$$\begin{aligned} \langle\sigma_n^2\rangle &= \langle(\alpha\delta\hat{X}_a^+)^2\rangle - \langle(\alpha\delta\hat{X}_a^+)\rangle^2 && (2.33)\\ &= \alpha^2\sigma^2_{X_a^+} && (2.34) \end{aligned}$$

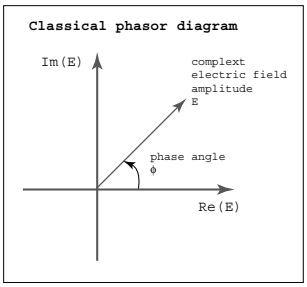

Figure 2.2: Classical phasor diagram

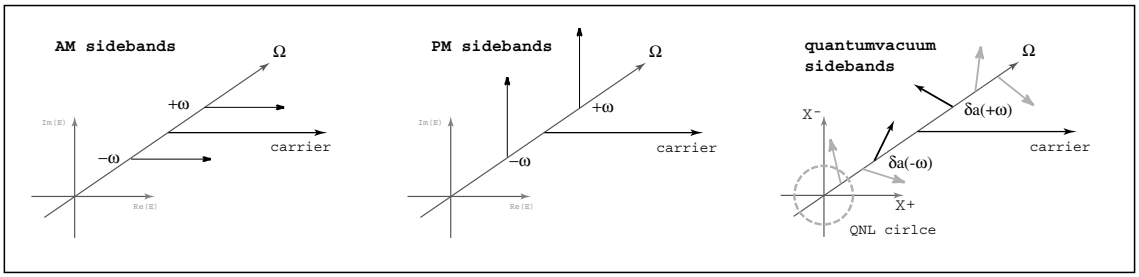

Figure 2.3: Sideband picture. LEFT: amplitude modulation. MIDDLE: phase modulation. RIGHT: Continuum of vacuum noise AM and PM sidebands beating with carrier.

This tells us that the variance of the photon number scales with the mean photon number. Hence for a coherent state ($\sigma^2_{X_a^+} = 1$) the measured intensity noise of a coherent state will have a variance proportional to the average intensity. This is the shot noise limit (SNL). Looking now at an amplitude squeezed state ($\sigma^2_{X_a^+} = e^{-2r}$ with squeezing factor $r > 0$) we find that the photon number variance becomes

$$\langle \sigma_n^2 \rangle = \alpha^2 e^{-2r} \tag{2.35}$$

As we can see, that the photon number noise has been squeezed below the shot noise limit. The best level of continuous (ie. not pulsed) squeezing observed in an experiment is around 7dB. See [5].

2.1.7 Sideband model

In classical electromagnetism, the electric field vector of a single mode of light is often expressed in complex notation, in a phasor diagram, see Figure 2.2 where the horizontal axis is the real component of the complex field and therefore the amplitude quadrature. The vertical axis is the imaginary component of the field which is the phase quadrature. Can we use this picture for quantum light? The quantum mechanical correspondence principle ensures that every classical observable has a corresponding quantum operator that is Hermitian. The corresponding quantum mechanical electric field vector operator looks like

$$\hat{E}_q(t) = i \sum_k \left(\frac{\hbar \omega_k}{2\epsilon_0} \right)^{\frac{1}{2}} [\hat{X}_k^+(t) \sin(\omega_k t) - \hat{X}_k^-(t) \cos(\omega_k t)] \tag{2.36}$$

The summation is over k continuum of frequency and polarization modes, and ϵ_0 is the permittivity of free space. So far our linearized operator treatment has been in the time domain. A fundamental mathematical result is that any continuous function $f(t)$ may

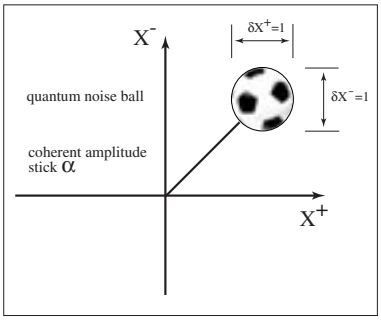

Figure 2.4: Ball on stick picture of coherent state.

be decomposed into a continuum of harmonic functions $\tilde{f}(\omega)$ by performing a Fourier transform

$$\tilde{f}(\omega) = \int_{-\infty}^{\infty} f(t) e^{-i\omega t} dt \tag{2.37}$$

In the frequency domain, our linearized operators become

$$\delta\hat{a}(t) \longrightarrow \delta\hat{a}(\omega) \tag{2.38}$$

$$\delta\hat{a}^t(\omega) \longrightarrow \delta\hat{a}^\dagger(\omega) \tag{2.39}$$

It may now be seen that we have sidebands $\delta\hat{a}(\omega)$ and $\delta\hat{a}^\dagger(\omega)$ either side of the carrier, ie. the field with amplitude α at frequency Ω. This can give us an intuitive idea of the origin of quantum noise and also the mechanism behind squeezing. The sidebands beat with the carrier to give phase and amplitude modulation. In a coherent state, the phases of all the sideband pairs are completely uncorrelated, and the result is an intensity noise spectrum that is flat. Squeezed light may then be explained as correlations between each sideband pair. For example, amplitude squeezing would result from the pairs of sidebands tending to align in the phase quadrature. Thereby lowering the AM fluctuations, and consequently increasing PM fluctuations.

2.1.8 Ball on stick picture

The ball on stick picture is a useful mental picture of the quantum state of light and is shown in Figure 2.4. It is a mixture of classical and quantum ideas. A slice is taken of the noise spectrum at every frequency (ω) where the horizontal and vertical axes correspond to the amplitude (X^+) and phase (X^-) quadratures respectively. The *stick* is the length of the classical amplitude α and the fuzzy *ball* represents the quadrature fluctuations, which cause the field amplitude to walk in length and phase angle with a Gaussain probability distribution (the Q-function). The fluctuation standard deviations are chosen as the boundaries of the ball, ie. (σ_{X^+} and σ_{X^-}). Ball on stick pictures is shown in Figure 2.5 where the QNL boundary is shown in dashed lines. The first diagram show a vacuum state that is of course QNL equal in width in both quadratures. In the second diagram the light is squeezed in the phase quadrature and therefore anti-squeezed in the amplitude quadrature. One can imagine that it is from this kind of diagram that the term *squeezing* originated.

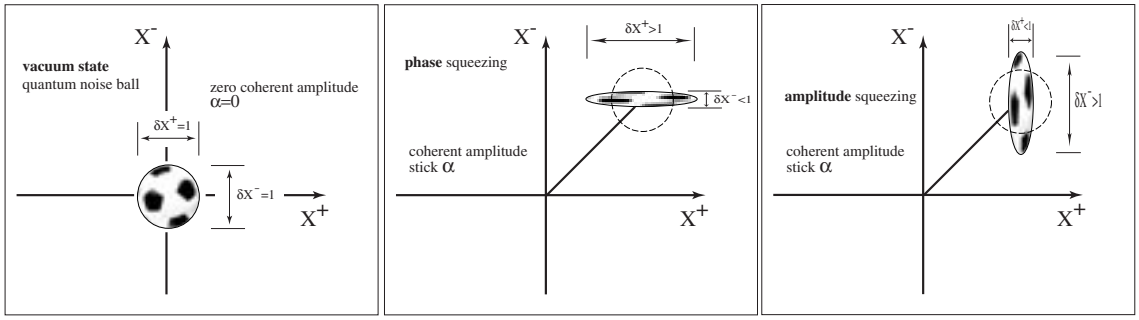

Figure 2.5: Ball on stick picture. LEFT: Vacuum state. MID: Phase squeezed state. RIGHT: Amplitude squeezed state.

2.2 Measurement

In this section we will develop the tools necessary for measuring the state of a light beam. And also model the effect of loss on our measurement. Note that from now on the hats will be dropped from the operators, and we will be working in the frequency domain, and the tilde denoting a fourier transformed operator will be dropped.

2.2.1 Direct detection with a photodiode

A photodiode gives an electric current proportional to the intensity of light that is incident on it. Intensity proportional to the number of photons detected per unit time. What we are interested in measuring are the fluctuations of the intensity at chosen frequencies, ie. we want to measure the intensity noise spectrum. In the previous section we already derived the variances of the photon number fluctuations, both for squeezed and coherent states. The measured photocurrent I would then be proportional to the photon number

$$I \quad \propto \quad |\alpha|^2 + \alpha\delta\hat{X}_a^+ \tag{2.40}$$

The important thing to see here, is that using a photodiode alone, we can only ever measure the steady intensity of the beam ($|\alpha|^2$) plus the amplitude quadrature fluctuations ($\alpha\delta\hat{X}_a^+$). This is because all phase information is destroyed in the conversion of light into electrical current in the photodiode. The field itself oscillates too quickly for any electronic circuit to be able keep up. And so if we want to measure the phase quadrature we must find another way.

2.2.2 Standard homodyning

A beamsplitter of intensity reflectivity η is shown in Figure 2.6. We have two beams described by the linearized operators

$$a \quad = \quad \alpha + \delta a \tag{2.41}$$

$$b \quad = \quad \beta + \delta b \tag{2.42}$$

each entering one port of a beamsplitter. Beam a is called the signal beam, and beam b is the local oscillator (LO). Due to energy conservation, one beam path in the beamsplitter will undergo a π change in phase shift (exactly which path it is be depends on the type of

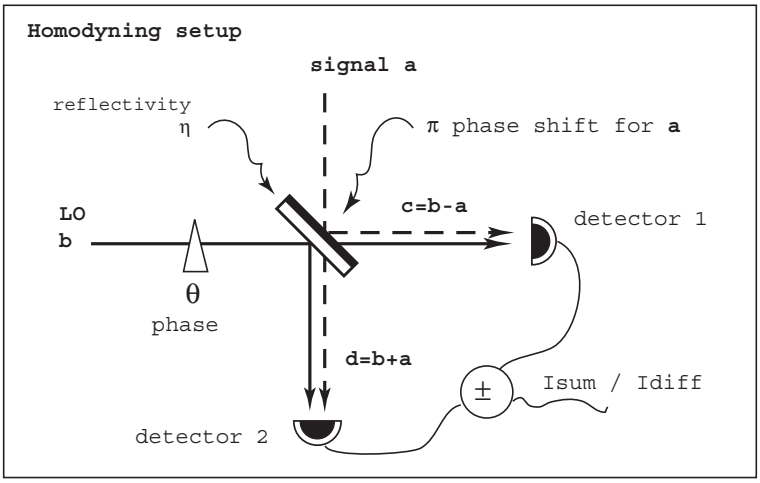

Figure 2.6: Standard homodyning setup.

beamsplitter and its relative orientation). The output fields are given by

$$c = b\sqrt{1-\eta} - a\sqrt{\eta} \tag{2.43}$$
$$d = b\sqrt{\eta} + a\sqrt{1-\eta} \tag{2.44}$$

The beamsplitter ratio is chosen to be balanced ($\eta = \frac{1}{2}$). Before passing through the beamsplitter, the LO is given an arbitrary phase shift θ. We will assume that the magnitudes of the coherent amplitude of the input field b is much greater than the magnitude of the input field a, that is ($|\beta| \gg |\alpha|$). With this assumption in mind and neglecting all quadratic terms, the photocurrents as measured by photodetectors placed at the output ports become

$$c^\dagger c \approx \frac{1}{2}\left\{|\beta|^2 + 2\alpha\beta\cos\theta + \beta\left[\delta X_a^{\theta+\frac{\pi}{2}} + \delta X_b^+\right]\right\} \tag{2.45}$$
$$d^\dagger c \approx \frac{1}{2}\left\{|\beta|^2 - 2\alpha\beta\cos\theta + \beta\left[-\delta X_a^{\theta+\frac{\pi}{2}} + \delta X_b^+\right]\right\} \tag{2.46}$$
$$\tag{2.47}$$

The two photocurrents are either added or subtracted and may be shown to be proportional to

$$I_{sum} \propto |\beta|^2 + \beta\delta X_b^+ \tag{2.48}$$
$$I_{diff} \propto 2\alpha\beta\cos\theta + \beta\delta X_a^{\theta+\frac{\pi}{2}} \tag{2.49}$$

Ignoring the steady terms and looking only at the fluctuations we get

$$\delta I_{sum} \propto \beta\delta X_b^+ \tag{2.50}$$
$$\delta I_{diff} \propto \beta\delta X_a^{\theta+\frac{\pi}{2}} \tag{2.51}$$

We can see that for I_{sum} we just get back the amplitude quadrature noise of the local oscillator. The reason for this is that we assumed $|\beta| \gg |\alpha|$ and a sum of photocurrents is effecitvely the same as one big detector. For a differential measurement I_{diff} we measure the noise on the signal beam scaled by the amplitude of the LO. The really neat thing

is that we can choose which angle of quadrature of the signal beam to be measured, simply by adjusting the relative phase shift θ. So for $\theta = \frac{\pi}{2}$ the amplitude quadrature is measured. And for $\theta = 0$ we measure the phase quadrature. This method is called *standard* homodyning. A variation on this is *self* homodyning when the input beam has zero coherent amplitude, ie. a vacuum state. The differential measurement I_{diff} will give us the exactly the shot noise limit (SNL) at the LO mean power level. This may then be used to calibrate the I_{sum} measurement to find the LO noise relative to the SNL.

2.2.3 Loss

The effect of loss in intensity η due to an inefficient detector may be modelled with a beamsplitter of intensity reflectivity η. Using the same setup as for the homodyning problem, our incident beam is $b = \beta + \delta b$ and we detect the transmitted field d of only one detector. Note that we must include the vauum state $a = \delta a$ entering in the unused port of the beamsplitter. The field d at the detector is then

$$\begin{aligned} d &= \sqrt{\eta}b - sqrt1 - \eta a & (2.52)\\ &= \sqrt{\eta}(\beta + \delta b) - sqrt1 - \eta\delta a & (2.53)\end{aligned}$$

The photocurrent will then be

$$d^\dagger d = \eta(|\beta|^2 + \beta\delta X_b^+) + \sqrt{\eta(1-\eta)}\beta\delta X_a^+ \quad (2.54)$$

Ignoring the constant term we have find

$$d^\dagger d = \beta\left[\eta\delta X_b^+ + \sqrt{\eta(1-\eta)}\delta X_a^+\right] \quad (2.55)$$

What this result is telling us is that effect of loss is the same as throwing away some of the input field, and also coupling in some vacuum fluctuations. For a squeezed state this means a loss in the level of squeezing, ie. loss brings any state closer to the quantum noise limit (QNL). It is for this reason that squeezed beams are often described as being *fragile*.

2.2.4 Mode mismatch

Classically, a mode mismatch occurs if we would like to interfere two light beams (like in a homodyning stage) but they do not overlap perfectly. The reason may be spatial, ie. the two beams have different mode shapes, or it could be polarization, ie. orthogonal polarizations do not interfere (by definition!). This is measured by what is called the visibility $\mathcal{V}$ of the interference, given by scanning the relative phase of the two beams and measuring the fringe maximum and minimum intensities, and plugging them into the relation

$$\mathcal{V} = \frac{I_{max} - I_{min}}{I_{max} + I_{min}} \quad (2.56)$$

The effect of a mode mismatch with visibility $\mathcal{V}$ on a homodyning measurement may be modelled using the linearized operators. The result which will only be quoted here, is that it effectively looks exactly like the beamsplitter loss calculation performed above. With an equivalent intensity loss proportional to the square of the visibility.

$$\eta = \mathcal{V}^2 \quad (2.57)$$

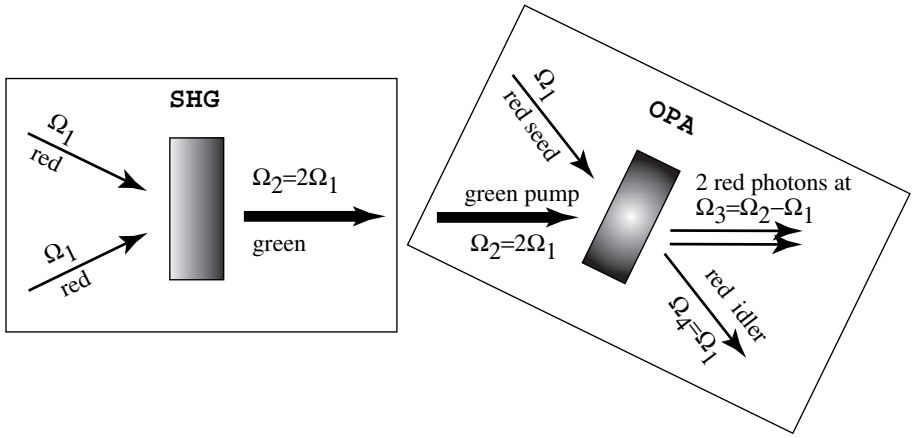

Figure 2.7: Three/Four-wave mixing. LEFT: second harmonic genration. RIGHT: Optical parametric amplification.

This highlights the importance of good mode matching in a squeezing experiment. If the detection system is standard homodyning, then every effort must be made to optimize the visibility between the LO and signal beams, otherwise the equivelent effective loss will throw away the hard earned squeezing and return the squeezed state back to the quantum noise limit.

2.3 Production of squeezed light

Fortunately, the two squeezers we used for our experiment were already built by Warwick Bowen and Dr. R Schnabel for their recent teleportation experiment [8]. The question is; how does on actually build a squeezer? It turns out that linear processes alone cannot produce squeezed light, what is required is the effect of a *non-linear* material. Our method of producing squeezed light used the second-order non-linear property of a crystal to be able to perform a four-wave mixing down conversion process known as optical parametric amplification (OPA). To squeeze a seed beam, the four-wave mixing process required an input pump light field at twice the seed frequency, ie frequency doubled, a process known as second harmonic generation (SHG). Note, that, only a brief coverage will be given here. For a detailed account of the theoretical predictions, and experimental results of OPA squeezing see [2].

2.3.1 Second Harmonic Generation (SHG)

The pump light of twice the seed beam frequency was produced in a three-wave mixing process in a second-order non-linear crystal. A second-order non-linear medium has a strong quadratic electrical susceptability response to an applied electric field. The medium would convert a component the oscillating field $E = \cos\Omega t$ into $E' = \cos^2\Omega t$, which oscillates at 2Ω. Our crystal was made from Mg:$LiNbO_3$ pronounced *magnesium oxide doped lithium oxide*. As can be seen in Figure 2.7 in the SHG process two photons at the same frequency Ω_1 are combined into a single photon of twice the frequency Ω_2, thereby conserving energy ($\hbar\Omega_2 = 2\hbar\Omega_1$). However, momentum must also be conserved, ie. the corresponding wave vectors must also satisfy ($k_2 = 2k_1$) which implies that the refractive

index of the material must be the same for both frequencies

$$\frac{n_2\Omega_2}{c} = 2\frac{n_1\Omega_1}{c} \tag{2.58}$$

This is often referred to as the phase matching condition, and must be satisfied along with the second-order nonlinearity for a medium to become a SHG. In our crystal this was achieved by using the birefringence property of the crystal to find a close match in refractive indices, this was then optimized and held by temperature control.

2.3.2 Optical Parametric Amplification (OPA)

The OPA process works basically like this: A low frequency photon (the seed) Ω_1 is mixed with a high frequency photon (the pump) Ω_2 to produce the new difference frequency photon ($\Omega_3 = \Omega 2 - \Omega 1$) and also an idler frequency photon Ω_4 at the same frequency as the seed photon ($\Omega_4 = \Omega_1$). For the degenerate case (DOPA) we have the pump frequency equal to twice the seed frequency, ie. ($\Omega_2 = 2\Omega 1$), both the idler and intermediate photons then have frequencies equal to the seed frequency ($\Omega_3 = \Omega 4 = \Omega 1$). This is shown in the diagram in Figure 2.5. In the degenerate optical parametric amplification (DOPA) process, ie. each pump photon is converted into two seed frequency photons. Although not possible to show with a quick derivation, the level of amplification depends on the phase of the pump relative to the seed beam. When π out of phase, the DOPA actually de-amplifies the seed. The effect of both modes of operation on the quadrature amplitude variances is shown in the ball on stick diagram in Figure 2.7. Remembering the sideband picture. The effect of phase dependent amplification is to correlate the sidebands either side of the carrier, to either align to PM to give amplitude quadrature squeezing, or to preferentially align in the AM direction to give phase quadrature squeezed light.

2.4 Spatial Squeezing

So far there has been no mention of spatial squeezing, this is because we have needed some time to develop the necessary tools and understanding of quantum light. From this point on, ordinary squeezing will be referred to as *temporal* squeezing, in an effort to distinguish it from *spatial* squeezing. The author realises that this may not be the best use of terminology since spatial squeezing measurements are actually still done in time, but nonetheless, it is hoped that the distinction will prove to be sufficiently clear.

2.4.1 Spatial differential measurements

As mentioned in Chapter 1, spatial differential measurements can be used to give information about light beam displacement. We also learned that there is a limit to the sensitivity of such a measurement set by the shot noise limit (SNL). Since we are now dealing with the spatial distribution and detection of light, it is not unreasonable to suggest that we must perform *multi*-spatial mode analyses in order to arrive at the correct results. A general treatment of multi-mode light in this context is given in [3].

Consider first a one-dimensional spatial differential measurement. The first question that comes to mind about a spatial differential measurements is; where does the noise come from? In the photon picture this is easy to answer because, like in a beamsplitter, each photon must choose to go either one way or the other, and it's the same with a

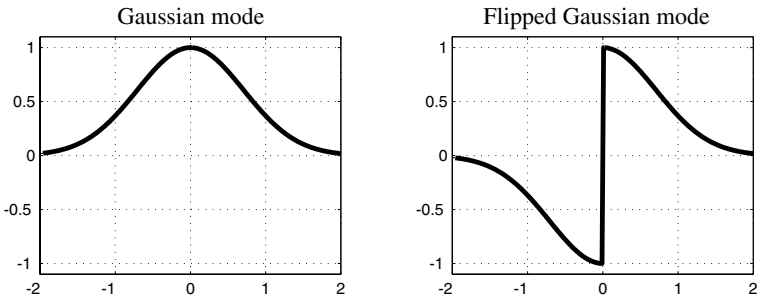

Figure 2.8: Field envelopes. LEFT: Gaussian mode. RIGHT: Flipped Gaussian mode.

split detector, because the photon may be anywhere in the wavefront plane, the photon must choose to hit either one of the detectors. One can imagine that since the decision is random, there will be moments when the balance of photons on each detector will be anti-correlated and other occasions when they will be correletated correlated. On differential measurement the correlations cancel out leaving only the anti-correlations that set up the shot noise limit. One may then reason that spatial squeezing is the reduction of these anti-correlations along the direction of the split detector elements. This is indeed the case, but how can we reconcile this picture with the operators that we have developed in this chapter? Drawing on the following analogy, a spatial differential measurement is identical to a self homodyning differential measurement. There is a light beam whose power is split into two and each half is separately detected. The separate photocurrents are then subtracted from each other to give the differential measurement. Now in the case of self-homodyning, the signal actually comes from the vacuum state entering the unused port of the beamsplitter. But where could a vacuum state enter on a spatial split detector? The answer is in the detail that a beamsplitter necessarily imparts a π phase shift to one of the input paths (to abide by the law of conservation of energy). If we extend the analogy, then we see that for a Gaussian beam incident on a two element spit detector, the vacuum state will enter the calculation disguised as a *flip-mode*. See Figure2.8. By flip-mode we mean the one half of the Gaussian beam is given a π phase flip relative to the other half. Can we, however, convince ourselves of this prediction? Perhaps counter intuitively, it is possible to perform a classical analysis that was given in the paper [11] to show that the vacuum state does indeed enter disguised as flip-mode.

We can define an orthonormal basis $\{u_i(x)\}$ for the spatial distribution of the electric field envelope of a light beam. We are free to choose any normalized function for the first mode $u_0(x)$ in the basis. We can define the second mode to be the flip of the first mode, by this we mean

$$u_1(x) = \begin{cases} -u_0(x) & , \quad x < 0 \\ +u_0(x) & , \quad x \geq 0 \end{cases} \tag{2.59}$$

This fulfills the condition of a basis because u_0 and u_1 are orthogonal. This is guaranteed only if their integrals on each half of the domain are equal in magnitude and also opposite in sign. We may then choose the rest of the basis modes $\{u_{i>1}\}$ to satisfy the basis requirement that the members are mutually orthonormal and also complete the space. To begin, we give only u_0 a mean field, but all the other modes are given the opportunity to contribute to the quantum noise as vacuum states. Each element of a split detector will receive the sum of all the modes. As we are interested in the intensity fluctuations we

consider only the interference cross terms incident on each half of the split detector.

$$I_{x<0}(u_i, u_j) = \int_{-\infty}^{0} u_i^*(x)u_j(x)dx \tag{2.60}$$

$$I_{x>0}(u_i, u_j) = \int_{0}^{+\infty} u_i^*(x)u_j(x)dx \tag{2.61}$$

The sum and difference photocurrents of the two detector elements then become

$$I_{sum}(u_i u_j) = I_{x<0}(u_i, u_j) + I_{x>0}(u_i, u_j) \tag{2.62}$$

$$I_{diff}(u_i u_j) = I_{x<0}(u_i, u_j) - I_{x>0}(u_i, u_j) \tag{2.63}$$

By explicit substitution of u_0 into u_1 it is quite easy to show that for any mode u_i the following relation holds true

$$I_{sum}(u_i u_1) = I_{diff}(u_i u_0) \tag{2.64}$$

By definition all $u_{i>1}$ are orthogonal to u_1 which implies that

$$I_{sum}(u_{i>1} u_1) = 0 \tag{2.65}$$

From equation 2.64 we get

$$I_{diff}(u_{i>1} u_0) = 0 \tag{2.66}$$

In words this means that none of the modes beyond $u_{i>1}$ contribute to the differential measurement. The only mode that does contribute is the flip-mode u_1, and it shares with u_0 a perfect differential measurement overlap integral

$$I_{diff}(u_0 u_1) = 1 \tag{2.67}$$

and therefore also a perfect interference visibility *for a differential measurement*. Returning now to the quantum operators and our previous analysis of the homodyning setup. We already knew that for perfect visibility of a differential homodyne measurement, the noise comes from the signal beam that underwent a π phase flip for one path relative to the bright local oscillator. And for spatial squeezing it is the same thing. The noise in a spatial differential measurement comes from the flipped mode (usually occupied by a vacuum state) of the bright beam which is acting like a local oscillator. This may be thought of as *spatial homodyning*, and will be referred to as such throughout this thesis.

2.4.2 The spatial homodyning condition

This was only a one-dimensional treatment, but note how no assumption had to be made as to the shape of the function $u_0(x)$. Keeping this result in mind, I will go through a linearized quantum operator analysis for a quadrant detector and field with a two-dimensional spatial distribution. In a sense, the following derivation has been done in reverse because we have already 'guessed' the correct modes required. Nevertheless it is completely valid for the case of a quadrant detector, whose elements put together detect the entire beam.

Consider an incident light beam with a two-dimensional mean field envelope $u_{00}(x, y)$ and a corresponding quantum operator $\hat{b} = \beta + \delta\hat{b}$ A quadrant detector allows three sets of differential measurements to be taken concurrently; hor-

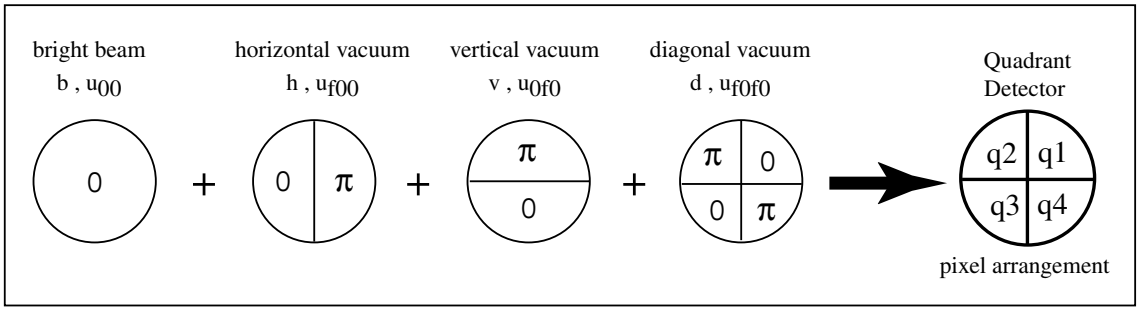

Figure 2.9: Arrangement of flip modes and quadrant detector pixels.

izontal $[H = (q1 + q4) - (q2 + q3)]$, vertical $[V = (q1 + q2) - (q3 + q4)]$ and diagonal $[D = (q1 + q3) - (q2 + q4)]$. See Figure 2.9 for the quadrant positions.

The **conjecture** is that each differential measurement would actually be a spatial homodyning measurement on the corresponding flip mode. For a H_{diff} measurement the corresponding vacuum state would be the horizontal-flip-mode denoted (u_{f00} with corresponding quantum operator $\hat{h} = \delta\hat{h}$). For vertical V_{diff} the state would be the vertical-flip-mode (u_{0f0} with $\hat{v} = \delta\hat{v}$). And for diagonal D_{diff} the state would be the double-flip-mode (u_{f0f0} with $\hat{d} = \delta\hat{d}$). All that remains is to actually *prove* the conjecture!

We shall use the linearized quantum operator formalism. Figure 2.9 shows how the problem is set up. Remembering the π phase flips for respective vacuum states, the field of each quadrant will be

$$\hat{q}_1 = \frac{1}{\sqrt{4}}\left[\hat{b} - \hat{h} - \hat{v} + \hat{d}\right] \tag{2.68}$$

$$\hat{q}_2 = \frac{1}{\sqrt{4}}\left[\hat{b} + \hat{h} - \hat{v} - \hat{d}\right] \tag{2.69}$$

$$\hat{q}_3 = \frac{1}{\sqrt{4}}\left[\hat{b} + \hat{h} + \hat{v} + \hat{d}\right] \tag{2.70}$$

$$\hat{q}_4 = \frac{1}{\sqrt{4}}\left[\hat{b} - \hat{h} + \hat{v} - \hat{d}\right] \tag{2.71}$$

After some algebra, the photon numbers of the quadrants become

$$N_{q_1} = \frac{1}{4}\beta\left[\beta + \delta X_b^+ - \delta X_h^+ - \delta X_v^+ + \delta X_d^+\right] \tag{2.72}$$

$$N_{q_2} = \frac{1}{4}\beta\left[\beta + \delta X_b^+ + \delta X_h^+ - \delta X_v^+ - \delta X_d^+\right] \tag{2.73}$$

$$N_{q_3} = \frac{1}{4}\beta\left[\beta + \delta X_b^+ + \delta X_h^+ + \delta X_v^+ + \delta X_d^+\right] \tag{2.74}$$

$$N_{q_4} = \frac{1}{4}\beta\left[\beta + \delta X_b^+ - \delta X_h^+ + \delta X_v^+ - \delta X_d^+\right] \tag{2.75}$$

The three differential measurements become

$$H_{diff} = \beta\delta X_h^+ \tag{2.76}$$

$$V_{diff} = \beta\delta X_v^+ \tag{2.77}$$

$$D_{diff} = \beta\delta X_d^+ \tag{2.78}$$

This proves the conjecture! The spatial differential measurements have returned the vacuum noise on their respective flipped modes of the bright beam. In other words this is spatial homodyning. This result will be used to advance the following defintion:

The *spatial homodyning condition* says that the quantum noise from a spatial differential measurement made on a bright coherent mode of light with envelope u will originate entirely from the mode of light denoted u_f whose envelope is flipped along the detector subtraction boundary.

2.4.3 Squeezed flip-modes

We can of course occupy the flipped vacuum states by replacing them with any desired signal beam. These could be beams with classical modulations carrying information. And we could put a *squeezed* flip mode to replace the vacuum. Thereby allowing beam displacement measurements below the shot noise limit (SNL). This is our experimental goal: To demonstrate that *two* dimensions of a displacement measurement can be squeezed below the shot noise limit. This will require the mixing of three beams. A bright local oscillator with a horizontally flipped squeezed mode, and also a vertically flipped squeezed mode.

2.5 Summary

In this chapter the quantum state of light was developed and it's operators linearized. The sideband model along with the ball on stick picture were introduced. The linearized operators were used to calculate the results for the beamsplitter that lead to useful tools and concepts applicable to an experiment. Particularly the technique of homodyning and the effect of loss on a squeezed beam. A treatise of one-dimensional spatial differential measurements was given that encouraged us to formulate a conjecture about an extension to two dimensions. The conjecture was proven to be true using the linearized quantum operators and its direct analogy to standard homodyning supported. The spatial homodyning condition was formulated and used to predict the required flip modes required for two-dimensional spatial squeezing.

Chapter 3

Special Optics

'If the physical laws of this world are autonomous, we are not free; if we are not free, then the physical laws are not autonomous.' Karl Popper

3.1 Overview

This chapter introduces the special optical components that were required for the experiment. The first of which being the waveplates that generated the flipped modes, the second being the mode-mixing cavity. Both the theory, and experimental characterization of these components will be discussed.

3.2 Why the need for special optics?

The fundamental idea behind spatial squeezing is that of mixing flipped-mode beams together with a local oscillator. Considering now the 1D spatial squeezing case, the flip-mode and local oscillator were mixed on an asymmetric beamsplitter. Due to the fragile nature of squeezed light, the balance was chosen in favour of the squeezed beam (92% power reflected), thus keeping losses to an absolute minimum. Of course this meant that most of the local oscillator was dumped, but this was of no major concern as its power level could be made arbitrarily high so as to compensate for this loss. The obvious extension of this method to two-dimensional spatial squeezing is by the addition of a second beamsplitter to mix the second squeezed beam together with the other one. However, it is impossible to make the ratios of the two beamsplitters such that both squeezed beams would encounter acceptable losses in the mixing process. In other words, a new method is required to mix the two squeezed beams. The solution to this problem lies in the very fact that the two beams are orthogonal spatial modes, and that the properties of an optical cavity are mode dependent.

3.3 Classical cavity properties

The most basic optical cavity is shown in Figure 3.1. It consists of two mirrors M1, M2 of amplitude reflectivities r_1, r_2, and transmittances t_1, t_2, spaced a distance L apart. A light field E_{in} is incident on M1. The light which passes through M1 undergoes multiple reflections and a phase shift ϕ as it travels back and forth from M1 and M2. The circulating intra-cavity field E_{circ} arrives at a steady state of equilibrium, where the input power compensates for the leaking field through M1, the output field E_{trans} through M2, and

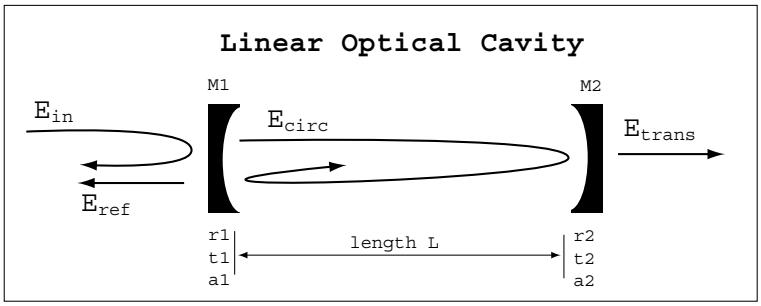

Figure 3.1: Schematic diagram of Fabry-Perot cavity. Relevent light paths and their respective electric field variables are shown.

any absorbtion a_1, a_2. The total field reflected from the cavity E_{ref} is equal to the sum of incident reflected light ($r_1 E_{in}$) and leaking circulating field ($t_1 E_{circ}$). The complex valued cavity equations may be written down as

$$E_{in} = E_0 e^{-i\omega_0 t} \tag{3.1}$$

$$\phi = \frac{\omega_0}{2L} \tag{3.2}$$

$$E_{circ} = t_1 E_{in} + r_1 r_2 e^{i\phi} E_{circ} \tag{3.3}$$

The steady state equation for circulating field Ecirc may be solved to give

$$E_{circ} = \frac{t_1 E_{in}}{1 - r_1 r_2 e^{i\phi}} \tag{3.4}$$

leading to explicit forms for

$$E_{trans} = t_1 e^{\frac{i\phi}{2}} E_{circ} \tag{3.5}$$

$$E_{leak} = t1r2e^{i\phi} E_{circ} \tag{3.6}$$

$$E_{ref} = -r1E_{in} + E_{leak} \tag{3.7}$$

Intuitively one might expect that the cavity would be a tuned system, as the phase shift ϕ encountered on a round-trip length L would differ depending on the wavelength of light. This is indeed the case. Functions for reflected and transmitted power (P_{ref}, P_{trans}) are plotted in Figure 3.2 along with the phase shifts encountered for each, relative to the input beam. The range from each transmission peak to peak is called the free spectral range (FSR) and is equal to $FSR = \frac{c}{2L}$. Peak width is $\delta\nu = \frac{FSR}{F}$ where F is the finesse of the cavity given by

$$F = \frac{\pi\sqrt{r_1 r_2}}{1 - r_1 r_2} \tag{3.8}$$

Therefore, a cavity of higher finesse will have smaller bandwidth. Cavity finesse is determined by the reflectivity of the mirrors. The analysis just performed assumed we were working with the first eigenmode of the cavity, ie. the first Hermite-Gaussian solution TEM_{00} to the paraxial Helmholtz equation for a spherical mirror resonator.

More generally, higher order $\mathrm{TEM}_{\mathrm{pq}}$ modes experience different phase shifts for a round-trip journey, ie. ϕ depends on the mode in question. This is called the Gouy phase

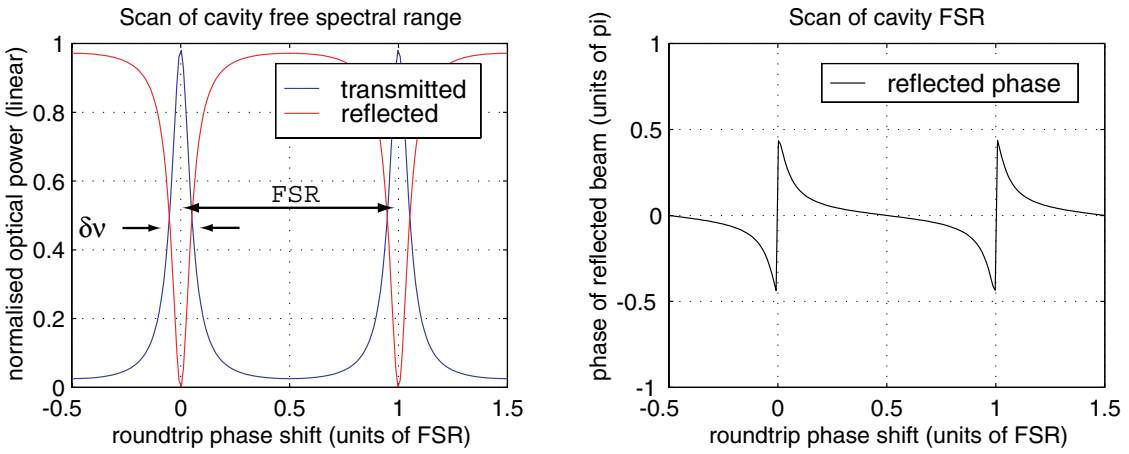

Figure 3.2: Classical cavity. LEFT: Theory plot of reflectedt/ransmitted power, and RIGHT: reflected phase while scanning the length of a linear cavity. Parameters; $r_1 = r_2 = 0.85$, $a_1 = a_2 = 0.05$.

shift and is given for mode indices (p, q) by

$$\Delta\phi_{Gouy} = \pi(p + q + 1)\Delta\zeta \tag{3.9}$$

$$\Delta\zeta = [\arctan\frac{z_1}{z_0}] - [\arctan\frac{z_2}{z_0}] \tag{3.10}$$

Where (z_1, z_2) are the positions of the mirrors relative to the internal cavity waist position, and Rayleigh range $z_0 = \pi\frac{W_0^2}{\lambda}$ set by the waist size W_0. This tells us that $\mathrm{TEM_{pq}}$ resonances will be spaced at $\Delta\phi_{Gouy}$ along the free spectral range. Note that modes for the same index sum $(n = p + q)$ will experience the same shift. A symmetrical confocal cavity is one where $(\Delta\zeta = 1)$ and every mode therefore lies either on resonance or halfway between (depending if n=even or n=odd). However, this is a special case. For the general case, only one mode will be resonant at a time, assuming of course that the cavity bandwidth is smaller than the Gouy phase shift separation, and that $(\Delta\zeta)$ is an irrational number.

It is this property of optical cavities that we have used to our advantage. The spatial homodyning condition allows us to make any choice for local oscillator envelope, because the differential measurement signal will be the flipped mode of the LO in the direction along the two detector pixels. One squeezed beam may then be chosen to be a $\mathrm{TEM_{00}}$ which could be transmitted through a cavity. The LO would then have to be a single-flipped (either vertically or horizontally) mode of $\mathrm{TEM_{00}}$ which we shall from now on denote $\mathrm{TEM_{f00}}$ for horizontal and $\mathrm{TEM_{0f0}}$ for vertical. The choice is arbitrary, but we will from now on use a $\mathrm{TEM_{f00}}$ local oscillator, which implies the squeezed $\mathrm{TEM_{00}}$ beam is the horizontal squeezing beam. Since our LO is $\mathrm{TEM_{f00}}$ then a vertical differential measurement would come from the vertical flipped-mode of $\mathrm{TEM_{f00}}$, denoted $\mathrm{TEM_{f0f0}}$. The second squeezing beam must therefore be a $\mathrm{TEM_{f0f0}}$ which happens to consist of a weighted sum over all odd-odd $\mathrm{TEM_{pq}}$ basis states.

The wonderful key idea is then this; the cavity could be locked to resonate with $\mathrm{TEM_{00}}$, ie. to transmit $\mathrm{TEM_{00}}$, where as the odd-odd $\mathrm{TEM_{pq}}$ would be reflected as they are off-resonance. Thereby combining the two squeezed beams with potentially zero power loss. But would the squeezed property of the two beams emerge from the cavity unscathed?

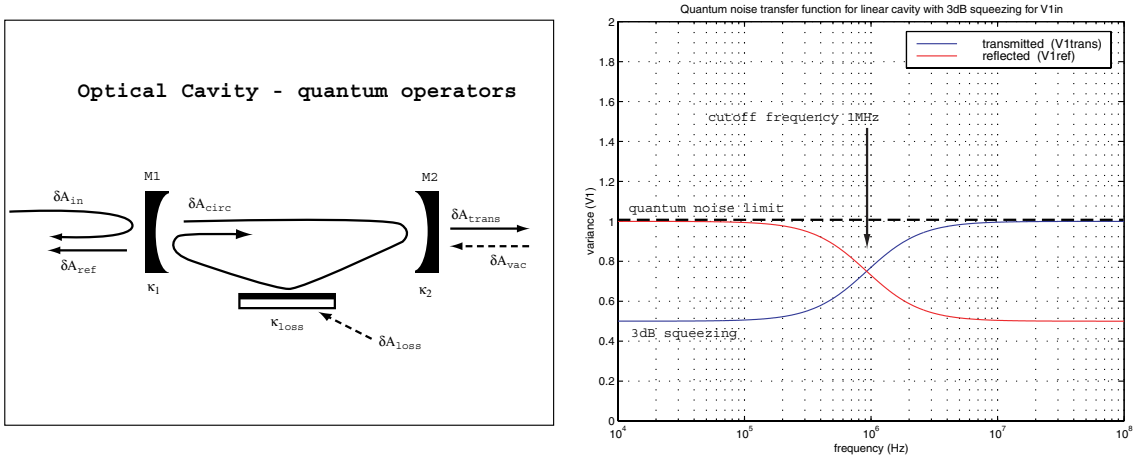

Figure 3.3: LEFT: Quantum operators for linear cavity. Schematic of a linear cavity (actually a third mirror is included to model losses). Relevant light paths and their quantum operators are shown. RIGHT: Quantum noise transfer functions. Scan of detection frequency for 3dB amplitude quadrature squeezing. Quantum noise limit at V1=1. Blue curve is the transmitted field, note that squeezing is transmitted below cutoff frequency at 1MHz, and reflected above cutoff frequency. Parameters; $\kappa 1 = \kappa 2 = 300000$, $\kappa_{loss} = 500$.

An answer to this question requires a quantum noise analysis of the system.

3.4 Quantum noise properties

Classically one can imagine a carrier light field which is being modulated in either phase or amplitude at frequency ω_m and therefore has sidebands at $\pm\omega_0$. Looking now at the transmission of this modulated beam through the cavity on resonance with the carrier, we find that provided the bandwidth $\delta\nu$ of the cavity is greater than the modulation frequency ω_0, then the sidebands will be transmitted along with the carrier. On other hand, if the sidebands lie outside the cavity bandwidth, then they will be so far off resonance as to be reflected, ie. the carrier has been stripped of its sidebands.

Applying this reasoning to squeezed light one may arrive at a similar answer, ie. if $\delta\nu$ is smaller than the frequency range being squeezed, then the carrier will be stripped of these sidebands and replaced by vacuum sidebands. The exact result, ie. the cavity quantum noise transfer functions may be derived using quantum operators. The problem can be set up shown in Figure 3.3.

The mirror loss coupling rates are; first mirror κ_1, second mirror κ_2, and intra-cavity loss represented by a third mirror κ_{loss}. As in chapter 2 for the homodyning calculation, we must include the vacuum state entering through the unused port (into M2) and also the vacuum state mixed in by optical loss. Here the input state is represented by the temporal operators; input state Ain, reflected A_{ref}, transmitted A_{trans}, circulating A_{circ}, vacuum state entering from unused port A_{vac}, and finally intra-cavity loss vacuum state A_{loss}. Linearising the operators and forming the rate of change in time of the circulating amplitude quadrature gives

$$\frac{d\delta\hat{X}1_{circ}}{dt} = -\kappa\delta\hat{x}1_{in} + \sqrt{2\kappa_2}\delta\hat{X}1_v ac + \sqrt{2\kappa_{loss}}\delta\hat{X}1_{loss} \tag{3.11}$$

Using the following boundary conditions at the mirrors

$$\delta\hat{X}1_{trans} = \sqrt{2\kappa_2} - \delta\hat{X}1_{vac}\delta\hat{X}1_{ref} = \sqrt{2\kappa_1} - \delta\hat{X}1_{in} \tag{3.12}$$

and performing a Fourier transform with the identity $\mathcal{F}\{\frac{df(t)}{dt}\} = 2\pi\Omega\mathcal{F}\{f(t)\}$ gives

$$\delta\hat{X}1_{trans} = \frac{\sqrt{4\kappa_1\kappa 2}\delta\hat{X}1_{in} + \sqrt{4kapp_1\kappa_{loss}}\delta\hat{X}_{loss} + (2\kappa_2 - \kappa_{loss} - i2\pi\Omega)\delta\hat{X}1_{vac}}{\kappa_{loss} - i2\pi\Omega} \tag{3.13}$$

Forming the expectation value of this to find the variance, one arrives at

$$V1_{trans} = \frac{4\kappa_1\kappa_2 V1_{in}(\Omega) + ((2\kappa_2 - \kappa_{loss})^2 + (2\pi\Omega)^2)V1_{vac}(\Omega) + 4\kappa_2\kappa_{loss}V1_{loss}(\Omega)}{\kappa_{loss}^2 + (2\pi\Omega)^2} \tag{3.14}$$

For the phase quadrature $V2_{trans}$ the equation is identical to the one above, except that $V1$ etc. are replaced by $V2$ etc. The derivation for reflected light is the same, it is sufficient to quote the results

$$V1_{ref} = \frac{4\kappa_1\kappa_2 V1_{vac}(\Omega) + ((2\kappa_1 - \kappa_{loss})^2 + (2\pi\Omega)^2)V1_{in}(\Omega) + 4\kappa_1\kappa_{loss}V1_{loss}(\Omega)}{\kappa_{loss}^2 + (2\pi\Omega)^2} \tag{3.15}$$

Once again replacing $V1$ etc. for $V2$ to get the phase quadrature $V2_{ref}$. Now what can all these equations tell us? Figure 3.3 is a plot of $V1_{ref}$ and $V1_{trans}$ as a function of frequency Ω for a squeezing value of 3dB in the amplitude quadrature, entering a typical cavity of coupling rates $\kappa_1 = \kappa_2 = 300000$ and $\kappa_{loss} = 500$. Immediately apparent is the cut-off frequency ν_{cut} at about 1MHz. Below this frequency, the squeezing passes through the cavity unaffected. Above ν_{cut} the squeezing is in a sense stripped from the carrier and reflected, the beam that emerges thereafter being shot noise limited (SNL), ie. the squeezed sidebands have been replaced by vacuum sidebands. The lesson to be learned here is that if we are going to use a cavity to combine two squeezed beams, then we must be sure to keep cavity finesse low enough to ensure the survival of a squeezed state upon transmission.

3.5 Ring cavity as mode-mixer (theory)

The attentive reader will have no doubt come to the conclusion that a simple linear cavity would be highly inconvenient for its proposed mode-mixing purpose, since it would require Faraday isolators to separate incoming and outgoing light. Another way of keeping incoming and outgoing beams spatially separate is by the choice of a ring cavity. Figure 3.4 is a schematic showing how such a ring cavity could be used to combine a $\mathrm{TEM_{f0f0}}$ with a $\mathrm{TEM_{00}}$. New classical and quantum noise analyses for the ring cavity are not required as in practice the internal mirror M3 is near 100% reflectivity, and this would not change our calculation results significantly. Before we can move on to modelling the properties of this mode-mixing cavity, it is necessary to find an expression for the double-flipped mode $\mathrm{TEM_{f0f0}}$ expansion coefficients in the $\mathrm{TEM_{pq}}$ basis. Due to the limited size of this margin, it is not possible for me to include the derivation in the main body of the text, the mathematically inclined reader is thus directed toward Appendix A.1 where a full

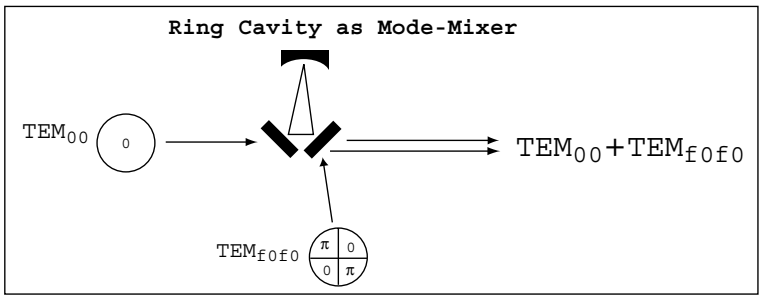

Figure 3.4: Ring cavity as mode-mixer. Schematic showing how a ring cavity could be used to combine the light paths of TEM_{00} with a $\mathrm{TEM}_{\mathrm{f0f0}}$.

derivation is to be found. The result of the expansion is

$$\mathrm{TEM}_{\mathrm{f0f0}} = \sum_{p=odd}^{\infty}\sum_{q=odd}^{\infty} c_{pq}\mathrm{TEM}_{\mathrm{pq}} \tag{3.16}$$

$$c_{p=2n+1,q=2m+1} = \frac{(-1)^{n+m}(2n)!(2m)!}{\pi n!m!2^{n+m-1}\sqrt{(2n+1)!(2m+1)!}} \tag{3.17}$$

Where $n = 0, 1, 2, 3, \ldots$ and $m = 0, 1, 2, 3, \ldots$ generate the odd-odd states. The first few non-zero coefficients are; $c_{11} = 0.6366$, $c_{13} = c_{31} = -0.2599$, $c_{33} = 0.1061$. The absolute values of the coefficients is monotonicaly decreasing, but at a rather slow rate. For the accuracy of numerical modelling purposes, we must then be sure to truncate our calculation at the highest mode number possible. Using these coefficients to form $E_{in} = c_{pq}e^{-i\omega_0 t}$ and substituting this equation as the initial field into the cavity equations 3.7 with the appropriate Gouy phase shifts, a scan of the cavity free spectral range for a reflected $\mathrm{TEM}_{\mathrm{f0f0}}$ could be modelled numerically. Cavity paramaters chosen are the actual values used in the real experiment and are as follows: coupling mirror reflectivities $R_p = 95\natural$, cavity round-trip length 200mm, centre mirror radius of curvature 250mm. These intial parameters set the following cavity properties: FSR=760MHz, finesse $F_p = 61$, bandwidth $\delta\nu_p$=12MHz. A plot of cavity reflected $\mathrm{TEM}_{\mathrm{pq}}$ power is shown in Figure 3.5. The contributions of each individual $\mathrm{TEM}_{\mathrm{pq}}$ basis component are shown in different colours. The total of all contributions, ie. the double-flipped mode $\mathrm{TEM}_{\mathrm{f0f0}}$ itself, is visible as the bold black line above all the others. The x-axis of the plot is centred at the resonance of TEM_{00}, ie. at FSR=0. Note how the deepest resonance for $\mathrm{TEM}_{\mathrm{fofo}}$, ie. the TEM_{11} component, occurs very close to the TEM_{00} resonance, and that each successive dip lies further away. This is no accident. It was designed to be this close so that the very first component, which contains the most power, would be sure to be reflected, and so then all modes up to $p + q = 10$ (before the pattern repeats) would be guaranteed to lie clear of TEM_{00} resonance. Also of concern were the phase shifts encountered by each component upon reflection. Initially the vast plethora of minute phase shifts (on the order of milli-radians) caused some concern. As a re-assurance I embarked on the quest to reconstruct the field of the mode itself. Analytic expressions for the $\mathrm{TEM}_{\mathrm{pq}}$ were obtained up to the 29th mode. The complex valued coefficients were used to reconstruct the double-flipped mode both before ($\mathrm{TEM}^{\mathrm{in}}_{\mathrm{f0f0}}$) and after reflection ($\mathrm{TEM}^{\mathrm{ref}}_{\mathrm{f0f0}}$), as plotted in Figure 3.6 respectively. A difference between the two was not discernable. As a check the overlap integral of before and after wavefunctions was taken. This consisted of the sum of products of the complex

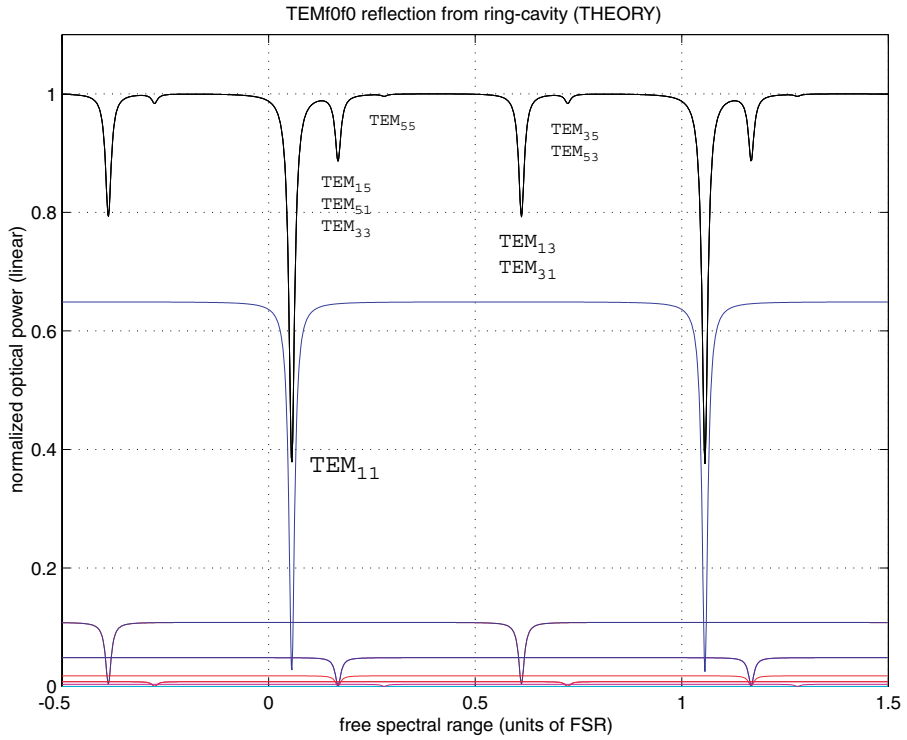

Figure 3.5: Mode structure of $\mathrm{TEM}_{\mathrm{f0f0}}$ in ring cavity. Numerical model up to the fifth mode. Individual contributions shown in colours. Total reflected power in black, peaks labelled for the modes they contain. TEM00 resonance coincides with (fsr=0)

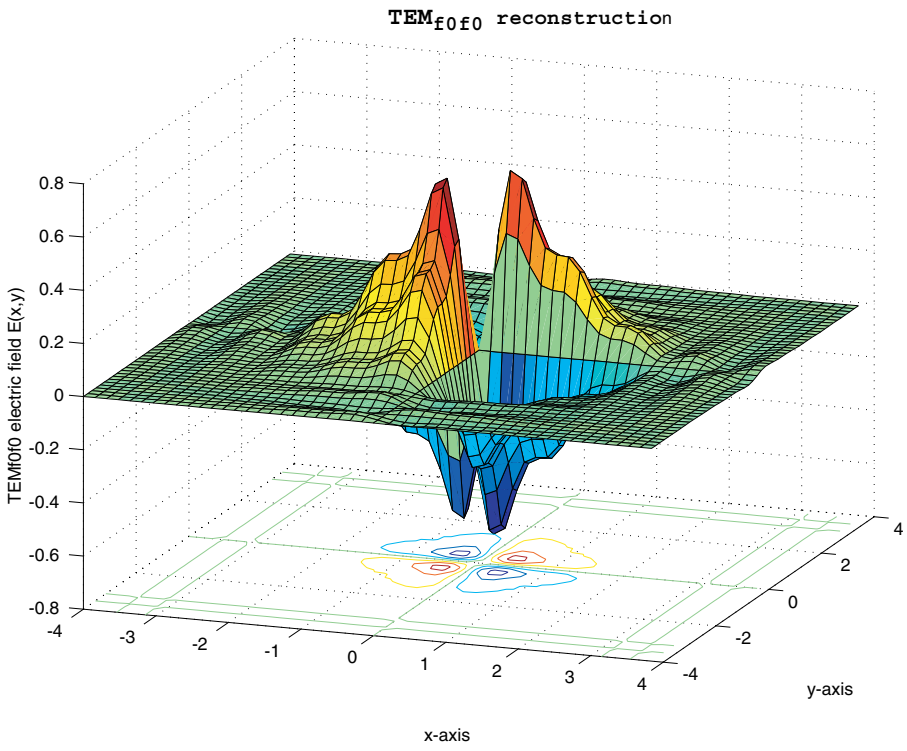

Figure 3.6: Double-flip-mode reconstruction at TEM_{00} resonance BEFORE reflection. Numerical model used up to and including $p = q = 29$ $\mathrm{TEM}_{\mathrm{pq}}$ basis wavefronts.

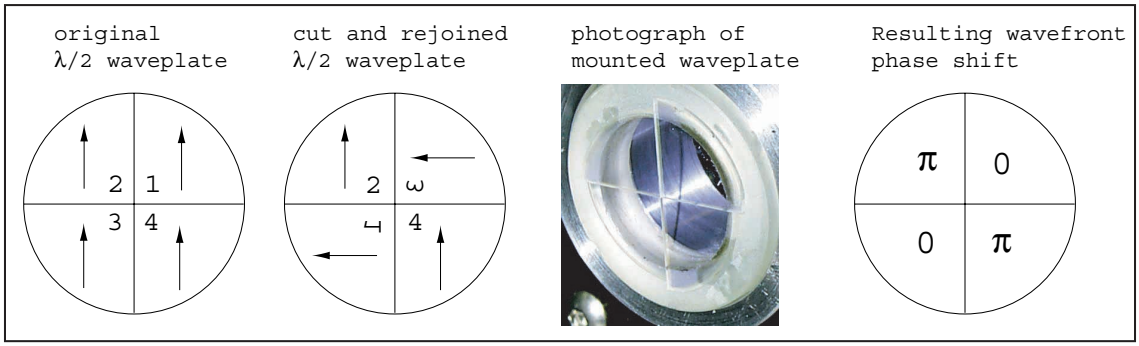

Figure 3.7: Special waveplate construction and function. FROM LEFT: Original plate aligned along optical axis and cut into quadrants. The pieces are re-arragned. Photograph of actual waveplate in the experiment. The resulting phase shift of the wavefront.

coefficients of each mode

$$I_{overlap} = \sum_{p=odd}^{29} \sum_{q=odd}^{29} c_{pq}^{in} c_{pq}^{ref} \tag{3.18}$$

The overlap integral value obtained was $I_{overlap} = 0.986 + 0.054i$. An overlap integral equal to exactly 1 would imply perfect reflection. Ignoring the harmless global phase shift of 55mrad, the absolute value becomes $|I_{overlap}| = 0.987$ which provides further evidence that the envelope of the $\mathrm{TEM_{f0f0}}$ mode should be preserved upon reflection. For the keen reader, Appendix B.1 contains a complete listing of the MatLab code written for the numerical analysis and figure generation of the FSR plots and mode reconstruction plots presented in this chapter. As a final point, it is interesting to guess what effect a spatial Fourier transform on the double-flipped mode might have had on the previous calculations. It is also useful because in the lab a spatial Fourier transform of a light beam is readily produced at the focal point of a lens. A property of the basis set $\mathrm{TEM_{pq}}$ is that they are invariant under a Fourier transform. The power in each mode remains constant, it is only the relative phases between the modes that is different. An optical cavity is however completely insensitive to these inter-modal phase differences. From the cavity's point of view, we are still only seeing the same old $\mathrm{TEM_{pq}}$ with the same old Gouy phase shifts. The conclusion we may draw from this is that none of the results from our previous calculations dealing with $\mathrm{TEM_{f0f0}}$ reflectivity would be any different.

3.6 Wave-plate characterization (experimental)

The rest of this chapter is devoted to experimental characterisation of the two special optical components. We begin by asking the question; how would one actually create a flipped-mode? There are two ways, waveplate or knife-edge, and both were explored in the paper ***ref***. The latter setup consisted of a Sagnac interferometer with a knife-edge cutting across half of the beam path. When the beams recombined, they did so with a π phase shift in one half, ie. a SFM. Due to the complexity of this technique, it was not used in our experiment. By far the most applicable method for our purposes was the former option. The waveplate begins its life as an ordinary half-waveplate, most often used in the lab for rotating the angle of linear polarised light. A half-waveplate is made from a flat piece of birefringent material such as calcite crystal, which is cut to a thickness such that there is a relative phase of π between the ordinary (o-ray) and extraordinary (e-ray) light

paths. The o-ray has its linear polarisation is aligned to the optical axis of the crystal, and the e-ray perpendicular to it. A double-flip-plate which would transform a TEM_{00} into $\mathrm{TEM}_{\mathrm{f0f0}}$ is made by cutting the half-waveplate into 4 quadrants aligned to the optical axis and rearranging the pieces, and therefore the optical axes themselves as shown in Fig3.***. This means that a beam centred on the plate and passing through the diagonal quadrants will undergo a π phase shift relative to the other diagonal quadrants, thereby creating the desired double-flipped-mode (DFM). A single-flip mode is likewise produced by sending the beam through only two of the quadrants.

Two questions worth asking are: 1) Will the joins between quadrants cause optical power loss? 2) What is the quality of the flip-mode produced? The answer to the first question is of course yes. We had two types of waveplate manufactured for us by ***Ref***, the four quadrant plate (4QP) mentioned earlier, and also a two quadrant plate (2QP). The reason for this stemmed from the topological conjecture that it's much more difficult to keep gaps small when joining four pieces together, than when joining only two. This allowed us the flexibility to choose which plates we could use in our experiment, but in practice the difference between them was in fact negligible, and this is most entirely due to the outstanding skills of the manufacturer. A direct power loss measurement was made on the 4QP by sending a 2mm beam through the waveplate centre, yielding a 5 percent drop in power. Loss was reduced to 3 percent when the beam was placed on only 2 quadrants of the 4QP. The only way we could minimize these power losses were to keep the beams as large as possible, ie. to distribute the energy of a wider area in comparison with the fixed area of the gap in the wave plate. The second aspect we had to test was the quality of the flip-mode generated by the waveplate. We did this by interfering the flipped-modes with other beams (both flipped and unflipped) of equal power, and scanning the relative phase between the two beams to see the fringes on each quadrant detector. The results can be seen in Figure 3.8 The first plot (TOP LEFT) of Figure 3.8 is the interference between TEM_{00} and $\mathrm{TEM}_{\mathrm{f00}}$ (produced by 2QP). What we can see is that each horizontal half of the detector (left = quadrants 2 and 3 , right = quadrants 1 and 4) interfere π out of phase, which is exactly what is to be expected, and proves that we indeed have produced a $\mathrm{TEM}_{\mathrm{f00}}$ mode. Note that the vertical dashed lines mark the positions in phase where constructive and destructive interference occur. They do not line up exactly, and are out by about 7°. This is what we call a phase mismatch, and is most likely due to the error in the original half-waveplate, ie. it did not give exactly the required $\frac{\lambda}{2}$ phase shift difference between the e-ray and o-ray (which can be tuned to some extent by tilting the plate off-axis). This means our flip is not exactly 180° but rather something more realistic like $(180 \pm 7)^\circ$ which is not the end of the world but does mean that our mode-matching in the experiment will suffer slightly as a result. A good measure of mode-matching is the *visibility* given by

$$V = \frac{I_{max} - I_{min}}{I_{max} + I_{min}} \tag{3.19}$$

Where $V = 1$ implies perfect mode-matching, and $V = 0$ implies the worst mode-matching possible. For this intereference run we obtained individual quadrant visibilities of around $V = 0.90$ which is a good indication the waveplate created a $\mathrm{TEM}_{\mathrm{f00}}$.

The second plot (TOP RIGHT) of Figure 3.8 shows the interference of two horizontal flip-modes, one produced by a 4QP the other from a 2QP. As one would have expected, all the quadrants of the detector interfered in phase. This means that the wavefront effect of one 2QP was cancelled out by the single-flip waveplate in the second beam. The measured individual quadrant visibilities are around $V = 0.91$. Which is further reassurance that

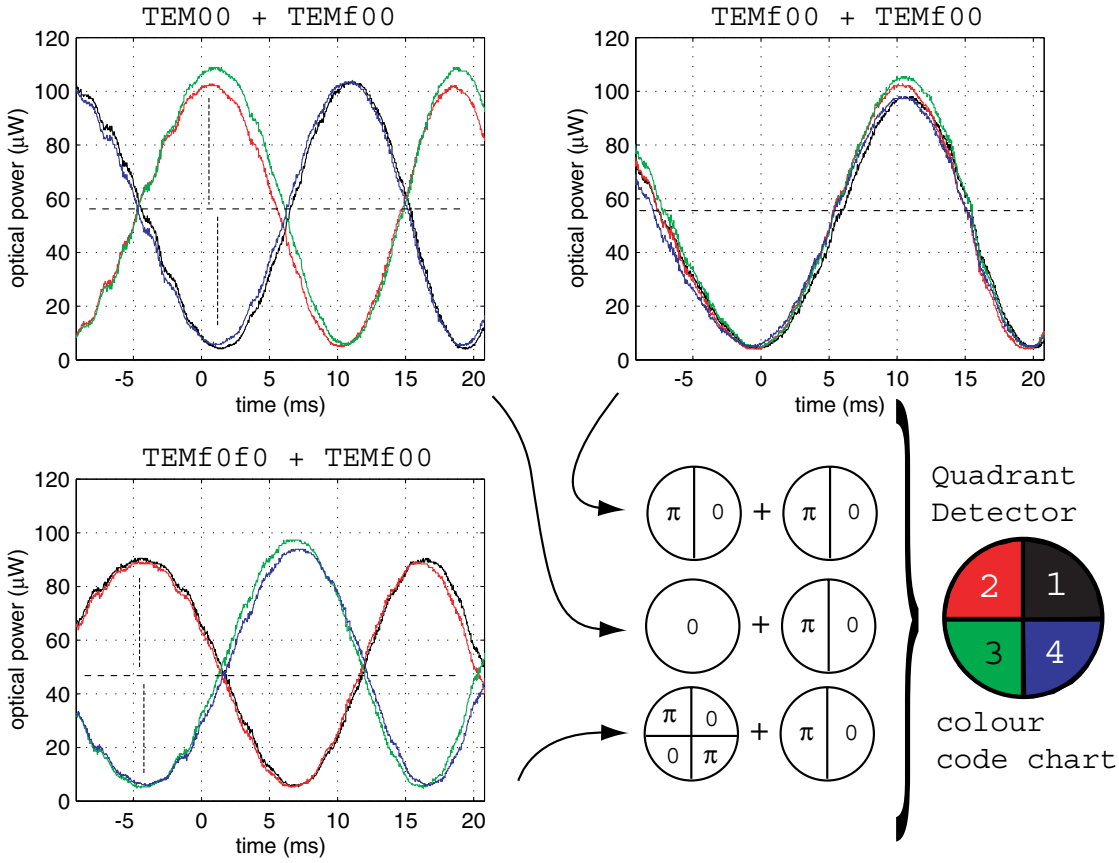

Figure 3.8: Multi-mode interference (experimental - quadrant visibility). Scans of visibility when interfering multi-mode light. Each quadrant detector has its own colour trace. Horizontal dashed lines are 50 percent quarter power. Vertical dashed lines show the slight phase mismatching in the waveplate. Top left, interference of TEM_{00} with single-flip waveplate (TEM_{f00}). Top right, the effect of single-flip waveplate cancelled by another single-flip waveplate on second beam. Bottom left, interference of single-flip waveplate with double-flip waveplate (TEM_{f0f0}).

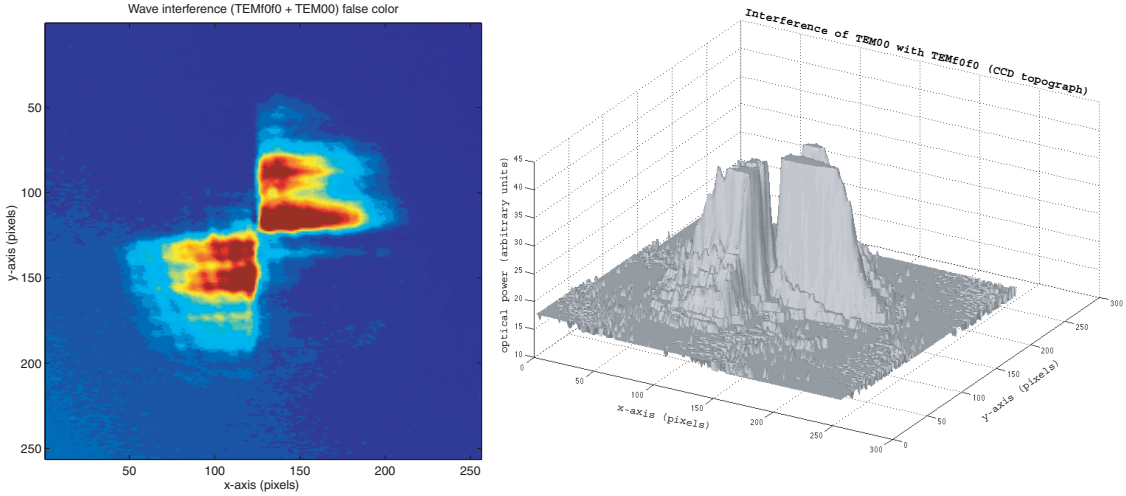

Figure 3.9: Multi-mode interference (experimental - CCD camera). Interference of double-flip mode with TEM_{00}, imaged with CCD camera (data corrected for CCD gamma=1.5 brightness scaling). LEFT: is a false-colour image, blue is dark, red is bright light. Note total destructive interference in the diagonal quadrants. Small ripples are due to interference fringes on CCD front filter/protector. RIGHT: same data as left, but processed into shaded topograph for visualisation. Note the 'sheer cliff' at the quadrant boundary this means that the double-flipped mode was precise and in focus. Note also that the top is flat due to clipping from CCD automatic gain control.

the 2QP were performing their single-flip duty correctly.

The third plot (BOTTOM LEFT) is the interference of a double-flipped mode $\mathrm{TEM}_{\mathrm{f0f0}}$ from a 4QP, with a single-flipped mode $\mathrm{TEM}_{\mathrm{f00}}$ from a 2QP. The phase mismatch is smaller than before at about 5°. Observe that the top and bottom halves of the quadrant detector (top = quadrants 1 and 2 , bottom = quadrants 3 and 4) have received fringes π out of phase with each other. Individual quadrant visibilities are $V = 0.88$. Which is lower than for the 2QP fringes, but this is to be expected, primarily because of the larger gap in the 4QP and the fact that there is more room for error when interefering through a total of size quadrants than for only four or two. However, this is still convincing evidence that the 4QP was performing it's double-flip duty correctly.

These results obtained so far are sufficient to show that our waveplates are performing their flipping dutes very well. As an aid to visualisation (and also for fun!), we imaged the interference of the double-flip-mode $\mathrm{TEM}_{\mathrm{f0f0}}$ with a TEM_{00} on a commercial CCD camera. The result is shown in false-colour on the left side of Figure 3.9

Where blue represents darkness, and red corresponds to bright light. One may also see that diagonal corners of the detector are opposite in phase, ie. (first-diagonal = quadrants 2 and 4 , second-diagonal = quadrants 1 and 3). Note however, the vertical *ripples* in the image. We believe that these are entirely fringe artifacts contained within the CCD camera chip itself, most notably interferences due to reflections from the microchip cover and a neutral density filter put in place for required attenuation. Neverthless, this is visually satisfying evidence that we have indeed generated a double-flip mode. Finally, the plot on the right in Figure 3.9 is a topographical map of the same data. Once again this is an aid to visualisation. Note especially the sheer cliff at the quadrant boundary where interference changes from destructive to constructive, which is also supportive evidence for the claim that we have a good double-flipped mode.

This section has been a very important aspect of the entire experiment because wave-

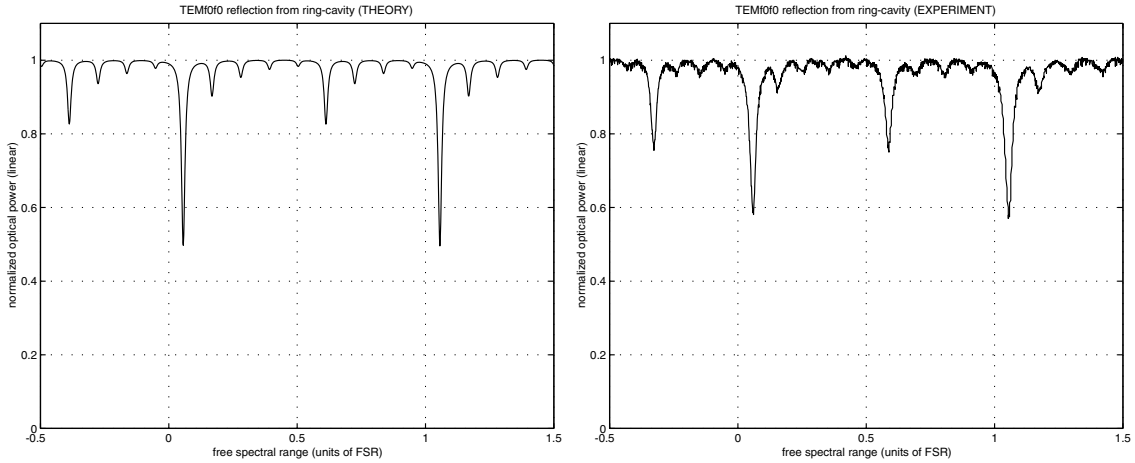

Figure 3.10: Ring cavity mode structure (comparison of theory and experiment). LEFT: Theory plot using numerical model of reflected power from the first total of p=q=29 $\mathrm{TEM_{pq}}$ modes that make up the double-flip-mode $\mathrm{TEM_{f0f0}}$. RIGHT: Experimental result of reflected power from the ring cavity of a Fourier transformed $\mathrm{TEM_{f0f0}}$ with the free-spectral-range scanned. Theory and experiment have identical initial parameters (same as the mode structure and mode reconstruciton numerical analyses performed in section 1.5). Observe that the experimental mode position structure agrees well with theory, and that the mode peaks are consistently shallower than in the theoretical prediction, which is consistent with intra-cavity amplitude loss of about 5??? percent. The main peaks are labelled for the modes they contain.

plate performance for flip-mode production is crucial to fulfilment of the spatial homodyning condition, and also, therefore, to any attempt of spatial squeezing.

3.7 Characterization of mode-mixing cavity (experimental)

In the prevous sections, by way of theoretical modelling and analysis, it was shown that a ring cavity could be used for the special purpose of mixing together two different spatial modes, specifically a $\mathrm{TEM_{f0f0}}$ with $\mathrm{TEM_{00}}$. As the reader may recall, the secret to the success of this technique rested upon the fact that odd-odd members of the $\mathrm{TEM_{pq}}$ felt their resonances at different regions in the cavity free spectral range away from the $\mathrm{TEM_{00}}$ resonance. It is precisely this cavity mode structure that may combine a $\mathrm{TEM_{00}}$ with a $\mathrm{TEM_{f0f0}}$.

We decided to experimentally verify the mode structure of our cavity. A $\mathrm{TEM_{f0f0}}$ was made using the 4QP, and mode-matched into the cavity. Reflected light was collected with a single photo-detector, and the length of the cavity scanned a few FSR. The results are shown on the RIGHT side of Figure 3.10. The theoretical prediction (at LEFT) was made using the same numerical model as in Section 1.5 with initial cavity parameters identical to those in the experiment, ie. coupling mirror reflectivities $R_p = 95\natural$, cavity round-trip length 200mm, centre mirror radius of curvature 250mm. These intial parameters set the following cavity properties: FSR=760MHz, finesse $F_p = 61$, bandwidth $\delta\nu_p$=12MHz. One can see quite clearly that the experimentally observed positions of the modes in the free spectral range agree very well with the theoretical predictions. The main peaks are labelled for the modes they contain. Notice also that the relative depths of the peaks also correspond very well between experiment and theory. There are however some slight

deviations, and it is thought that in the experiment the initial beam used was not a pure Gaussian beam before entering the waveplate. Any deviation from an initial Gaussian beam would contain higher order $\mathrm{TEM}_{\mathrm{pq}}$ modes, which would be slightly over represented in the final results. Nevertheless, these results are not only a good indication that our cavity has the properties we desire, it also reinforces our previous evidence pertaining to the quality of the double-flip-mode.

Now is probably the best moment to mention that the experimental setup we used for the results in Section 1.6, and the data presented in Figure 3.8 and Figure 3.9 in particular, were obtained by the reflected beam from the mode-mixing cavity used in *this* section. In other words for these results we used the final configuration of the experiment. This is perhaps the conclusive piece of evidence needed to show that both special optical components did indeed work well, and in harmony.

3.8 Summary

This chapter began with an explanation as to our need for two special optical components, namely, the mode-flipping waveplates and the mode-mixing cavity. Theoretical analyses of these components were performed, not only to highlight their mechanisms, but also for the creation of predictions that could be compared to the experimental results that followed. And since the results of theory and experiment compared quite favourably, we felt confident that these optical components could perform their respective duties that are in fact the key to the full 2D spatial squeezing experiment.

Chapter 4

The Experiment

'Art is a lie that lets us recognise the truth'. Pablo Picasso

4.1 Overview

The purpose of this chapter is to give a description of the experiment detailed enough so that it could in principle be rebuilt. To achieve this goal, the chapter begins with a run through of the key stages and their control systems. Important design considerations are discussed, followed with a view of the experiment in its entirety. The last section is a prelude to the results chapter, and deals with initial parameters, precautions, and data analysis.

4.2 The basic experiment

How did the experiment work? Drawing from previous discussions, the main idea is this: The spatial homodyning condition tell us that if we would like to squeeze the horizontal and vertical differential measurements on a split detector, ie. 2D spatial squeezing, then we must mix together two squeezed beams that are flipped along their respective axes, ie. horizontal and vertical, relative to the local oscillator that they must finally be combined with before detection. Note that from insights gained in the previous chapter on the mode-mixing cavity, we have chosen the local oscillator envelope to be a single-flip-mode (TEM_{f00}). This implies that the beam being transmitted through the cavity, which is an ordinary Gaussian beam (TEM_{00}), will correspond to the horizontal squeeze (H) beam. And that the reflected beam, which is a double-flip-mode (TEM_{f0f0}), will correspond to the vertical squeeze beam (V). A schematic diagram of this setup is shown in Figure 4.1. Starting at the laser (LA), the light is split, most for supplying the production of green light (SHG). The light that is left over is used for supplying the local oscillator (LO) and seed beams for the optical parametric amplifiers (OPA1 and OPA2). Each squeezer consists of a single OPA that is fed a seed beam, and is pumped by green from the SHG. The squeezed beams from OPA1 and OPA2 are combined on the mode-mixing cavity (ET). The envelope of OPA2 is an ordinary Gaussian TEM_{00}. Prior to mixing on the (ET) cavity, OPA1 beam is sent through a double-flip waveplate (4QP) to turn it into a TEM_{f0f0}. The local oscillator (LO) is sent through a single-flip waveplate (2QP) to produce a single-flip mode (TEM_{f00}) before being mixed on a beamsplitter (BS) with the two squeezed beams OPA1 and OPA2. At the homodyning stage (HD), all three beams finally arrive at their destination on the quadrant detector (QD), whose signals are suitably added/subtracted for viewing on a spectrum analyser (SA). An artificial displacement transducer (DT) was

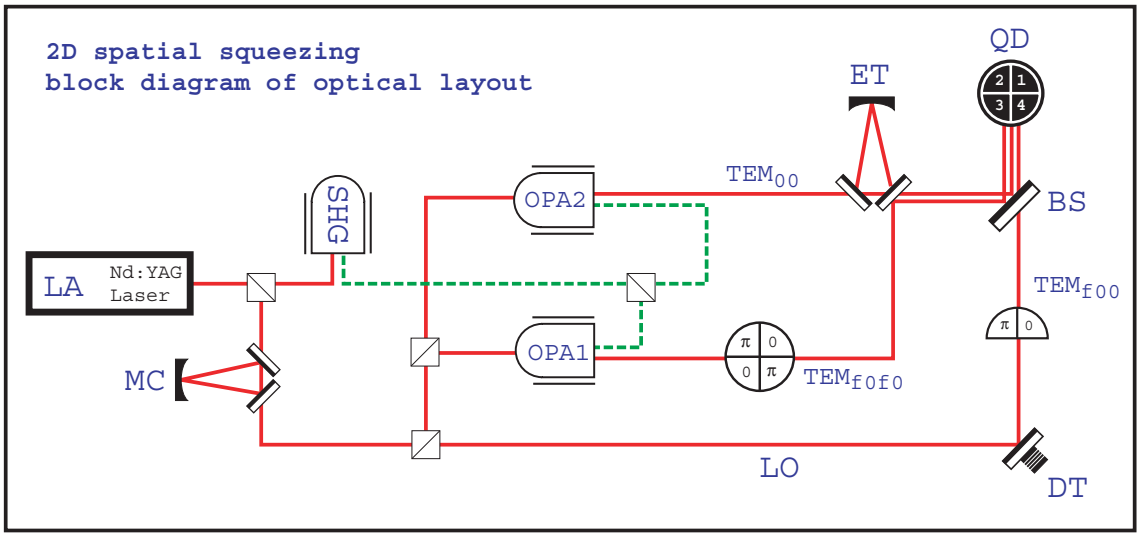

Figure 4.1: Schematic of basic experiment. LA: laser, MC: mode cleaner, ET: mode-mixing cavity, LO: local oscillator, DT: displacement transducer, BS: mode-mixing beamsplitter, QD: quadrant detector.

placed in the path of the local oscillator before the beampsplitter.

An important point that we must clarify for the reader, is that we did not build any of the stages from the laser up to and including the two squeezers, ie. stages LA, MC, SHG, OPA1 and OPA2. A complete account of their design and construction is given in [8]. What we did design and build in this honourse project were all the stages from the squeezers onwards (ET, 4QP, 2QP, and HD containing BS, DT, QD). Details of each stage will be further discussed.

4.3 Stages

4.3.1 Laser (LA)

The laser was a non-planar ring oscillator Nd:YAG operating at 1064nm with a maximum power output of 1.5W. The lasing frequency was adjustable (±8GHz). In the slow regime (on the order via a temperature servo loop. And in the fast regime by way of a piezo electric (PZT) actuator that changed the length of the Nd:YAG crystal. There was a relaxation oscillation at about 500kHz, but and above 25MHz the light was shot noise limited. The output beam shape was a slightly elliptical TEM_{00}.

4.3.2 Mode-cleaner (MC)

The mode-cleaner (MC) was a three mirror ring cavity. From what we have learned in Chapter 3, we know that a cavity will usually resonate for only one spatial mode at a time, depending on the exact round-trip optical path length. This property was used to our advantage. The wavelength of the laser was tuned to resonante a TEM_{00} with the cavity. This spacially filtered the beam because it rejected the other higher order modes, ensuring a clean TEM_{00}. In addition to spatial filtering, the MC played another role in filtering out classical amplitude and phase noise upon beam transmission for frequencies above the 2MHz linewidth of the cavity. The cavity was constructed from a metallic material with

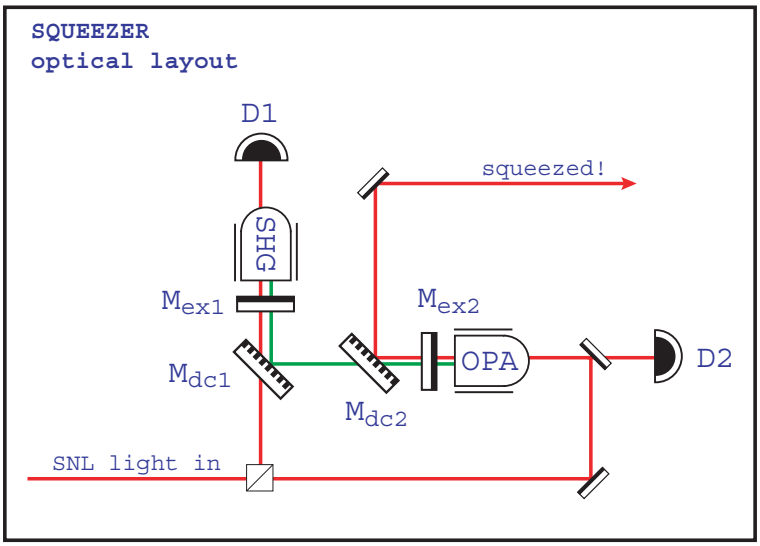

Figure 4.2: Schematic of squeezer. Mex1/Mex2: External cavity mirrors, Mdc1/Mdc2: dichroic mirrors, D1/D2:photodetectors.

the propoerty of a first order thermal expansion rate of zero. This ensured long term stability against thermal drift and hence was a reference for the entire experiment.

4.3.3 Two squeezers (OPA1, OPA2 and SHG)

The two squeezers are of course *the* most important elements in the 2D spatial squeezing experiment. The theory behind their operation was given in Chapter 2. Here we will look at their construction and function in the actual experiment. Figure 4.2 shows a detail of one of the squeezers (both have identical designs and construction). Focussing our attention initially on the generation of 532nm green light produced by the SHG crystal. The curved surface of the crystal is highly reflective, and forms a cavity with the external mirror M_{ex1} for red light. Green makes a single pass through M_{ex1} which is optimised for high green transmission. An external cavity setup allows one extra control over mode-matching and fine tuning. About 200mW of 1064nm light ('red') passes through the dichroic mirror M_{dc1} and into the cavity. The 532nm light ('green') is produced in the SHG process discussed in Chapter 2, and leaves the cavity, then reflecting from M_{dc1} toward the OPA. The light that leaks from the curved end of the SHG crystal is collected by detector D_1 for locking purposes (which will be treated in the control theory section that follows). Turning our attention to the OPA, which we can see is another external cavity formed by mirror M_{ex2} and the OPA crystal curved surface. The green is sent through a dichroic mirror M_{dc2} and into the back of the OPA crystal. It makes only one pass since M_{ex2} is high transmission of green. Meanwhile a red seed beam, which was tapped from the LO is sent through a dichroic M_{dc3} and into the cavity via M_{ex2}. The green tap-off from M_{dc3} is detected on D_2 and used for locking of green with the red seed beam. When locked, the green beam de-amplifies the seed by a factor of one third, thereby squeezing the seed. The emerging squeezed beam then reflects from M_{dc2} and on to the rest of the experiment. The power in the squeezed beam is about 150μW. The SHG and OPA crystals do not sit in the open air, they each have their own temperature controlled ovens operating at 105°C. Milli-kelvin temperature control is necessary for maintaining the required refractive indices, ie. equal at both 1064nm and 532nm. Mounted on both

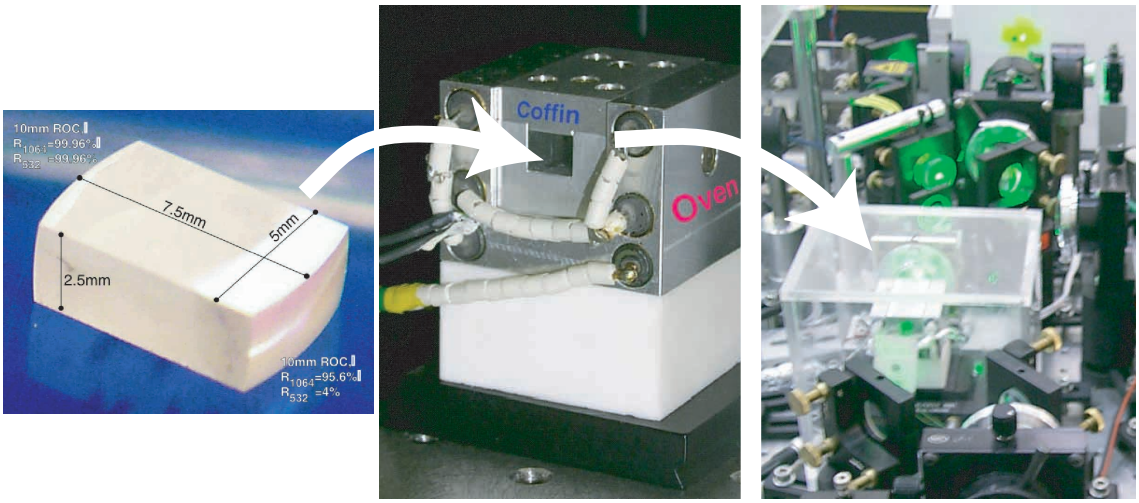

Figure 4.3: OPA photographs. LEFT: the OPA crystal by itself. MID: the temperature oven. RIGHT: OPA1 setup in the experiment with green pump light.

SHG and OPA crystals are piezo-electric crystals (PZTs) capable of producing a strain in the crystal, these are used for the purpose of locking. Neglected in this picture have been the numerous steering mirrors and lenses necessary for mode-matching purposes. Where the squeezer fit into the setup as a whole is presented in a Figure 4.10. Even though both squeezers use the same components and construction, there is some variability in squeezing. OPA2 seemed to be the better squeezer out of the two, producing about 4dB of temporal squeezing. OPA1 managed to produce a respectable 3dB of temporal squeezing. These were measured using the usual temporal homodyning technique.

4.3.4 Special optics

We have already devoted an entire chapter for the optical components. However in an effort for completeness their roles shall be briefly revisited. 2D spatial squeezing requires at least two flipped modes to satisfy the spatial homodyning condition. We chose the LO to be a $\mathrm{TEM}_{\mathrm{f}00}$ created by a two-quadrant waveplate (2QP). And the squeezed light from OPA1 to be a $\mathrm{TEM}_{\mathrm{f0f0}}$ produced by a four-quadrant waveplate (4QP). The squeezed beam from OPA2 was kept as a TEM_{00} and passed through the mode-mixing cavity (ET). The $\mathrm{TEM}_{\mathrm{f0f0}}$ from OPA1 reflected off ET, thereby combining the two beams. Most of the details concerning their functioning were given in chapter 3. However, we did not mention the reason as to why the mode-mixing cavity was set to operate at high finesse. This was because we found that although low finesse passed the OPA2 beam more efficiently, this was at a detriment to the double-flipped OPA1 beam reflection. We found that high finesse was a good compromise for reflection efficiency of the double-flipped mode, while not losing too much power with OPA2 transmission. Typical cavity transmission efficiencies were; for OPA2 $\eta = 96\%$, and for OPA1 $\eta = 95\%$. These figures are the fraction of total TEM_{00} light reflected when the cavity on resonance (all flipping waveplates removed). The efficiency of OPA1 is worse because its mode shape was not as Gaussian as OPA2. The poor mode shape originated from the OPA crystal/cavity itself, and was largely beyond our control.

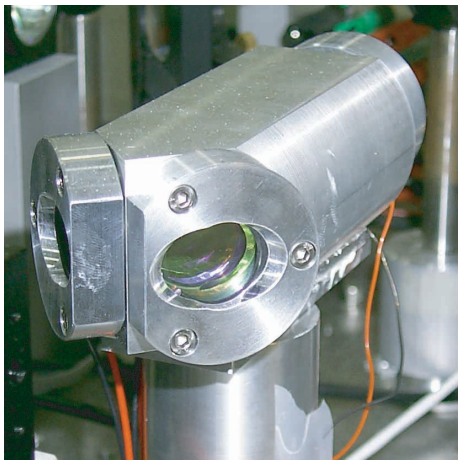

Figure 4.4: Photograph of mode-mixing cavity (ET).

4.3.5 Homodyning stage (HD)

The actual measurement of squeezing is made at the homodyning stage. This is where the two squeezed beams are mixed on a beamsplitter with the local oscillator (LO). The ratio of the beamsplitter was chosen to be 95 percent reflective for the squeezed beams. The reason for this derives from the fragile nature of squeezed light. Any loss to a squeezed beam reduces the level of squeezing by mixing in vacuum state and bringing it closer to the shot noise limit. The undesirable, and unavoidable consequence of this was that 95 percent of the LO power was dumped and wasted. This meant that we had to supply as much LO power as possible, to keep it sufficiently high in power above the squeezed beams, so that the homodyning condition could be satisfied. The three mixed beams were then sent to the quadrant detector. The quadrant detector (name: EPITAXX ETX 505Q) consists of 4 individual photodiodes. Each diode is a square 0.5mm a side, and they are packed so close together as to have a gap of not more than $25\mu m$ between them. The signals from each photodiode are boosted by four independent custom built amplifiers. The outputs are calibrated to respond with 1mV per 0.1mW input optical power. The signals are then split and added/subtracted appropriately to perform horizontal and vertical differential measurements. These two signals were then sent to a spectrum analyser (in later runs, we were able to get hold of a second spectrum analyser) where their noise powers could be measured. Typical fringe visibilities were; for OPA2 $\mathcal{V} = 98.5\%$, and for OPA1 $\mathcal{V} = 95.8\%$. These figures are for TEM_{00} on each beam, ie. no waveplates placed in the beampaths. OPA1 is worse than OPA2 for mode matching. Once again this is because the mode shape from the original OPA1 (prior to waveplate insertion) was poor, and this effect was exacerbated by the fact the OPA2 was being mode cleaned by ET and OPA1 wasn't. These were effects we had little control over.

4.3.6 Displacement Modulator/Transducer (DT)

An important aspect of the experiment was to simulate the presence of a signal by creating a displacement of the beam at frequencies around where we were going to make the squeezing measurements (around 5MHz). We did this using a small mirror mounted on a PZT, with the beam arriving at an angle of 45°. A PZT (piezo-electric crystal) changes its length for a given voltage applied to it. This modulation was applied on the LO only,

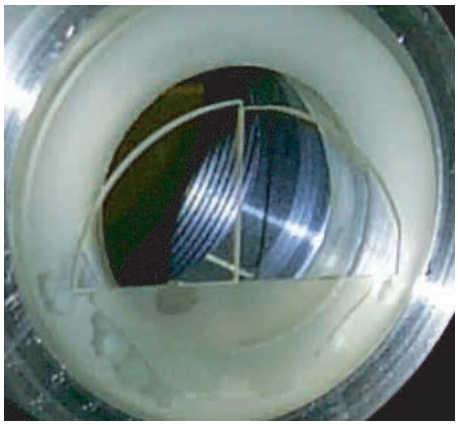

Figure 4.5: Photograph of two-quadrant mode-flipping waveplate (2QP).

before the beamsplitter that mixes it with the squeezed beams. Now in a real world type beam displacement measurement, this would be crazy, as most of the light is dumped on that beamsplitter. Our reason for putting the modulation there was not by choice, but rather necessity, since the optical benchtop is of finite size, and there was just not sufficient space to fold the light path once more. Note however, that for an experimental demonstration, there has been no loss of generality in doing it this way. We could produce 20Åof displacement for both horizontal *and* vertical at the same time. How can this be? In theory a mirror mounted on a single PZT should only give a horizontal displacement, ie. a displacement along the plane of the folded light path. The reason we could produce *diagonal* modulation was because of one of the the oridinarily undesirable properties of PZTs. A PZT actually consists of a stack of piezo-electric material slices. When a voltage is applied to the stack, it not only expands/contracts along the principal axis, but also sways ever so slightly at an angle away from the axis. We used this defect of our PZT to our advantage to get a diagonal modulation. However, our control of this effect was rather limited, and could only be altered by changing the driving frequency of the PZT near resonance.

One big aspect of the experiment that has so far been side-stepped in this brief tour of the various stages, is the all important issue of servo-locking. What locking is, why it was needed, and how it was achieved, are the topics of the next section.

4.4 Control Theory

Light is a wave phenomenon, and therefore has a of phase. If what we would like to measure is the interefernce of two light beams, then we must have some way of *controlling* their relative phase. Another situation where we must be in control, is for the adjustment of an optical cavity round-trip path length. This is an absolute necessity for keeping the incident light on resonance, otherwise the free-spectral-range of the cavity would drift aimlessly around the centre frequency of the light beam, falling on/off resonance beyond our control. Optical control may be achieved in at least two ways: By changes of refractive index in a medium (such as the electro-optic-effect), thereby changing the optical path length; or via the bulk motion of a mirror mounted on a piezo-electric crystal (PZT), creating a change in the geometrical pathlength. For its inherent convenience, we utilised only the latter type of control within the relevant elements of our experiment. What we

have dealt with so far is only half of the picture. We must of course have some form of feedback to inform us of which way, and by how much, our parameter has drifted from the preferred value, in order that we may correct for its deviation. This is what we call the extraction of an *error signal* from a system. And when the parameter is maintained at its preferred value, we regard the system as being *locked*. A useful error signal has must satisfy two criteria: 1) It must be proportional to the deviation of the locking parameter and therefore must change in sign (ie. from positive to negative or vice versa); 2) Is must also be above undesirable background noise . Once these conditions are satisfied, it is possible to process the signal, most often with a proportional-integral-differentiator (PID), to drive the controllers of the system, be it actuators, temperature controllers etc. For the locking of phase, a *modulation* locking method is usally applied. For the locking of a cavity we have two main techniques at our disposal, modulation locking and tilt locking. Modulation locking has three further variations. These will now be discussed in further detail.

4.4.1 PDH locking

A cavity locking technique named after its inventors; Pound, Drever and Hall. The signal beam is phase modulated at frequency ω_m thereby creating sidebands at $\pm\omega_m$ around the carrier of frequency ω_0. There are two regimes of operation depending on the bandwidth ($\delta\nu$) of the cavity; 1) $\omega_m < \delta\nu$; 2) $\omega_m > \delta\nu$. For the former, a cavity of bandwidth $\delta\nu$ less than the PM frequency ω_m will impart to the sidebands negligble phase shifts, hence the sidebands become a reference for the carrier. If the carrier is exactly on resonance, ie. zero phase shift, then everything is essentially the same as before. If, however, resonance should deviate from the carrier, a phase shift shall be incurred. This has the effect of rotating the modulation from PM to AM. The AM siganl can be recovered by detecting the reflected beam on a photodiode and *de-modulating* the photocurrent signal with the same frequency as the original phase modulation. The procedure of demodulation is essentially an electronic circuit that multiplies the two signals, after which a low-pass filter rejects the high frequency components. This gives an error signal proportional to the resonance deviation from the carrier, and also changes sign at zero-crossing. For the second regime where the sidebands lie within the cavity bandwidth PM is also converted to AM, but this time it's because the sidebands are differentially attenuated. Using the same demodualtion method one can obtain a zero-crossing error signal whose polarity depends on which way the resonance has deviated from the carrier.

4.4.2 Dither Locking

Dither locking is a variation on the PDH theme. Here the optical path length of the cavity itself is modulated, and the carrier acts as both a source and reference. When the carrier is off resonance, the cavity modulation produces two sideband AM sidebands. The strengths of the two sidebands are asymmetrical depending on which way, and how far the carrier is from resonance. The AM signal can then be demodulated and used for control.

4.4.3 Tilt locking

Tilt locking was developed by D. Shadock and M. Gray. A thorough account is given in their paper [9]. Here is the basic idea behind tilt-locking. A TEM_{00} incident on a cavity that is slightly mis-aligned to the beam will cause some of the power to be coupled into

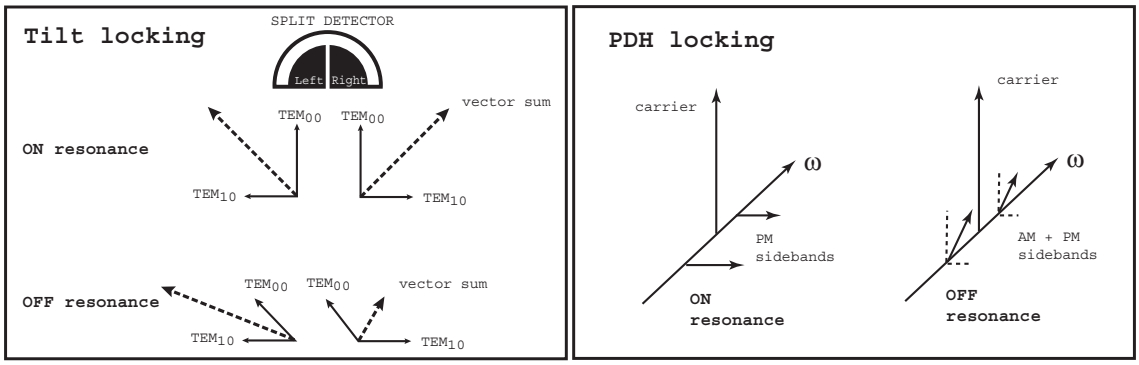

Figure 4.6: LEFT: Vector diagram of tilt-locking.RIGHT: Sideband picture of PDH locking.

the next higher order mode, ie. TEM_{10}, which will be reflected along with a fraction of the original TEM_{00}. We already know that a cavity gives a reflected a phase shift that is mode dependent. The TEM_{10} which is far from resonance acts as a reference for the TEM_{00}. When the TEM_{00} is precisely on resonance, the relative phase between the central maximum of TEM_{00} and the two maxima of TEM_{10} are $+\frac{\pi}{2}$ and $-\frac{\pi}{2}$ respectively, ie. the situation is symmetric. When slightly off resonance, the TEM_{00} phase angle changes, thereby increasing the relative angle between one TEM_{10} maximum, and decreasing the angle of the other maximum. See Figure 4.6. A vectorial addition of the vectors leads to the conclusion that there is now an asymmetry, in the intensity on each half of the beam straddling the TEM_{10} maxima. If the reflected beams are shone onto a split detector (ie. a detector with two elements side by side) and allowed to interfere, then the total power collected by each element will also by asymmetric. If the difference of the two photocurrents is taken then we have an error signal that is proportional to the deviation, and very importantly changes sign exactly at resonance. The error signal could be suitably processed to drive the cavity via an actuator or temperature controller. Tilt locking is a highly desireble method as it does not require cumbersome phase modulators and electronic demodulation to produce an error signal.

4.4.4 Modulation locking for homodyne detection

Modulation locking is used for locking the phase angle θ of a signal beam relative to a local oscillator. In homodyning this is crucial, as θ corresponds to the quadrature of the signal beam being measured. For example, in our case we wanted to lock to the amplitude quadrature in order to detect squeezing. This may be achieved by using a beam that has PM sidebands. When the $\theta = 0$, we are measuring the amplitude quadrature, and so we don't even see the PM sidebands. The moment we drift away from $\theta = 0$, we will begin detecting the PM sidebands as an AM signal in our differential measurement. This can be demodulated using the usual techniques to extract an error signal with zero-crossing.

4.5 Every cat has nine locking loops

As the title of this section suggest, we had a total of nine locking loops to operate. They are given here in the order that they are cascaded. A diagram of all the locking loops with detectors and drivers is given in Figure 4.7

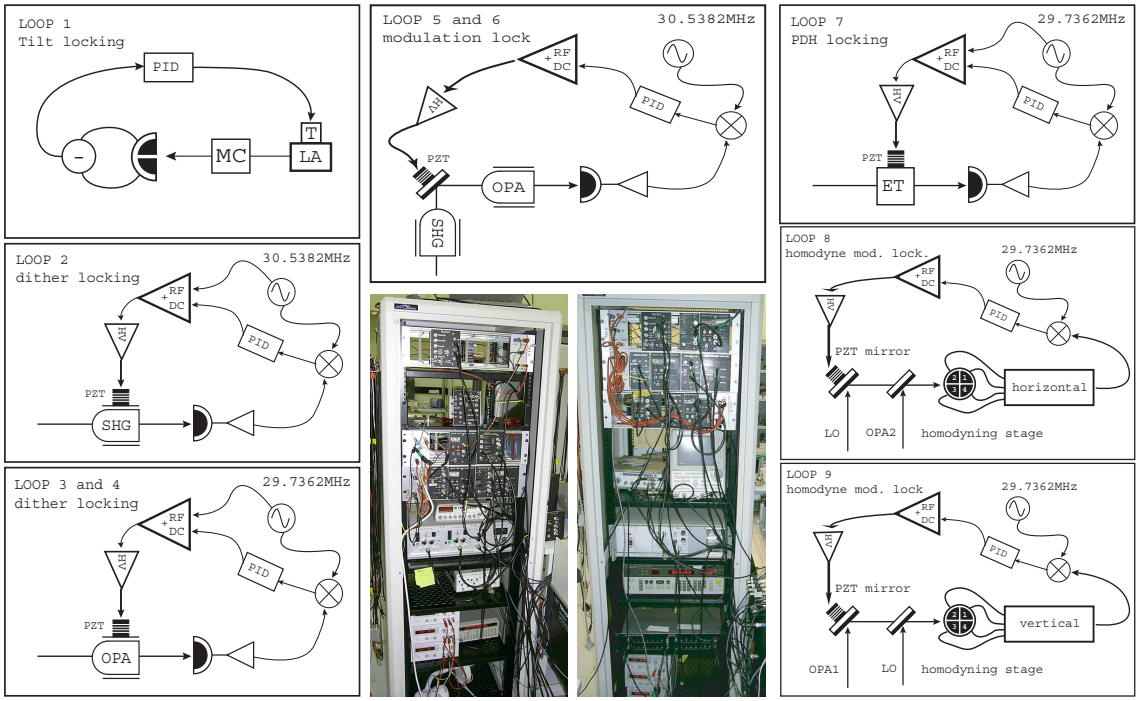

Figure 4.7: Locking loops surround photographs of the two control racks.

1. The mode-cleaner supplies the LO and the seed beams for both OPAs. It had no actuators to control it's resonant frequency. Instead, it was the laser whose frequency was locked to the mode-cleaner. The mode-cleaner was therefore *the* reference for the entire experiment (and consequently fastened very securely to the bench!). A locking error signal was obtained by the tilt locking technique, the benefit of this was that no phase modulation had to be applied on the original laser carrier itself. The laser frequency was adjustable on short time scales via a PZT bonded to the lasing crystal which could stress it appropriately. Long time scales were taken care of with a temperature controller. When the error signal was zero-crossed properly the mode-cleaner could stay locked all day.

2. The SHG did not require (1) to be locked first as it recieved a tap-off from the laser before the mode-cleaner. For the SHG to work, its resonance had to be locked to the red input beam. The method used was dither locking, ie. the cavity itself was modulated by the application of a high voltage sinusoid at precisely 30.5382MHz. This created sidebands in the transmitted beam which were transformed in the usual way, detecter, mixer, and low pass filter into a useable error signal that in turn drove the high voltage via a PID unit. This locking was very stable and could stay locked for the entirety of a session.

3. In all the loops that follow it was required that the mode-cleaner be locked. A tap-off from the local oscillator supplied the seed beam for OPA1. The OPA cavity was locked to the seed by dither locking. The high voltage that was applied to the crystal, was modulated at exactly 29.7362MHz. The reflected beam was detected, and the usual dither locking method for error signal extraction was used. This locking was

fairly stable, but a sharp tap given to the table with an Allen key was enough to make it drop lock.

4. For OPA2 the story is exactly the same as OPA1 (even the same modulation frequqency).

5. Next the green had to be locked to the OPA1 red seed beam in order to de-amplify and therefore squeeze the seed beam. This was accomplished by the method of modulation locking. Since the green had PM sidebands at 30.5382MHz, these were transferred to the red seed by the de-amplification process. The photocurrent from the OPA1 seed locking detectror was then demodulated at 30.5382MHz, and an error signal derived to control the SHG phase relative to the OPA1 seed.

6. The same story for OPA2.

7. We now have two squeezed beams ready to be combined on the mode-mixing cavity (ET). Reflected OPA2 beam was detected, demodulated at the dither locking frequency, giving a PDH lockinh error signal which was then processed by a PID. The PID output was amplified to drive the cavity PZT mirror. By itself, this locking was fairly stable (mainly attributed to the temperature stability of the lab), but when the OPA1 beam was added it was more difficult to lock. This may have occured because both OPA1 and OPA2 were dither locked at the same frequency. Therefore any TEM_{00} component of OPA1 could have been transmitted through the cavity and into the locking detector, thereby upsetting the error signal. Fortunately, it was not impossible to lock it, and it was unnecessary to change the modulation frequency of OPA1.

8. Now that we have OPA2 being transmitted through ET, we would like to make the horizontal spatial squeezing homodyne measurement. We must of course have the phase angle between LO and OPA2 locked together at a phase angle $\theta = 0$ to detect the amplitude quadrature. The PM sidebands from OPA2 were still sufficiently strong to provide a signal for modulation locking. If say, the LO and OPA2 drifted apart in phase, the homodyne setup would then begin detecting some of the phase quadrature, and therefore the PM signal. This was used to extract an error signal to control a PZT mirror for the LO before the mode-mixing beamsplitter (BS). Note that this PZT mirror is a separate one to that of the displacement modulator (DM).

9. The final task is to lock the phase of OPA1 to the LO in order to perform an amplitude quadrature homodyne measurement, and the technique is exactly the same as for loop (8).

Hopefully this has given the reader some idea of the complexity involved in running this experiment.

4.6 Electronic Equipment

Optical components are of course only half the story. A quantum optics experiment requires a whole array of electronic units; detectors, PIDs, HV amplifiers, signal amplifiers, mixers, signal arithmetic, digital oscilloscope and the all important spectrum analyser. Here is some information about a few of these units.

Figure 4.8: Photograph of quadrant detector (QD).

4.6.1 PID, HV and PZT units

These units are the real work-horses of the experiment. Their job is to keep everything locked. The PID or proportional-integral-differentiator, takes a raw error signal and processes it to make it suitable for driving an actuator. It essentially filters the signal with a low-pass filter and provides amplification at the desired gain setting. The output from the PID is sent to a high voltage amplifier (HV unit) to drive the PZT. The usual procedure in an experiment, is to set manually the DC offset on the PID to find the desired locked position. The integrator is switched on, and the gain adjusted to just below PZT oscillation. The locked position is then fine-tuned using the integrator offset.

4.6.2 Quadrant arithmetic and mixing

After the quadrant detector, the signal must be suitably added/subtracted to perform the necessary differential measurement, ie. horizontal=$[(q_1+q_4)-(q_2+q_3)]$ and vertical=$[(q_1+q_2)-(q_3+q_4)]$ where $[q_1, q_2, q_3, q_4]$ refer to the quadrant as ordered in the cartesian plane. We needed to perform both horizontal and vertical measurements at the same time. This involved splitting each photodiode current before performing the arithmetic.

4.6.3 Spectrum analyser

For our purposes, the inner workings of a spectrum analyser can be thought of as a tunable narrow-bandpass filter, whose averaged power output (varance of the signal) is monitored. For this discussion we will keep the centre frequency of the narrow-bandpass filter at a fixed value. There are two important settings to specify on a spectrum analyser, RBW and VBW. Resolution bandwidth (RBW) is the width of the narrow-band-pass filter. It sets the limit for what range of frequencies that are included in the power measurement. The measurement time is inversely proportional to the RBW. This is because the internal calibration algorithm of the specturm analyser requires this much time to converge to the correct power value. Video bandwidth (VBW) is the level of averaging performed on the power output after the narrow-band-pass filter. Trace averaging is a way of effectively lowering the VBW. It has the effect of smoothing out the trace. The last consideration is one of the electronic noise floor in a spectrum analyser. It is always present, but as long as it is below the signal of interest, its effect may be corrected by subtracting it (in linear

scale) from the desired signal. This method is known as dark noise correction because detectors whose photocurrent we are measuring must be kept in the dark to take this measurement.

4.7 Important design considerations

There were two main aspects of design that had to be considered when building the experiment. The first, which is common to all quantum optics experiments, is the necessity of mode-matching into cavities and interferometers such as a homodyning stages. The second, was a problem unique to our experiment because the waveplates were very abrupt phase objects which underwent diffraction.

4.7.1 Polarization and spatial mode-matching

In a homodyning stage, the LO and signal beams must overlap as closely as possible. In other words, the interference fringe visibility must be very good. This is only possible for beams which are actually the same mode shape and polarization. In our experiment we dealt only with linear polarization whose angle is easily changed by the rotation of an ordinary half-waveplate. Spatial mode-matching however requires the Gaussian waist position and waist size to coincide for both beams. A cavity has its own eigenmode for a Gaussian beam. If one does not mode match either the waist size, position or angle of entry correctly, then power will be coupled from the orignal Gaussian beam into higher order $\mathrm{TEM}_{\mathrm{pq}}$ modes, thereby leading to all sorts of profanities spewed forth from the frustrated experimenter.

For the general case of solving mode matching problems, three lenses are required to go from one waist size and position to a new waist size and position. Things are simplified when the original beam is very thick, and therefore has a long Rayleigh range and slow divergence. In this circumstance one may achieve the desired results with one lense of the correct focal length, but more often than not, two lenses are required to do the job. There are two ways of doing this. The first is to use a lens of long focal length to effectively perturb the focal length of the second lens to get the desired value. The second method creates a new waist close to the first lens, and the second lens position may be worked to get the desired result. In an effort to speed up the often difficult process of mode-matching when building up the experiment, I wrote a MatLab code which is listed in Appendix D, that numerically solved the Gaussian ABCD matrix problem.

4.7.2 Imaging system

We must remember that the special waveplates used to generate the flipped-modes are *phase objects* and will therefore diffract the original Gaussian beam. The effect of diffraction can be reversed with an imaging system. Therefore we needed an image of the OPA1 double-flip waveplate on the quadrant detector. We also needed an image of the LO single-flipped waveplate on the quadrant detector. As can be seen in the right of Figure 4.9, this was achieved by imaging the OPA1 waveplate before the mode-mixing beamsplitter. This allowed us to place the LO waveplate *itself* at the same distance from the beamsplitter as the OPA1 image. Then by use of a lens, both the OPA1 waveplate *image*, and the LO waveplate *object*, were then imaged onto the quadrant detector, just as required. The OPA1 beam had to be mode-matched into the ET cavity, which was simply done with

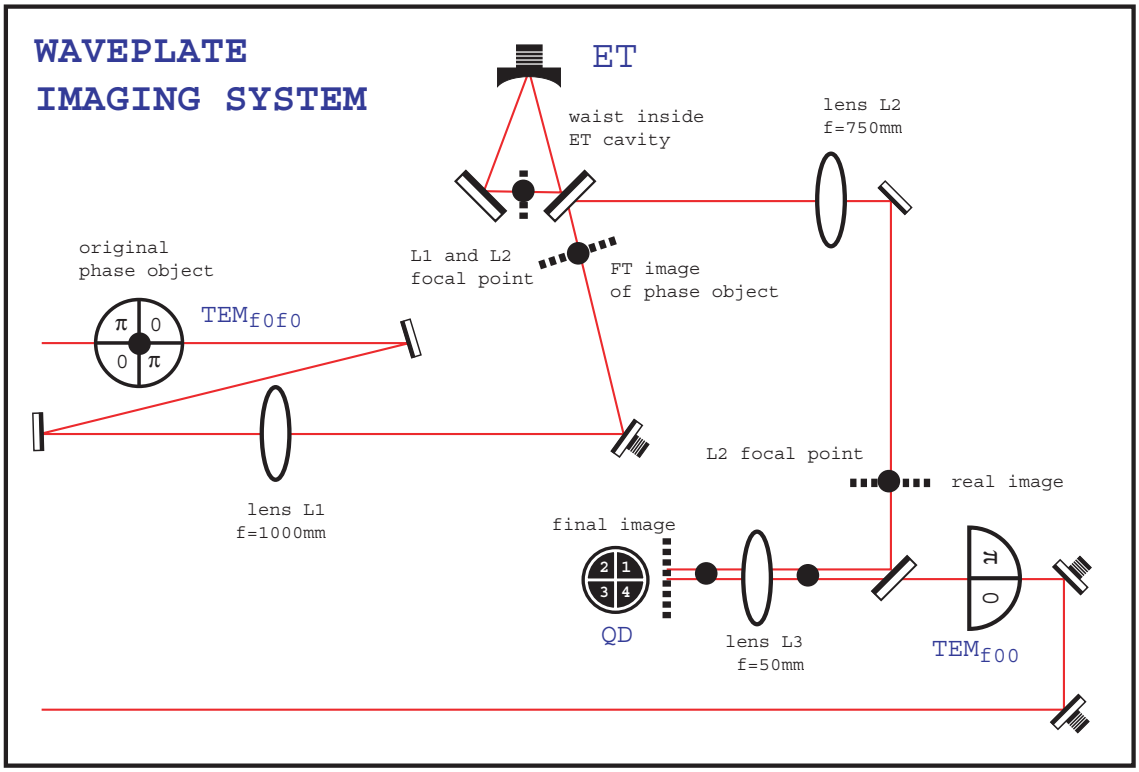

Figure 4.9: Imaging system. The wave-plate is the object, which had to be imaged onto the quadrant detector (QD). The large black dots refer to the focal points of the lenses and also to the ET cavity waist position. The thick dashed lines refer to the images formed by the lenses (L1, L2 and L3).

a single lens (L1). This can be seen near the left side of Figure 4.9. Notice the rather counter-intuitive placement of the new OPA1 waist position *outside* of the cavity. This can be made conceptually clear by tracing the light path in *reverse* from the quadrant detector. As can be seen, this requires an equal distance from the ET waist and the OPA1 waveplate image; something that can only be achieved by positioning the new OPA1 waist outside of the cavity by exactly one half of the intra-cavity waist position. Due to space restrictions on the optical bench we used only a single lens to perform this operation, and consequently the image at ET is the Fourier transform of the original object. Remember though, that this does not change the cavity-reflective properties of the double-flipped mode. Following now the entire path of the OPA1 we can see that it is imaged twice by two lenses that are spaced so that their focal points touch. This is a telescopic configuration, and so recreates exactly (aside from loss of the highest spatial modes due to aperturing) the electric field distribution of the phase object with the magnification M given by the ratio of focal lengths $M = f1/f2$. The imaging problem has been solved!

4.8 Initial parameters and precautions

In order to be sure that our measurements were faithful to reality, several initial parameters had to be taken and analyzed so as to fulfill the requirements of important assumptions that go into obtaining a squeezing result.

4.8.1 Method for obtaining squeezing results

Our instrument for measuring the state of light was a homodyning system. A homodyning system has two requirements that need to be satisfied, (i) the local oscillator (LO) must have an amplitude much greater than the signal beam, and (ii) the detectors must be sufficiently balanced to reject common-mode noise from the LO. In our experiment the LO was a factor of about 50 greater in power than the squeezed beam. This ensured that condition (i) was satisfied, and therefore the signal detected actually corresponded to the signal beam, and not some mixture of both signal and LO as can happen if their ratio of powers are not sufficiently high. For condition (ii), note that our laser was shot noise limited above 4MHz and so we did not require a high degree of common-mode rejection, but in our setup, a high level of common-mode rejection was guaranteed because the alignment procedure ensured that the quadrant detector was always centred.

Measurement of squeezing in the lab required the acquisition of three concurrent sets of data from a spectrum analyser. The squeezing result is obviously just a spectrum analyser trace taken while the two signal beams are squeezing, but by itself this information is practically useless. It must be calibrated against the shot noise limit (SNL). As long as the homodyning conditions are satisfied, then the SNL is measured by simply blocking the two squeezing beams. The noise measured will come from the flipped vacuum and hence will be SNL. There is one further matter of inconvenience, and that is the fact that no electronic ciruits are absolutely quiet. This is referred to as dark noise because it is measured by shading the detector from all light and taking a trace on the spectrum analyser. The procedure for obtaining a normalized squeezing measurement was then as follows. All traces were converted from dBm scale to linear. The average of dark was taken and subtracted from the shot and squeezing values, ie. dark-corrected. The mean of the dark-corrected squeezing noise is formed and divided by the dark-corrected shot noise to obtain a normalised noise power. In linear scale, the SNL is exactly equal to one, classical

noise rises above one, and squeezing lies below one. Of course squeezing results are most often quoted in dB scale in which the SNL sits at exactly zero, consequently classical noise is positive and squeezing is negative. Note that when we refer 3dB of squeezing what we really mean is a normalised noise power of -3dB. This terminology arrises because squeezing is akin to an attenuator of shot noise, and therefore de-amplification by 3dB really means an amplification of -3dB. It is hoped that no confusion will arise from this terminological anomaly, most especially in the next chapter where the results are to be presented.

4.8.2 Which shot noise?

The shot noise calibration method discussed earlier gives a slightly pessimistic squeezing result, ie. one closer to shot noise than it is in actuality. This is because we have not fulfilled the homodyning condition exactly. We have made an approximation in allowing the LO to be only about 50 times the power of the squeezed beam. Note that we can not make the squeezed beam zero power, otherwise it would not be possible to keep it locked. The consequence of this is that a shot noise taken by blocking both squeezed beams will lower the power incident on the detector, and therefore lower the noise power level. When the squeezing measurement is normalised, it gives a result that is slightly worse than it actually is. However, this is a totally fair measurement as our squeezing result is on the SNL side. An alternative method for obtaining shot noise is to block only one squeezed beam at a time, ie. if measuring horizontal shot noise, we blocked only the horizontal squeezing beam. This should reduce the previously mentioned effect by a factor of a half. There is one more method of obtaining shot noise that we tried. This involved blocking the green pump to the OPAs, which had the effect of switching the squeezing off. A side-effect of this was the OPA output beams rose in power by a factor of (3/2) because the beam was no longer being de-amplified by the green. This method is difficult because the OPA power must be restored to its orignal value with the use of neutral density filters, otherwise the squeezing will be on the 'unfair' side of the SNL. It is for this reason, that this method was not used for any of the results presented in this thesis. Instead, our usual method was either the all squeeze block, or the alternate squeeze block (one squeeze beam blocked at time). This guaranteed that all squeezing measurements were on the fair side of the shot noise limit.

4.8.3 Calibration of displacement modulation

We came to the conclusion that it was sufficient to use the SNL itself as a calibration. This is because even if the beam is held as steady as possible, the differential measurement will have a noise that looks like a displacement of roughly $d_{SNL} = \frac{\lambda}{\sqrt{N}}$ where N is the number of photons collected in the measurement. This is only an approximation. The exact value for a TEM_{00} beam (or a $\mathrm{TEM}_{\mathrm{f}00}$ as it's the intensity that is measured on the split detector, not the electric field) may be found in [11] and looks like

$$d_{SNL} = \omega_0 \sqrt{\frac{\pi}{8N}} \tag{4.1}$$

Where ω_0 is the Gaussian waist size of the beam at the photodetector. The number of photons may be found by measuring the power in the beam, and knowing the measurement time. The measurement time is given by the inverse of the resolution-bandwidth (RBW)

setting on the spectrum analyser. The number of photons is then simply the total energy acquired during the measurement, divided by the energy of each photon

$$N = \frac{P}{h\nu(RBW)} \tag{4.2}$$

Where ν is the laser frequency and h is Planck's constant. Our parameters were ($\nu = c/1064\text{nm}$, $RBW = 1\text{kHz}$, $\omega_0 = 0.53\text{mm}$) and the shot noise limit displacement was equal to $d_{SNL} = 0.56\text{Å}$. This means that for a differential measurement to have a signal to (shot) noise ratio $SNR = 1$ would correspond to a displacement modulation with amplitude $d_{SNL} = 0.56\text{Å}$. If the beam is shot noise limited this is the smallest measurement allowed. However, for a squeezed beam, which has fluctuations below d_{SNL}, a smaller measurement is in theory possible. Results from this type of measurement will be presented in the next chapter.

4.8.4 Error analysis

Error analysis is an important aspect to any physics experiment. Effort must be made by the experimenter to uncover any possible systematic errors that could have plagued the system, both in data analysis, and in the experiment itself. A search of our experiment revealed that the only systematic error that *did* occur, was the one mentioned earlier, in the shot noise normalisation, and is harmless in the sense that it always quotes a squeezing result closer to SNL. In practice we have found that for our queezing measurements, the systematic error is certainly smaller than 5%, which translates to about 0.2dB uncertainty in a 3dB measurement. In a measurement there is also the statistical error. This may always be reduced to an arbitrarily low level by gathering more data. For our results, we made sure that the statistical error in our quoted levels of squeezing were always smaller than 5%.

4.9 The complete experiment

4.9.1 Daily alignment procedure

We have now seen the entire experiment. The question that remains is how to run it. Since the experiment could not be run non-stop 24 hours a day, it was given the chance to sleep overnight. This allowed the optical components to drift, thereby losing optimum alignment. Before a squeezing run could begin, it was necessary to perform a cascade of alignments. I will not go into too much detail here, only enough to give an idea of the steps that were involved.

1. Switch on laser and move all waveplates out of beam paths.
2. Check mode-cleaner tilt-locking error signal.
3. Align and lock SHG to produce maximum amount of green possible.
4. Optimize alignment and locking of seed injection into OPA1 and OPA2.
5. Check mode-shapes of OPA1 and OPA2 - tweak by slightly tilting OPA cavities.
6. Optimize alignment and locking for green injection into OPAs.

7. Mode-match OPA1 and OPA2 beams into ET cavity and check efficiency.
8. Lock OPA2 to ET cavity.
9. Homodyning mode-match LO to the reference OPA2 and check visibility.
10. Homodyning mode-match OPA1 to LO and check visibility.
11. Centre quadrant detector.
12. Insert single-flip waveplate on LO.
13. Insert two quadrants of the OPA1 double-flip-plate to cancel the LO single-flip-plate.
14. Centre the OPA1 double-flip waveplate.
15. Lock LO phase to OPA2 for homodyning (horizontal).
16. Lock OPA1 phase to LO for homodyning (vertical).
17. Ready for squeezing!

Note that this day-to-day variability of alignment also translated into levels of squeezing that changed from day to day. But by using this method of alignment, over a period of two weeks we converged at the optimum level of squeezing that our experiment could give.

4.10 Summary

Hopefully the reader has gained enough insight into the experiment, that it would be possible, at least in theory, to repeat the experiment if so desired. We have had to visit control theory, and locking loops along the way, as well as the special considerations that went into the design of the experiment. The rudiments of data analysis were discussed along with some intitial conditions that needed to be satisfied. We concluded with a view of the experiment in its entirety and the procedure needed to bring it into alignment. Now lets start squeezing!

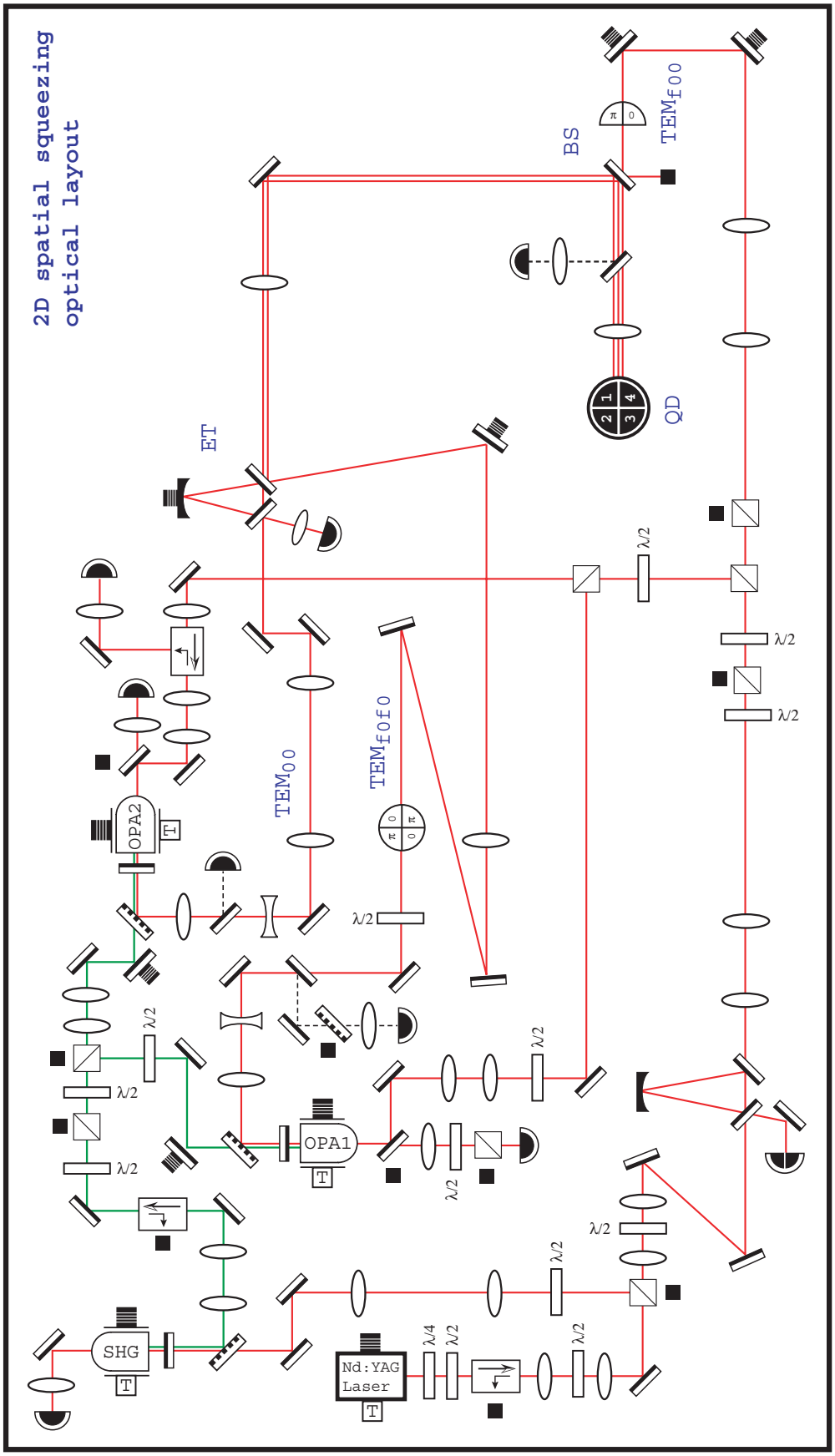

Figure 4.10: The complete optical layout

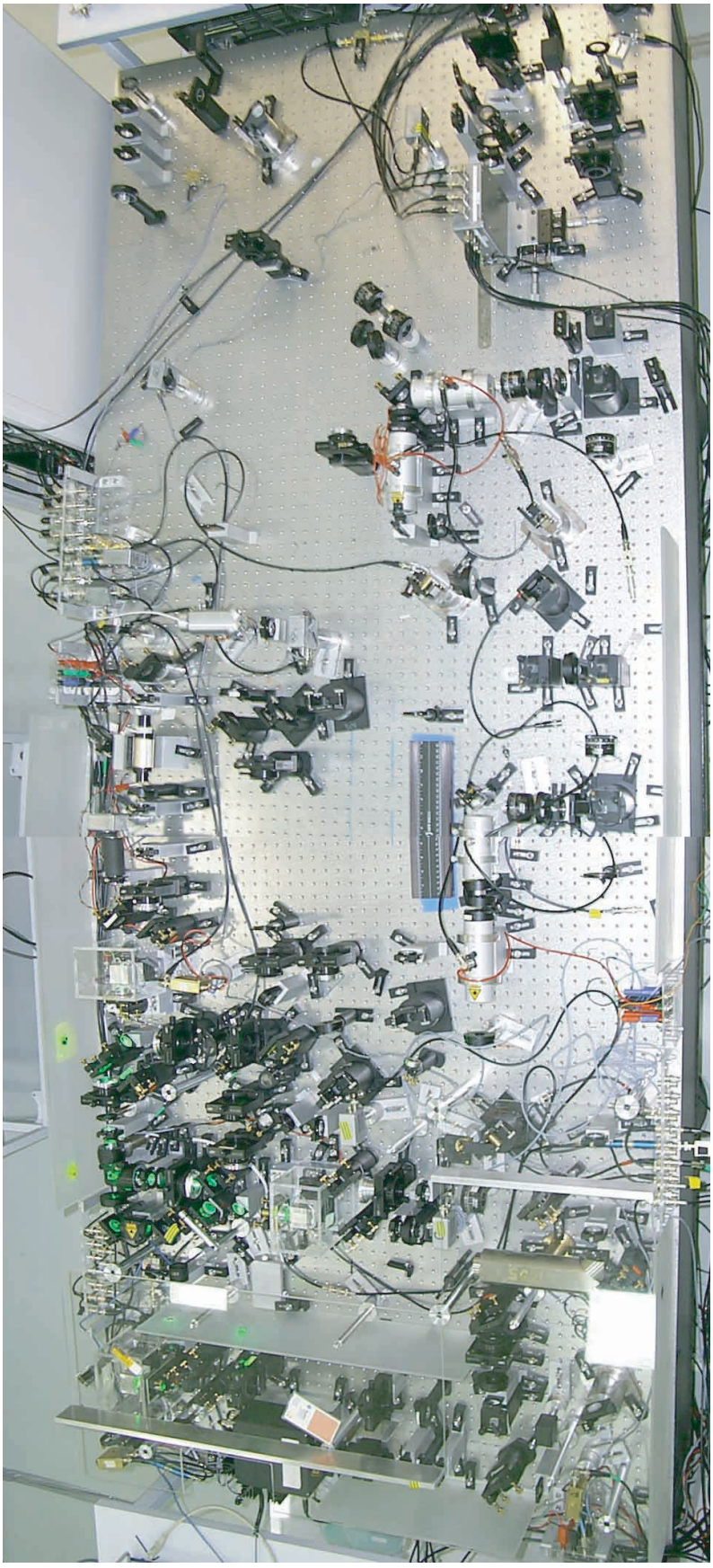

Figure 4.11: Photograph of the optical bench

Chapter 5

Experimental Results

'I could be bounded in a nutshell and count myself king of infinite space, were it not that I have bad dreams.'

William Shakespeare (Hamlet)

The previous chapter contained a discussion and analysis of initial experimental parameters and precautions. As these issues were dutifully addressed, the way is now paved for an uninterrupted presentation of the results.

5.1 Results

5.1.1 Scan of quadrature amplitudes

The traditional presentation of temporal squeezing results is to measure the noise power at a fixed frequency and scan the phase of the local oscillator relative to the squeezed beam, thereby scanning through all angles of quadrature. The resulting curves bare an uncanny resemblence to the M in a McDonalds logo, but are of course totally unrelated and mentioned purely for descriptive purposes. This method is also the simplest to implement

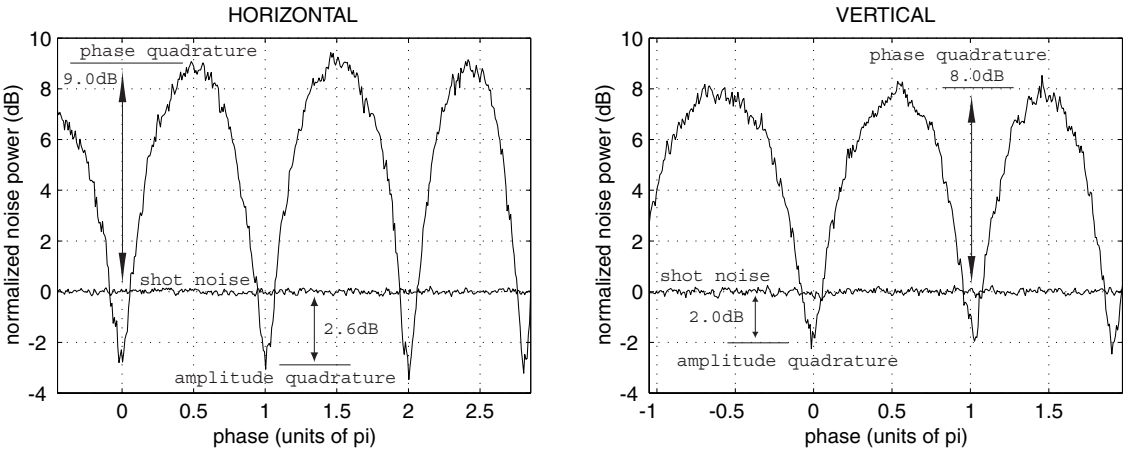

Figure 5.1: 'McDonald' curves. A scan of local oscillator phase relative to squeeze beams for 2D spacial squeezing. Minima are at phase integer multiples of π and correspond to amplitude quadrature squeezing for both horizontal and vertical measurments yielding H=-2.6dB and V=-2.0dB. Maxima are at phase half-integer multiples of π and correspond to phase quadrature anti-squeezing of horizontal and vertical measurements yielding H=+9.0dB and V=+8.0dB. Spectrum analyzer settings zerospan@4.976MHz, RBW=100kHz, VBW=100Hz, no average.

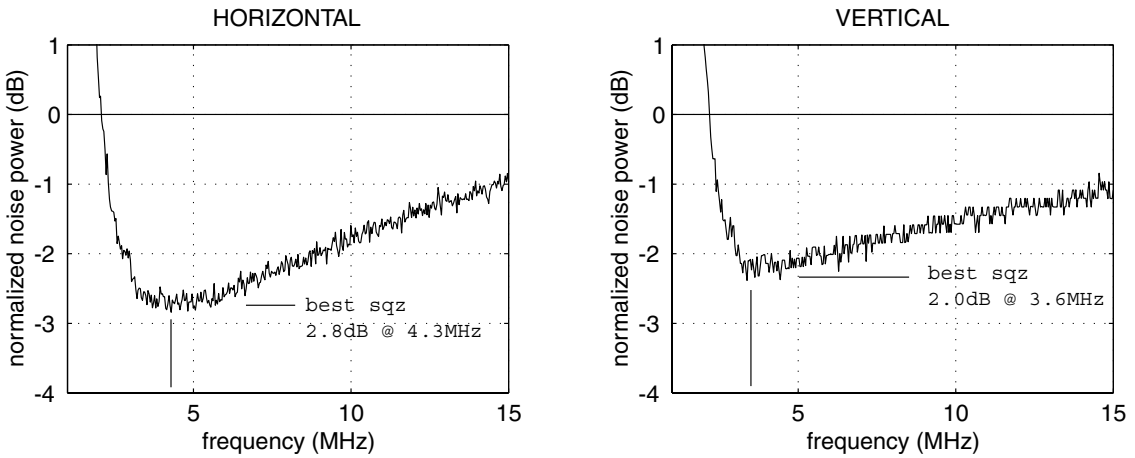

Figure 5.2: Wide frequency range. Noise spectrum of 2D spatial squeezing from 1MHz to 15MHz normalized at each frequency. Raw data is at top, and dark noise corrected normalized data at bottom. Spectrum analyzer settings span form 1MHz to 15MHz, RBW=100kHz, VBW=100Hz, average 10 traces.

in an experiment as it is not necessary for the homydning stage to be locked. We have made this type of measurement for 2D spatial squeezing and it is presented in Fig5.1. The minima correspond to the squeezed quadrature, which in our case was amplitude, and is manifest at phase angles of integer multiple π. The phase quadratue is visible at half integer multiples of π and correspond to the maxima. Reading directly from the graph, the levels of squeezing in the amplitude quadrature are H=-2.6dB and V=-2.0dB for horizontal and vertical differential measurements respectively. Note that for convenience, horizontal and vertical measurement will be denoted by and H and V. The level of anti-squeezing in the phase quadrature was measured to be H=+9.0dB and V=+8.0dB. Using these values for the normalized variances to find the uncertainty products gives $V_H^+ V_H^- = 4.4$, $V_V^+ V_V^- = 4.0$ which are greater than one, and therefore satisfy the Heisenberg uncertainty principle.

5.1.2 Wide frequency range

In Fig5.2 a wide frequency range from 1MHz to 15Mhz allowed us to search for a single frequency we could work at that had the best possible squeezing for both H and V. The general behaviour is that below 2MHz the squeezed beams are above 0dB and therefore not even shot noise limited. Above 2MHz the squeezing rapidly gets stronger until reaching peaks of H=2.8dB @ 4.3MHz and V=2.0dB @ 3.6MHz. Moving higher in frequency the squeezing became gradually weaker at a slope of H=0.2dB/MHz and V=0.1dB/MHz. Note that H squeezing degrades more rapidly with increasing frequency than V squeezing. This is due to the 12MHz linewidth of the ET mode-mixing cavity acting as a low pass filter for H transmission. Since the V is reflected it does not experience the coupling in of SNL vacuum state as does the H, and hence its squeezing to not degraded as much. We chose 4.976MHz as the frequency we would work with as it was a good compromise for both H and V squeezing, and also coincided with a good response from the displacement modulator.

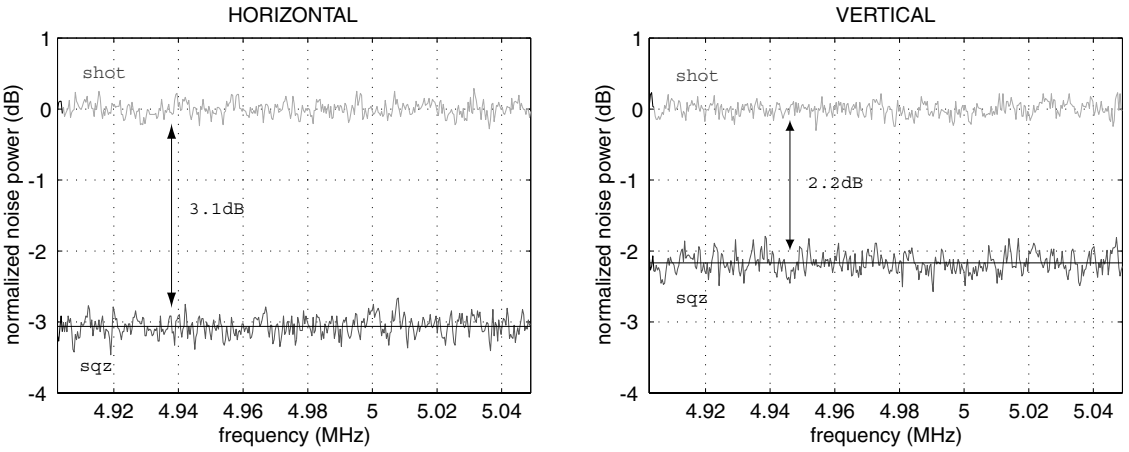

Figure 5.3: Best results! Noise spectrum of 2D spatial squeezing of 3.1 ± 0.1dB horizontal and 2.2 ± 0.1dB vertical. Upper curve is shot noise, lower curve is squeezing with a line through the mean value. Spectrum analyzer settings 150kHz span@4.976MHz. RBW=100kHz, VBW=100Hz, average 10 traces.

5.1.3 Best horizontal and vertical squeezing

The strongest levels of both H and V squeezing that we achieved are presented in Figure 5.3. For V the squeezing was 2.2dB which in linear scale is a factor 0.6 below shot noise limit. For H the squeezing was 3.1dB. In linear scale this means that the squeezing beam lowered the noise of the horizontal measurement by a factor 0.5 (one half!) of the shot noise limit, which translates into a factor of two increase in spatial resolution.

5.1.4 Stability

Good stability in any squeezing experiment is highly prized, as it not only allows the acquisition of measurements to be convenient, but more importantly, demonstrates its desirability for possible applications. Of course with much attention to engineering, squeezing

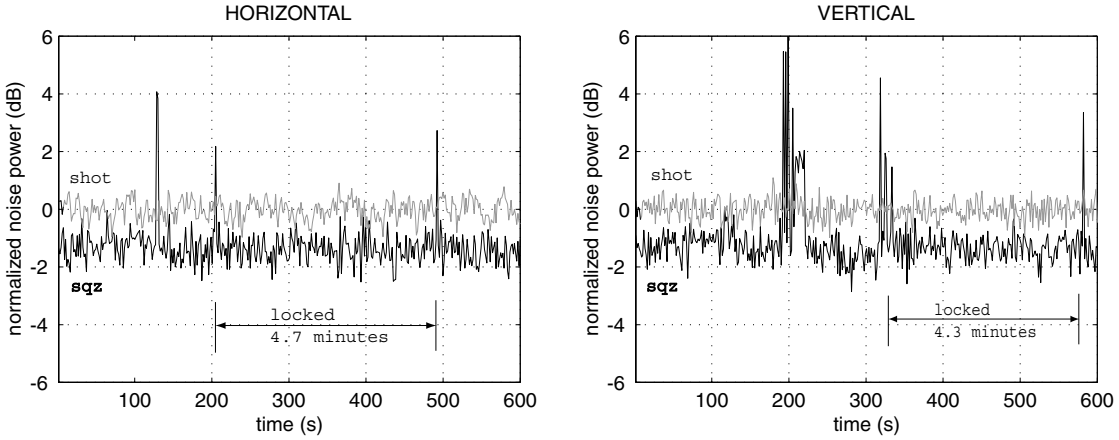

Figure 5.4: Long period locking stability. Noise spectrum of 2D spatial squeezing. Upper curve is shot noise, lower curve is squeezing. Spectrum analyzer settings zerospan@4.976MHz, RBW=100kHz, VBW=100Hz, no average.

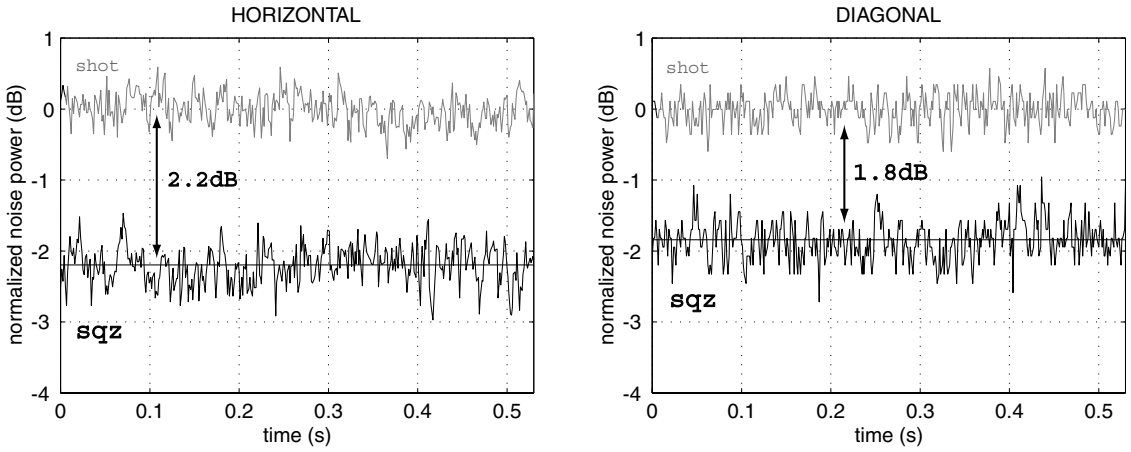

Figure 5.5: Diagonal and horizontal squeezing noise spectra. Diagonal (1.8 ± 0.3)dB and horizontal (2.2 ± 0.3)dB. Upper curve is shot noise, lower curve is squeezing with a line through the mean value. Spectrum analyzer settings zerospan@4.976MHz, RBW=100kHz, VBW=100Hz, no average sample mode.

could be made as stable as required. Figure 5.4 shows our long-time squeezing run. The spectrum analyser was set to scan for 10 minutes. It is thought that drops in our locking system, visible as spikes in Figure 5.4 were due to loud audio vibrations in the air caused by other researchers present in the lab at the time. Due to the relatively small range of PZT servos, we believe that once sound proofing has been addressed, long term stabilty is ultimately determined by thermal stabilty.

5.1.5 Diagonal Squeezing

This next run was a demonstration to highlight the configuration flexibility of two-dimensional spatial squeezing. We altered out vertical squeezed beam to For a quadrant detector there is another differential measurement possible other than H and V. It is the diagonal measurment (D) taken by summing opposite corners and subtracting one diagonal from the other. The noise detected when performing a diagonal spatial homodyning measurement comes from the vacuum mode that is double-flipped relative to the local oscillator. Since our local oscillator was a horizontal flipped mode ($\mathrm{TEM}_{\mathrm{f}00}$) then the squeezed beam required was a vertical flipped mode ($\mathrm{TEM}_{0\mathrm{f}0}$). The wave-plate in the OPA1 beam was shifted to lie on only two quadrants to give a vertical flip. OPA2 beam was left untouched to provide its usual horizontal spatial squeezing. Figure 5.5 shows the results from this 2D spatial squeezing measurement. Horizontal squeezing H=2.2dB, and diagonal squeezing D=1.8dB.

5.1.6 1D proper configuration

A variation on the theme of spatial squeezing was the reconfiguration of our experiment to perform a 1D-proper measurement. The 1D-proper configuration used the ET mode-mixing cavity to combine the squeezed beam from OPA2 together with the beam from OPA1 which was suitably boosted in power to act as a local oscillator. The phase plate in the path of the local oscillator was postioned to give a vertical phase flip, thereby fulfilling the spatial homodyning condition. The result of 1D-proper vertical squeezing is shown in Figure 5.6. We achieved a level of H=2.5dB below shot noise. The motivation

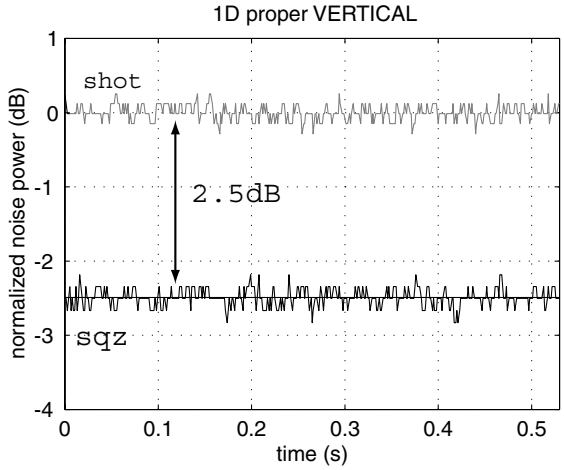

Figure 5.6: Proper 1D vertical squeezing (2.5 ± 0.3)dB. Upper curve is shot noise, lower curve is squeezing. Spectrum analyzer settings zerospan@4.976MHz, RBW=100kHz, VBW=100Hz, average 20 traces.

for performing a 1D proper measurement is this: Ordinary 1D spatial squeezing suffers from one significant ailment. The local oscillator beam is forced to undergo heavy loss at the mode-mixing beamsplitter whose splitting ratio is highly in favour of the fragile squeezed beam. This is in effect defeating the purpose of spatial squeezing. If we had used all the power in the local oscillator, and forgotten entirely about squeezing, our beam displacement mesurements would be more sensitive (but still at the shot noise limit). The 1D-proper configuration is free from this ailment entirely, as it combines the two modes on the mode-mixing cavity which has no obvious fundamental limit to how low local oscillator losses can be made.

5.1.7 Displacement Signal

We wanted to test if spatial squeezing really could improve the sensitivity of a beam displacement mesurement. Our method was to periodically displace the local oscillator beam by reflection from a mirror mounted on a PZT (see Chapter 4 for details). The displacement modulation was set at a frequency of 4.976MHz with amplitudes 5.0Åand 2.5Åfor horizontal and vertical respectively (calibrated to the shot noise limit with $d_{SNL} = 1.8$Å). The configuration used was the usual horizontal and vertical two-dimentional spatial squeezing setup. Squeezing levels were $H = 2.84$dB and $V = 1.80$dB. The results are shown in Figure 5.7. The broad peak corresponds to the displacement signal. Measurements of diplacement were taken from the maximum of the peak. For the SNL beam, the displacement modulation signal to noise-floor ratio was $SNR_{shotH} = 2.8$ and $SNR_{shotV} = 1.4$ For the squeezed beam, the displacement signal to noise-floor ratio was $SNR_{sqzH} = 5.2$ and $SNR_{sqzV} = 1.9$ As we can see, the squeezed beam has improved the signal to noise ratios of horizontal and vertical displacement measurements by factors of $\frac{SNR_{sqzH}}{SNR_{shotH}} = 1.9$ and $\frac{SNR_{sqzV}}{SNR_{shotV}} = 1.4$ We have therefore shown that two-dimensional spatial squeezing can indeed improve the sensitivity of beam displacement measurements.

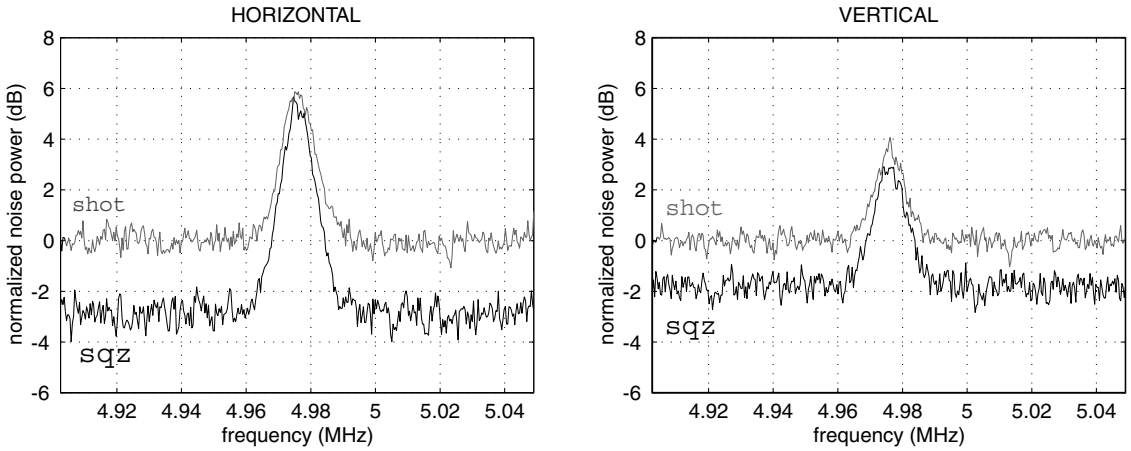

Figure 5.7: Displacement modulation. Noise spectrum of 2D spatial squeezing of $H = 2.8 \pm 0.4$dB and $V = 1.8 \pm 0.4$dB with displacement modulation at 4.976MHz. Upper curve is shot noise, lower curve is squeezing. Spectrum analyzer settings 150kHz span@4.976MHz, RBW=10kHz, VBW=100Hz, average 20 traces.

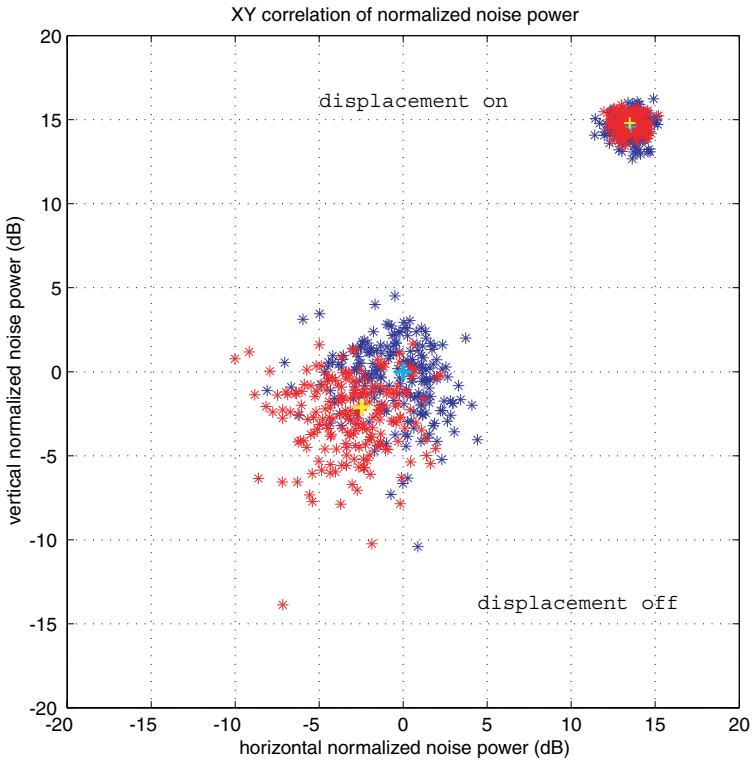

Figure 5.8: Noise power correlation plot of modulation on/off while 2D spatial squeezing ($H = 2.5$dB and $V = 2.1$dB) in a dB scale normalised to SNL. Shot noise data points are blue, squeezing points are red. The shot and squeezing mean values are marked by cyan and yellow coloured plus signs respectively. Two spectrum analyzers were used with settings zerospan@4.976MHz, RBW=1kHz, VBW=1kHz, average 6 traces.

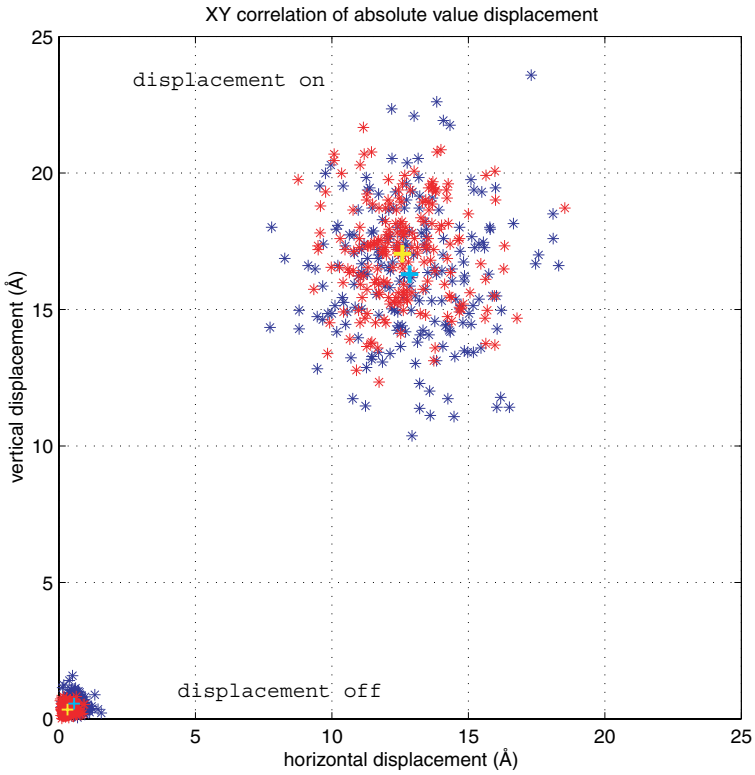

Figure 5.9: Calibrated absolute value displacement correlation plots of modulation on/off while 2D spatial squeezing (H = 2.5dB and V = 2.1dB) on a calibrated linear scale. Shot noise data points are blue, squeezing points are red. The shot and squeezing mean values are marked by cyan and yellow coloured plus signs respectively. Two spectrum analyzers used with settings zerospan@4.976MHz, RBW=1kHz, VBW=1kHz, average 6 traces.

5.1.8 Correlation plots (dB scale)

With the addition of a second spectrum analyser linked to trigger together with the first, we had the opportunity to construct correlation plots of horizontal verses vertical signals as shown in Figure 5.8. We performed this measurement both displacement modulation on and off. The scale in the graph is in dB and normalized to the shot noise limit. Our level of squeezing was H = 2.5dB and V = 2.5dB. For displacement-off it is quite apparent that the squeezing data points are lower than the shot noise. The displacement amplitude is about 13dB above shot noise for both horizontal and vertical squeezing. For displacements this large, the improvements in signal to noise ratio for squeezing over shot are very small.

5.1.9 Correlation plots (calibrated linear scale)

The same data from Figure 5.8 is plotted again in Figure 5.9 but this time in a calibrated linear scale. The scale was calibrated by the shot noise limited displacement noise floor of d_{SNL} = 0.56Å. Although difficult to see in this plot, the diplacement noise floors for displacement-off squeezing were d_{Hsqz} = 0.32Åand d_{Hsqz} = 0.34Å. As mentioned earlier this displacement is about 13dB above the noise floor, corresponding to about 15Å. For such a large SNR ($\approx$ 20) we expect that there would be little difference in the measured values of displacement for squeezing or just shot noise. But what we see for squeezing is that there is a small descrepancy of about (1Å) less horizontal, and (2Å) extra vertical, on

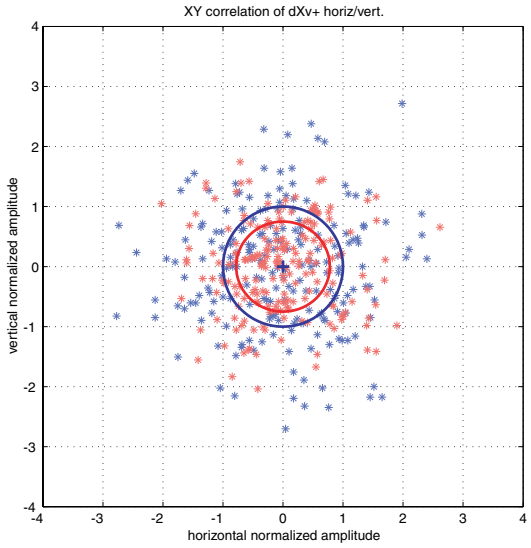

Figure 5.10: Direct amplitude quadrature operator correlation plots using the modulation-on data. Linear scale proporional to quadrature amplitude. Shot noise data points are blue, squeezing points are red. The shot mean value is marked by a blue coloured plus sign. The blue and red circles are drawn at the standard deviations for shot, and squeezing data, respectively. The data has been rescaled to make the standard deviation circle of the shot noise equal one. Two spectrum analyzers used with settings zerospan@4.976MHz, RBW=1kHz, VBW=1kHz, average 6 traces.

the measured displacements when compared with shot noise. This is what we referred to as the modulation-excess-feature, and was only present for large displacement measurements. It turns out that it does not change our measured values of squeezing, or the improvements measured for small displacements. The modulation-excess-feature is further addressed in the discussion section.

5.1.10 Correlation plots (extraction of amplitude quadrature)

Using the data from Figure 5.9 it was possible to extract the amplitude quadrature fluctuations in the light. This was done by taking the square roots of the data points for modulation-on, and then subtracting away the square roots of the mean of modulation-on. This was shown by [10] and we have

$$\delta X^{+} \approx \sqrt{V_{Hmod}} - \sqrt{\langle V_{Hmod} \rangle} \tag{5.1}$$

Where V_{Hmod} is the signal containing both the quantum fluctuations and the steady displacement signal. We used this method for both horizontal and vertical data points and it is presented in Figure 5.10 along with circles marking out the standard deviations of the data points. This is not a ball on stick picture! Because there is no phase quadrature axis, and therefore the HUP does not apply. We are effectively performing a spatial homodyning measurement on only the amplitude quadratures of the horizontal and vertical squeezed beams. The data has been re-scaled to the shot noise limit circle. The circle is not actually a circle but an ellipse. The axes of the ellipse are $R_H = 0.78$ and $R_V = 0.75$. Note that these are 2nd order standard deviations (ie. the fourth moment of the data) and should still correspond to the measured values of squeezing since quantum noise is flat spectrum. However, these 2nd order standard deviations do not correspond to

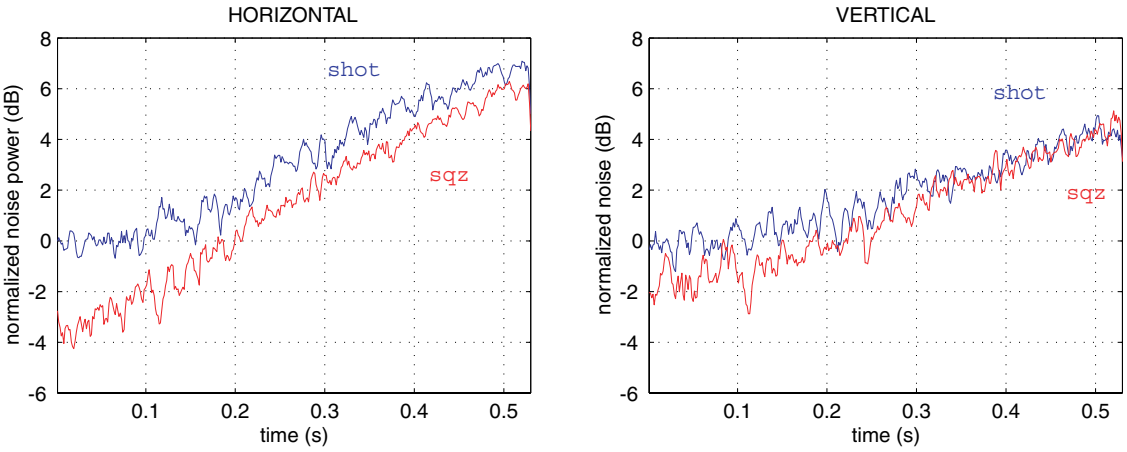

Figure 5.11: Ramp run. Normalised noise power for horizontal and vertical displacment ramp. Blue is shot noise, red is squeezing ($H = 2.7$dB and $V = 1.7$dB). Spectrum analyzer settings zerospan@4.976MHz, RBW=1kHz, VBW=1kHz, average 20 traces, 5 seat boxcar average.

precisely the 1st order measurements of squeezing. When squared and expressed in dB scale they become $H = 2.2$dB and $V = 2.5$dB. The measured values using the usual technique gave $H = 2.5$dB and $V = 2.1$dB. This is most likely due to processing in the two spectrum analysers (Horizontal was Hewlitt-Packard, and Vertical was Agilent Technologies) even thought there settings were she same. It is for this reason that 2nd order variances/standard-deviation measurements have not been quoted in any of our squeezing results in this thesis. The 1st order variance results are however believed to be reliable. We should then use caution for the interpretation of the correlation diagram in Figure 5.10 and use it instead as a conceptual tool to aid the visualization of two dimensional spatial squeezing.

5.1.11 Displacement Ramp (dB scale)

Earlier in this chapter we showed our results for the improvement in the SNR of an actual displacement measurement (see Figure 5.7). Our next ambition was to see exactly how small a displacement measurement we could make below the shot noise limit using two-dimensionally squeezed light. We achieved this by ramping the amplitude of the displacement from zero up to 0.6Åat a rate of 2Hz and measuring the signals from squeezed, and then shot noise limited light beams. The results for horizontal and vertical measurements are presented in Figure 5.11. The y-axis scale is in dB and normalised to shot noise. The x-axis is the time of the ramp to rise. Zero displacement starts at zero time. Concentrating for the moment on the horizontal plot. For shot noise, initially the signal is invisible as it lies below the noise floor. As the displacement gets larger, it eventually manages to rise above and become visible. For squeezing we can see that the displacement signal rises much earlier out of its noise floor. The same is also true for the vertical trace, but since there is less squeezing on the vertical ($V = 2.1$dB) than the horizontal ($H = 2.7$dB), it is not as obvious.

5.1.12 Displacement Ramp (signal to noise ratio)

The qualitative view from the previous section can be made quantitative by calculating the signal to noise-floor ratios from the previous data set. These are plotted in Figure 5.12.

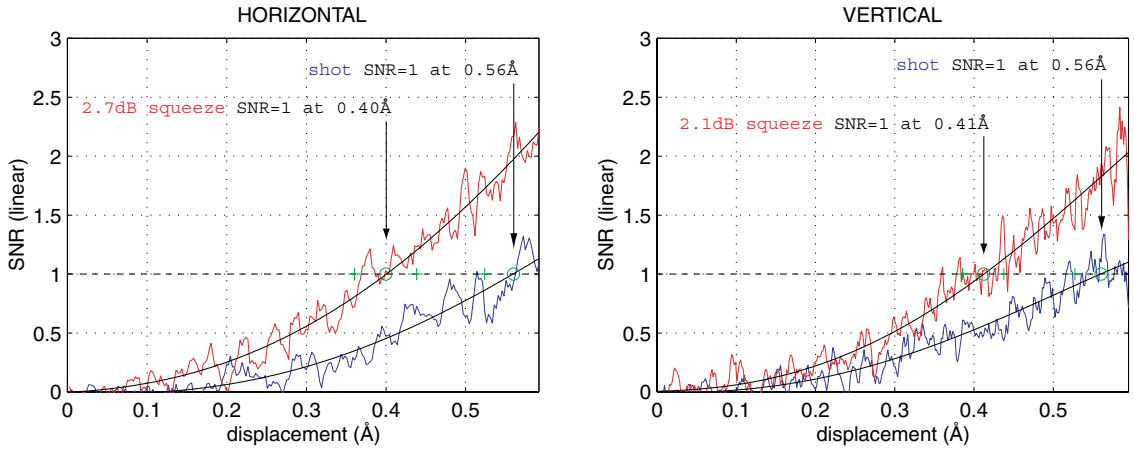

Figure 5.12: Ramp run. Signal to noise-floor ratios (SNR) of a displacement being ramped. Blue is shot, red is squeezing (H = 2.7dB and V = 1.7dB). Solid black lines are fitted to the data. Dashed black line marks SNR=1. Intersections with SNR=1 are labled. Spectrum analyzer settings zerospan@4.976MHz, RBW=1kHz, VBW=1kHz, average 20 traces, 5 seat boxcar average.

The x-axis has been calibrated to the shot noise displacement of (d_{SNL} = 0.56Å). The y-axis is the signal to noise ratio, where noise refers to the respective noise-floors of shot and squeezing for each trace. Note that the curve produced is quadratic in shape. This is because we are measuring the variances of the noise, which correspond to squared quantities of the differential intensity of the light, and are therefore squares of the displacement amplitude. The question is; at what point can we confirm that a signal has been detected? A standard rule of thumb is that the signal has a strength comparable to the noise floor, ie. a signal to noise ratio equal to one ($SNR = 1$). Using this as our guide, we can read of these detectivity points from Figure 5.12. Noticed that shot noise is always at (d = 0.56Å) this is because we have indeed calibrated the x-axes to the shot noise displacement. What we can see is that for the measurements taken with squeezed light, we could confidently read a displacment signal at the detectivity point as (d_H = 0.40Å) for horizontal and (d_V = 0.41Å) for vertical. This means we have surpassed the spacial resolution shot noise limit by linear factors of (1.4) for horizontal and (1.4) for vertical displacement measurements.

5.2 Discussion

5.2.1 Modulation-excess-feature

We continue here the discussion on the modulation-excess-feature begun in Section 1.1.9. Here are the relevent facts. i) This feature made only itself apparent as a discrepency in the measured displacement signals for displacements at least 13dB above the shot noise limit. ii) It gave unbalanced response to horizontal verses vertical measurements. iii) It was persistent from day to day. In order to find out more about it, we made the following checks. iv) It was not electrical/radio frequency pickup. v) It depended, but in no predictable way, on which shot noise was taken, ie. all a) sqz block, b) alternate sqz block, and c) all green block (discussed in detail in Chapter 4).

Collecting these facts together we arrived at a few ideas that may have caused the effect. The undesirable mode shape of OPA1 (vertical squeezer) was perhaps at fault. The

OPA1 mode shape was not a pure Gaussian and so did not produce a perfect flip mode to interfere with the local oscillator. The contribution from this undesirable component could have made unbalanced differential measurements that would have scaled with the displacement amplitude. Another cause may have been the non-linearity in the PZT crystal used to perform the displacement. Remember that we relied on the defects of the PZT to produce diagonal modulation. Any higher order non-linearities would most likely have made themselves more pronounced with larger amplitude displacements. Therefore, it is probably safe to say that the modulation-excees-feature was caused by the contribution of the two factors just mentioned.

Note, that the feature did not affect the squeezing mesurements , as they were performed without modulation at all. And they also could not have affected the very small displacement measurements (on order of 0.5Å), such as in the ramp runs of section 1.1.12 and 1.1.13.

5.2.2 Squeezing level agreement with measured losses

It is a good exercise to be able to trace the optical losses from the OPAs to the detector, and check if the level of spatial squeezing agrees with the temporal measurements performed at the very beginning. From Chapter 2 we learned that losses in quantum optics could be modelled with a beamsplitter. The following losses that we have identified and measured in our experiment are.

For OPA1: 95% transmission through four-quadrant waveplate. 95% reflection from ET cavity. 92% reflection from mode-mixing beamsplitter. 92% efficiency for homodyning.95% detection efficiency at the quadrant detector. This gives an overall transmission of 73%. Starting with 3dB of temporal squeezing this should result in 2.0dB of spatial squeezing and corresponds within 5% of the value measured a maximum of 2.2dB.

For OPA2: 96% transmission from ET cavity. 92% reflection from mode-mixing beamsplitter. 92% efficiency for homodyning.95% detection efficiency at the quadrant detector. This gives an overall transmission of 0.80%. Starting with 4dB of temporal squeezing that we measured with a temporal homodyning setup, this should result in 2.9dB of spatial squeezing and corresponds within 5% of the value measured a maximum of 3.1dB.

This analysis has confirmed that we could indeed account for losses to the squeezed light through the key experimental components.

5.3 Summary of results

This has been the first demonstration ever of two-dimensional spatial squeezing. We obtained 3.1dB and 2.2dB of squeezing below the shot noise limit for horizontal and vertical measurements respectively. Our sevo-locking was stable to the order of at least 5 minutes. We improved the spatial sensitivity of a two-dimensional beam displacement measurement by a factor of (1.4) below the shot noise limit for each axis. We produced the first ever one-dimensional spatially squeezed beam of light (2.5dB below shot noise level) that did not require either of its initial beams to undergo loss.

Chapter 6

Conclusion and future work

Prediction is difficult, particularly about the future. Niels Bohr

In this thesis I have reviewed quantum optics theory and its extension to spatial squeezing. The special optical components were modelled and characterised, and a record of important experimental details was given. The results were then presented and discussed.

6.1 Conclusion

In this experiment, we have achieved the first ever demonstration of simultaneous two dimensional spatial squeezing. Our best levels of squeezing for horizontal and vertical spacial differential measurements were respectively (3.1dB) and (2.2dB) below the shot noise limit. We improved the sensitivity of both horizontal and vertical measurements of an actual beam displacement by a factor of (1.4). We experimentally demonstrated the first ever generation of one-dimensionally squeezed light (2.5dB below shot noise) that did not required any of the beams to undergo loss prior to mixing.

- The results from this experiment will be included in the material for a paper on two-dimensional spatial squeezing being submitted for the journal *Science*.
- A detailed follow up paper covering higher-dimensional squeezing and mode-mixing techniques is planned.

6.2 Future work

This is not the end of the story! It is in the spirit of inquiry that I dare to a peek into the future.

6.2.1 Application to AFM

There would not have to be any major modifications made in our experiment to use two-dimensionally squeezed light in an atomic force microscope (AFM). Recent developments in AFM technology are pushing toward high bandwidth scanning of a surface, ie. video AFM. These would be useful in biological studies of living cells in action. Due to short integration time in collecting video frames (at least 5 per second) the compromise for sensitivity may be reached, one that only spatial squeezing can overcome.

p	N
2	1
4	3
6	10
8	35
10	126
12	462
14	1716

Table 6.1: The number of possible differential measurements N as a function of the number of pixels p.

6.2.2 Multi-pixel measurements - quantum imaging

Two-dimensional spatial squeezing is really just the beginning. The spatial homodyning condition says that, for every balanced spatial differential measurement, there is a corresponding flipped mode that could be squeezed to lower the fluctuations of the local oscillator beam for that measurement. The formula for p number of pixels and N number of differential measurements is

$$N = \frac{p!}{2\left[(p/2)!\right]^2} \tag{6.1}$$

The first few values are given in Table 6.1. Note especially how quickly the number of measurements rises with increasing pixel number. For a one mega-pixel CCD array of pixels the number of differential measurments is staggering (and too big too evaluate in Maple!). Of course, one need not use all possible configurations for an imaging application. As we have seen, the step from 1D to 2D spatial squeezing required the development of a new mode-mixing techinique. The step to higher dimensions will require an extension of this technique, and although the step may not be obvious, there is as yet, no known fundamental limit to the number of multi-mode beams that may be mixed.

6.2.3 Spatial connection with temporal quantum optics

Perhaps the most intriguing developments will come from the search for connections between spatial quantum optics and the traditional temporal quantum optics. This means that the familiar ideas in temporal quanutm optics such as, entanglement, dense-coding, teleportation, and cryptography, could have their analogs in spatial quantum optics.

Bibliography

[1] H.-A. Bachor. *A Guide to Experiments in Quantum Optics*. VCH Publishers, New York, 1 edition, 1998.

[2] B. Buchler. *Electro-optic Control of Quantum Measurements*. PhD thesis, Department of Physics, The Austalian National University, 2001.

[3] C. Fabre, J. B. Fouet, and A. Maître. Quantum limits in the measurement of very small displacements in optical images. *Optics Letters*, 25-1:76, 1999.

[4] P.K. Lam. *Applications of quantum electro-optic control and squeezed light*. PhD thesis, Department of Physics, The Austalian National University, 1999.

[5] P.K. Lam, Ralph T.C., Buchler B.C., McClelland D.E., Bachor H.-A., and Gao J. Optimization and transfer of vacuum squeezing from an optical parametric oscillator. *J. Opt. B*, 1:469, 1999.

[6] K. McKenzie. *Experimental Demonstration of a Gravitational Wave Detector Configuration Below the Shot Noise Limit*. PhD thesis, Department of Physics, The Austalian National University, 2002.

[7] E. Polzik, J. Carri, and H. J. Kimble. m. *Appl. Phys. B*, 55:279, 1992.

[8] R. Schnabel, W. P. Bowen, N. Treps, H.-A. Bachor, and P. K. Lam. Quantum correlations in continuous variable polarization states. *Phys. Rev. Lett.*, 88:093601, 2002.

[9] D.A. Shaddock, M. B. Gray, and D. E. McClelland. Frequency locking a laser to an optical cavity by use of spatial mode interference. *Opt. Lett.*, 24:1499, 1999.

[10] N. Treps. Private communication 2002.

[11] N. Treps, U. Andersen, B. Buchler, P. K. Lam, A. Maître, H.-A. Bachor, and C. Fabre. Surpassing the standard quantum limit for optical imaging using non-classical multimode light. *Phys. Rev. Lett.*, 88:093601, 2001.

[12] D. F. Walls and G. J. Milburn. *Quantum Optics*. Springer-Verlag, Berlin, 1 edition, 1994.

Expansion of double-flip-mode in TEMpq basis

What follows is the analytical decomposition of the double-flipped TEM_{00} mode in the TEM_{pq} basis. We begin by defining the action of the flip operators on an arbitrary function

$$\hat{F}_x(g(x,y)) = \begin{cases} -g(x,y) & , \quad x < 0 \\ g(x,y) & , \quad x \geq 0 \end{cases} \tag{A.1}$$

$$\hat{F}_y(g(x,y)) = \begin{cases} -g(x,y) & , \quad y < 0 \\ g(x,y) & , \quad y \geq 0 \end{cases} \tag{A.2}$$

Consider the set of normalized Hermite-Gaussian functions as a basis

$$u_p(x) = A_p H_p(x) e^{-\frac{1}{2}x^2} \tag{A.3}$$

$$A_p = \frac{1}{\sqrt{\sqrt{\pi} 2^p p!}} \tag{A.4}$$

$H_p(x)$ are the Hermite polynomials generated by the recursion relation and initial conditions

$$H_{p+1}(x) = 2xH_p(x) - 2nH_{p-1}(x) \tag{A.5}$$

$$H_0(x) = 1 \tag{A.6}$$

$$H_1(x) = 2x \tag{A.7}$$

Appropriate scaling factors and oscillating functions aside, the TEM_{pq} field envelope of the Helmoltz solutions for the propagation of an electromagnetic wave take the form

$$TEM_{pq}(x,y) = u_p(x)u_q(y) \tag{A.8}$$

Applying the flip operators, the double-flipped-mode of the TEM_{00} will be

$$TEM_{f,00} = \hat{F}_y(\hat{F}_x(TEM_{00})) \tag{A.9}$$

The aim here is to express $TEM_{f,00}$ as a weighted summation of $\{TEM_{pq}\}$ basis members

$$TEM_{f,00} = \sum_{p,q}^{\infty} c_{pq} TEM_{pq} \tag{A.10}$$

The task at hand is to find an analytical expression for the coefficients. Multiplying both sides of Eq. A.10 by the $\{TEM_{pq}\}$ set, and then integrating over all space and invoking the orthogonality of the functions, the coefficients are presented thus as

$$c_{pq} = \int_{-\infty}^{+\infty} \int_{-\infty}^{+\infty} \hat{F}_y(\hat{F}_x(TEM_{00}))TEM_{pq}dxdy \tag{A.11}$$

A solution to this integral must be found. Returning now to the more explicit forms of these functions, as products of Hermite-Gaussian functions, it becomes clear that the functions, and therefore the integrals, are indeed separable

$$c_{pq} = \int_{-\infty}^{+\infty} \hat{F}_x(u_0(x))u_p(x)dx \int_{-\infty}^{+\infty} \hat{F}_y(u_0(y))u_q(y)dy \tag{A.12}$$

Due to the fact that u_0 is an even function, the integrals may be split and recombined to integrate over only one quadrant of the plane

$$\begin{aligned} c_{pq} &= \left[\int_0^{+\infty} u_0(x)u_p(x)dx - \int_{-\infty}^{0} u_0(x)u_p(x)dx\right] \int_{-\infty}^{+\infty} u_0(y)u_q(y)dy & \text{(A.13)} \\ &= 2\int_0^{\infty} u_0(x)u_p(x)dx \left[\int_0^{+\infty} u_0(y)u_q(y)dy - \int_{-\infty}^{0} u_0(y)u_q(y)dy\right] & \text{(A.14)} \\ &= 4\int_0^{\infty} u_0(x)u_p(x)dx \int_0^{\infty} u_0(y)u_q(y)dy & \text{(A.15)} \end{aligned}$$

Whilst retaining the normalization constants, the functions are separated into their respective Hermite and Gauss parts

$$\begin{aligned} c_{pq} &= 4\int_0^{\infty} A_0H_0(x)A_pH_p(x)e^{-x^2}dx \int_0^{\infty} A_0H_0(y)A_qH_q(y)e^{-y^2}dy & \text{(A.16)} \\ &= 4A_0^2A_pA_q \int_0^{\infty} H_p(x)e^{-x^2}dx \int_0^{\infty} H_q(y)e^{-y^2}dy & \text{(A.17)} \end{aligned}$$

The mathematical text REF1 yielded the following helpful integral solution

$$\int_0^z e^{-x^2}H_p(x)dx = H_{p-1}(0) - e^{-z^2}H_{p-1}(z) \tag{A.18}$$

This general solution may be more useful for our purposes by taking the limit as $z \to \infty$

$$\begin{aligned} \int_0^{\infty} H_p(x)e^{-x^2}dx &= \lim_{z\to\infty}\left[H_{p-1}(0) - e^{-z^2}H_{p-1}(z)\right] & \text{(A.19)} \\ &= H_{p-1}(0) & \text{(A.20)} \end{aligned}$$

From REF1 an expression for the exact values of $H_p(0)$ are found to be

$$H_p(0) = \begin{cases} (-1)^n\frac{(2n)!}{n!} & , \quad p = 2n & , \quad n = 0,1,2,3,\ldots \\ 0 & , \quad p = 2n+1 & , \quad n = 0,1,2,3,\ldots \end{cases} \tag{A.21}$$

Substitution of this result into Eq.A.17 reveals that

$$c_{2n+1,2m+1} = 4A_0^2A_pA_q\left[(-1)^n\frac{(2n)!}{n!}\right]\left[(-1)^m\frac{(2m)!}{m!}\right] \tag{A.22}$$

Upon further simplification, we arrive at the formula for the double-flip-mode expansion coefficients

$$c_{2n+1,2m+1} = \frac{(-1)^{n+m}(2n)!(2m)!}{\pi n!m!2^{n+m-1}\sqrt{(2n+1)!(2m+1)!}} \tag{A.23}$$

Appendix B

MatLab code for numerical modelling of TEMf0f0

The following MatLab code was used to numerically the explore the mode structure of a double-flip-modeTEM_{f0f0} incident on a ring cavity. The coefficients for its expansion were used to reconstruct the wavefunctions of both before and after reflection from the cavity.

```
%Ring Cavity Model 2D - Guoy phase shift
clear;
format long

lmax=11;%%% truncate series to mode numver

%%%%%%%%.............define cavity properties...........%%%%%%%%%%%
c=3e8;
lambda=1064e-9;
d=198e-3;%round-trip cavity length

Rp=0.85;%polarization dependent -
Rs=0.95;% intensity reflectivities

r0=0.9999;%reflectivity amplitudes
r1=sqrt(Rs);
r2=r1;

fsr=c/(2*d);%free spectral range
F=pi*sqrt((r0*r1*r2)^1)/(1-((r0*r1*r2)^1));%Finesse
dnu=fsr/F;%resonant line width

a0=0;%absorption
a1=0.;
a2=0;

t0=sqrt(1-r0^2-a0^2);
t1=sqrt(1-r1^2-a1^2);
t2=sqrt(1-r2^2-a2^2);
```

```
%%%%%.....calculate cavity properties.....%%%%%%%%%%
R1=-250e-3;%radius of curvature for mirror 1 (negative means concave)
R2=R1;%radius of curvature for mirror 2 (negative means concave)

%Check cavity stability
G1=1+(d/R1);
G2=1+(d/R2);
GG=G1*G2;
if GG>=0 & GG<=1
%display('Stable')
else
display('Unstable')
end

z1=(-d*(R2+d))/(R2+R1+(2*d));%mirror 1 distance the the left of waist
z2=z1+d;%mirror 2 distance to the right of waist
z0=sqrt((-d*(R1+d)*(R2+d)*(R2+R1+d))/((R2+R1+(2*d))^2));%depth of focus
W0=sqrt(lambda*z0/pi);%waist size inside cavity

%%%%%%......calculate Guoy phase shift
z=d/2;%waist is halfway between two mirrors
zeta=2*atan(z/z0);%this is Mr Guoy in radians (two reflections * double pass)

%%%%%%%%%%%%%%%%%%%%%%%%%%%%%%%%%%%%%%%%
%2D  - HG normalization constants and flip-mode coefficients
c=[];
for n=0:fix(lmax/2);
for k=0:fix(lmax/2);
l=2*n+1;
m=2*k+1;
c(l+1,m+1)=(((-1)^(n+k)).*prod(1:2*n).*prod(1:2*k)./(pi*prod(1:n).

*prod(1:k).*(2.^(n+k-1)).*sqrt(prod(1:(2*n)+1).*prod(1:(2*k)+1)));
A(l+1)=1/(sqrt(sqrt(pi)*(2.^(2*n+1)).*prod(1:2*n+1)));
end
end
%re-normalize truncated series
%AA=sum(sum(c,1),2);

%%%%%%.....................All cavity modes.....................%%%
phi=(-1.5*2*pi :  1e-2  : 1.5*2*pi); % scan cavity
a=size(phi);
na=1:a(2);
a=[];
for l=0:lmax
for m=0:lmax;
qq=l+m;
```

```
dphi=phi+(qq*zeta)-pi;

E0=1*c(l+1,m+1);
Ein=E0*exp(i*0);
Ecirc=(t1*Ein)./(1-(r0*r1*r2*exp(i*dphi)));
Eout=Ecirc*t2;
Eleak=-Ecirc*(-r2)*(-r0)*t1.*exp(i*dphi);
Eref=Eleak+(Ein*r1);

Ereff(l+1,m+1,na)=Eref;
%Iout(l+1,m+1,na)=conj(Eout).*Eout;
Iref(l+1,m+1,na)=conj(Eref).*Eref;
%phiout(l+1,m+1,na)=angle(Eout);
%phiref(l+1,m+1,na)=angle(Eref);
end
end

%%%%%%........add up all the odd-odd modes........%%%%%%%%%%%%
l=0:lmax;
m=0:lmax;
Itotalref(na)=sum(sum(Iref(l+1,m+1,na),1),2);
%Itotalout(na)=sum(sum(Iout(l+1,m+1,na),1),2);

%%%%%%%%.......plot results.......%%%%%%%%%%%%%%%%%%%%%%%%%
l=1:lmax;
m=1;
phix=phi(na)/(2*pi);
funk(l,na)=Iref(l+1,m+1,na);
figure(1)
%plot(phi/(2*pi),Iout(0+1,:),'-r',

  phi/(2*pi),Itotalout,'-k' ,  phi/(2*pi),Iout(l+1,:));
cp=1/max(Itotalref);
plot(phix,Itotalref*cp,'-k',phix,funk*cp);
%plot(phix,Itotalref*cp,'-k');
axis([-0.5 1.5 0 1.1])
title('TEMf0f0 reflection from ring-cavity (THEORY)')
xlabel('free spectral range (units of FSR)')
ylabel('normalized optical power (linear)')
%plot(phix,Itotalout,'-k'  ,  phix,funk);


%%%%%%calculate flipmode reflection efficiency..%%%%%%
AA=sum(sum(conj(c).*c , 1),2);%truncation re-normalization constant
[Y,M]=min(abs(phi));%find TEM00 resonance position
AAref=Itotalref(M);%the actual reflected flip-mode total power
eff=AAref/AA%truncation normalized
%actual reflected flip-mode total power
```

```
%%%%%%....check if we still have a flip-mode...%%%%%%%%%%
l=0:lmax;
m=0:lmax;
cp(l+1,m+1)=Ereff(l+1,m+1,M);
B=sum(sum(conj(cp).*c,1),2)/AA;%perform overlap integral and re-normalize
BB=abs(B);%absolute value of overlap integral
Bphi=angle(B)*1e3;%reflected phase angle in mrad

%%%%%%%%%%%%%%%%%%%%%%%%%%%%%%%%
%%%%%%%%%%%%%%%%%%%%%%%%%%%%%%%%%%%%
%%%%%%%%%%%%%%%%%%%%%%%%%%%%%%%%%%%%%%%
%%%%%%%%%.........2D plot of reflected flip-mode reconstruction......%%
u=[];
H=[];
G=[];
l=[];
m=[];
N=[];
Nx=[];
Ny=[];
z=[];
zzzz=[];

%%%.........set 2D plot limits....%%%%%%%
umin=-4;
umax=+4;
Nmax=50;
N=1:Nmax;
u=umin+((N-1)/Nmax)*(umax-umin);

%.....here come the Hermites!.....
H(0+1,N)=1;
H(1+1,N)=2*u;
H(2+1,N)=4*u.^2-2;
H(3+1,N)=8*u.^3-12*u;
H(4+1,N)=16*u.^4-48*u.^2+12;
H(5+1,N)=32*u.^5-160*u.^3+120*u;
H(6+1,N)=64*u.^6-480*u.^4+720*u.^2-120;
H(7+1,N)=128*u.^7-1344*u.^5+3360*u.^3-1680*u;
H(8+1,N)=256*u.^8-3584*u.^6+13440*u.^4-13440*u.^2+1680;
H(9+1,N)=512*u.^9-9216*u.^7+48384*u.^5-80640*u.^3+30240*u;
H(10+1,N)=1024*u.^10-23040*u.^8+161280*u.^6-403200*u.^4+302400*u.^2-30240;

%%% for space considerations,
%%%%I have removed Higher order modes up to H(29+1,N)

%...recursion formula....
```

```
for l=28+1:lmax+1
H(l+1+1,N)=2*u.*H(l+1,N)-2*(l+1).*H(l+1-1,N);
end
%.......here comes Mr Gauss!....
G(N)=exp(-(1/2)*(u.*u));

%%%%.........form the TEM's......%%%%%%%%%
for l=0:lmax;
for m=0:lmax;
Hx(N)=H(l+1,N);
Hy(N)=H(m+1,N);
[Nx,Ny]=meshgrid(1:Nmax);
cc=real(cp(l+1,m+1));
%cc=real(c(l+1,m+1));
z(l+1,m+1, : , : )=cc*((A(l+1).*Hx(Nx).*G(Nx)) .* (A(m+1).*Hy(Ny).

*G(Ny)));
end
end

%%%%.a pure Gaussian is always a handy thing to have around.%
%GG(:,:)=G(Nx).*G(Ny);

%%%%%%.......add up all TEM's.....%%%%%%%%%
zzzz(:,:)=sum(sum(z,1),2);
H=[];
G=[];
c=[];
l=[];
m=[];
N=[];
z=[];
%%%%%%%%..........plot.......%%%%%%%%%
figure(2);
surfc(u,u,zzzz);
%shading interp
%colormap(gray);
view(20,20)
title('TEMf0f0 reconstruction')
xlabel('x-axis')
ylabel('y-axis')
zlabel('TEMf0f0 electric field E(x,y)')

%%%%%%%%%%%%%%%%%%%%%%%%
%%%%THE END
```

Appendix C

MatLab code for numerically solving Gaussian ABCD matrix

The following MatLab code solves the Gaussian ABCD matrix for propagation through two lenses. It was used primarily for choosing lens focal lengths and positions when building the mode-matching optical stages in the experiment. The user specifies the initial parameters; initial waist size and position, the focal lengths of two mode-matching lenses (f1, f2) and the desired waist size. The program then finds the spacing L between the lenses to get the desired waist size, and also its position from the second lens.

```
%%%%%%%%ModeMatcherABCD.m
%%%%use SI units everywhere
clear
format short
display('------->W0<---z----(f1)---L----(f2)----D---->W0pp<------------')

lambda=1064e-9%laser wavelength
W0=1.652e-3%laser waist at the first lens
z0=pi*(W0^2)/lambda;
z=0;%position of first waist left to the first lens
W0pppp=0.2005e-3%the desired waist
f1=150e-3%focal length of first lens
f2=100e-3%focal length of second lens

%%%scan the distance between second lens and the inter-lens waist
%%%there are two solutions depending on lens configuration
%%%one is positive and the other negative
%%%have to choose where to scan

%post-solution
zppstart=abs(f1+f2);
zppend=abs(f1+f2)*1.5;

%pre-solution
%zppstart=1e-3;
%zppend=abs(f1+f2);

nmax=1e3;
```

```
for n=1:nmax;
zpp(n)=zppstart+(zppend-zppstart)*(n/nmax);%scan

q1=z+i*z0;%q parameter at the first lens

A1=1;%first lens
B1=0;
C1=(-1/f1);
D1=1;
M1=[A1 B1
C1 D1];
q2=(A1*q1+B1)./(C1*q1+D1);
z2=-real(q2);%how far is inter-lens waist from first lens?
z02=imag(q2);
W02=sqrt(lambda*z02/pi);

A2=1;%free space between lenses
B2=zpp(n);
C2=0;
D2=1;
M2=[A2 B2
C2 D2];
q3=(A2*q2+B2)./(C2*q2+D2);
z3=-real(q3);
z03=imag(q3);
W03=sqrt(lambda*z03/pi);

A3=1;%second lens
B3=0;
C3=(-1/f2);
D3=1;
M3=[A3 B3
C3 D3];
q4=(A3*q3+B3)./(C3*q3+D3);
z4(n)=-real(q4);
z04=imag(q4);
W04(n)=sqrt(lambda*z04/pi);

end

%locate the lens position for which the desired waist is present
err=abs((W04/(W0pppp))-1);
[Y,I]=min(err);
error=Y%error in estimate
THEzpp=zpp(I);%I have found the optimum\\
 lens position relative to inbetween waist
THEz4=z4(I);%This is where the new\\
 waist lies relative to lens
```

```
L=THEzpp%This is the spacing between the two lenses
D=THEz4%This is where the new \\
waist is positioned relative to the second lens

%%%....plot shows waist size as \\
function of lens separation (blue curve)
%%%....red line is desired waist, \\
first asterix is solution to lens separation (L)
%%%....second asterix is where \\
the new waist will be relative to first lens (L+D)
%%%....this is to give an idea of the \\
optical layout and validity of the solution
plot(zpp,W04,'-b',zpp,W0pppp,'-r',L,W04(I),'*k',L+D,W04(I),'pk');
xlabel('lens separation (L) in metres');
ylabel('new waist size (W0pp) in metres');
zoom on
grid on

%%%%%%%..How much does the waist size grow with a change...%%%
%%%%%%%..in second lens position???.....%%%%%%%%
%%%%%%%..These are gradients for waist size...%%%%%%

%dW04dL=(W04(I+1)-W04(I))/(zpp(I+1)-zpp(I))
%dDdL=(z4(I+1)-z4(I))/(zpp(I+1)-zpp(I))

%%%%THE END
```